FERRIMAGNETISM AND MAGNETIC ENTROPY CHANGE OF TM/RE MULTILAYERS

by

MARIA RODICA HOSSU

Presented to the Faculty of the Graduate School of

The University of Texas at Arlington in Partial Fulfillment

of the Requirements

for the Degree of

DOCTOR OF PHILOSOPHY

THE UNIVERSITY OF TEXAS AT ARLINGTON

December 2008

ACKNOWLEDGEMENTS

I would like to express my gratitude to my advisor, Dr. Ali Koymen for his support and guidance through the duration of this work. I would also like to thank Dr. Y. Hao, J. Fry, P. Liu, and A. Weiss, for serving in my dissertation committee and their constructive questioning. I appreciate the technical assistance of Douglas Coyne and the support that I got from the faculty and staff of Physics Department at UTA. I am very grateful to all my family, for encouragement and patience.

November 17, 2008

ABSTRACT

FERRIMAGNETISM AND MAGNETIC ENTROPY CHANGE OF TM/RE MULTILAYERS

Maria R. Hossu, PhD.

The University of Texas at Arlington, 2008

Supervising Professor: Ali R. Koymen

Multilayers of Co/Tb, Ni/Gd, NiFe/Gd, CoFe/Gd and CoNi/Gd multilayers have been synthesized using dc magnetron sputtering. and have been investigated experimentally by SQUID magnetometry. Due to the antiferromagnetic coupling between the transition metal and rare earth layers these systems behave like artificial ferrimagnets, with a minimum in total magnetic moment at compensation temperature. The measurement of magnetic moment (M) as a function of temperature (T) shows that magnetic phase transition occurs at different temperatures during the heating (superheating) and cooling (supercooling) cycles resulting in thermal hysteresis curve for M (T).

Magnetic entropy change has been measured for CoFe/Gd and CoNi/Gd nanolayers. ΔS (T) associated with first order magnetic phase transitions, has a minimum during the cooling cycle and a maximum during the heating cycle. The magnetic phase transitions with entropy change can be controlled over 20-300K interval with small applied magnetic fields. The order-order magnetic phase transitions observed in M (T) and ΔS (T) are explained due to the temperature dependence of the Gd moment associated with the existence of an anisotropy field in the transition metal layers. The same multilayer can show none, one, or two-phase transitions by varying an external magnetic field in a small range and by changing the starting point in the cooling/heating cycles.

TABLE OF CONTENTS

LIST OF ILLUSTRATIONS

LIST OF TABLES

CHAPTER 1

INTRODUCTION

Magnetic properties of substances are induced by the existence of orbital and spin magnetic moments of electrons. Their interactions are the basis of creating macroscopic ordered substances that have various behaviors when interacting with a magnetic field.

The magnetic dipole moment of an atom is:

$$\vec{\mu}_J = (\vec{\mu}_L + \vec{\mu}_S) = g\mu_B \vec{J} \tag{1.1}$$

$\vec{\mu}_L$ is the orbital magnetic moment of the atom,

$\vec{\mu}_S$ is the spin magnetic moment of the atom,

$\vec{J}$ is the total angular momentum of the atom

$$\mu_B = \frac{eh}{4\pi m} = 9.27\ 10^{-24}\ \frac{J}{T} \quad \text{Bohr magneton} \tag{1.2}$$

$$g = 1 + \frac{[(J+1) + S(S+1) - L(L+1)]}{2J(J+1)} \quad \text{splitting factor} \tag{1.3}$$

J-angular momentum quantum number, L-orbital quantum number, and S-spin quantum number, m-mass of the electron and e -electric charge of the electron.

The characterization of magnetic properties is made using magnetization M and magnetic susceptibility χ

$$M = \frac{m}{V}, \text{ m magnetic moment, V volume} \quad (1.4)$$

$$\chi = \frac{M}{H}., \text{ H magnetic field} \quad (1.5)$$

The variation of these parameters with temperature (T) and external field: M(H), M(T) and χ(T) is generally investigated and used to describe magnetic properties of substances.

The following classification distinguishes the ordered substances based on the collective interaction of atomic moments.

1.1 Paramagnetism

This behavior is observed for atoms which have a net magnetic moment due to unpaired electrons in partially filled orbitals. In the presence of an external field there is a partial alignment of the atomic moments with the field direction, resulting in a net positive magnetization. However, the magnetization is zero when the external field is removed because there is no cooperative interaction between magnetic moments. The Curie law $\chi = \frac{C}{T}$ gives a temperature dependent susceptibility.

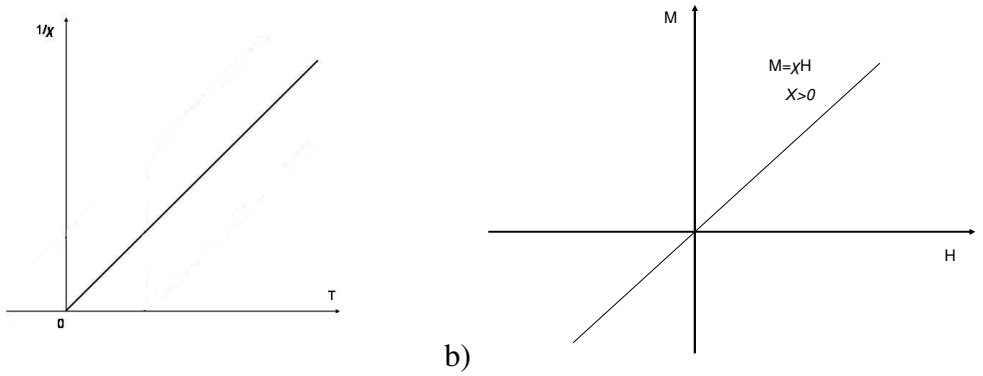

a) b)

Figure 1.1 Paramagnetic system: a) Inverse susceptibility dependence with temperature, b) Magnetization as a function of external magnetic field

1.2 Diamagnetism

Diamagnetism is a week magnetism which is characteristic to materials with no atomic magnetic moments. The main characteristics are a temperature independent susceptibility and a negative magnetization produced under an external field.

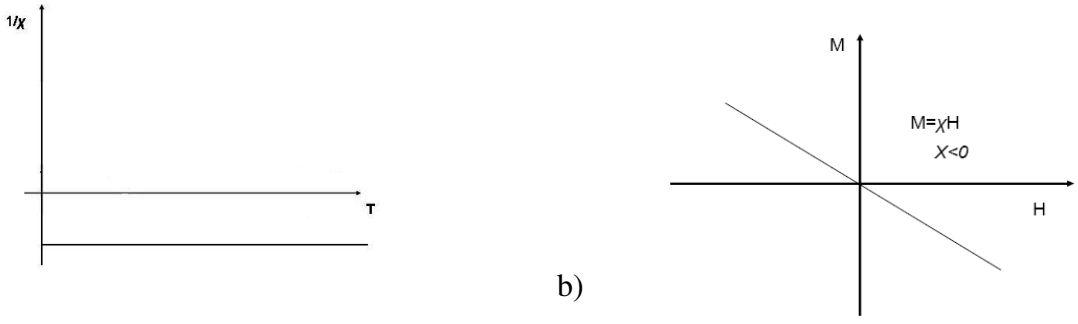

a) b)

Figure 1.2 Diamagnetic systems: a) Inverse susceptibility dependence with temperature, b) Magnetization as a function of the external magnetic field

1.3 Ferromagnetism

Ferromagnetism is characteristic for atoms which have permanent magnetic moments. There is strong interaction between atomic moments which keep them aligned even in the absence of an applied magnetic field.

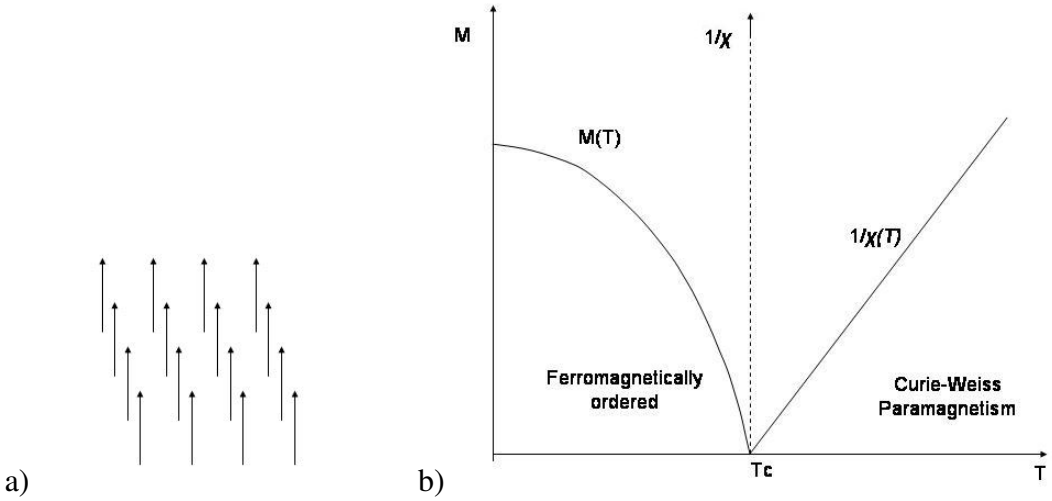

Figure 1.3 a) Ferromagnetic order below T_c, b) Magnetization and inverse susceptibility dependence with temperature

Above T_C, Curie temperature, the special order disappears and the substance is paramagnetic: the orientation of the moments is random due to the thermal agitation, each moment acting independent of the others. Below T_C, the individual magnetic moments of the atoms are lined up and they act together as a very large magnetic moment.

1.4 Antiferromagnetism

In the case of antiferromagnetic order the magnetic moments are lined up but the adjacent moments are aligned in opposite directions to each other. The result will be

a small value of magnetic moment M. M (H) is similar with a paramagnet, but the origin is quite different: the antiferromagnetic state is a long range order state.

Above a certain temperature, Neel temperature - T_N (figure 1.4), the substance is paramagnetic, and the same Curie-Weiss law, $\chi = \frac{C}{(T-\theta)}$, will describe the susceptibility temperature dependence, with the paramagnetic temperature, $\theta<0$, $\theta \neq T_N$

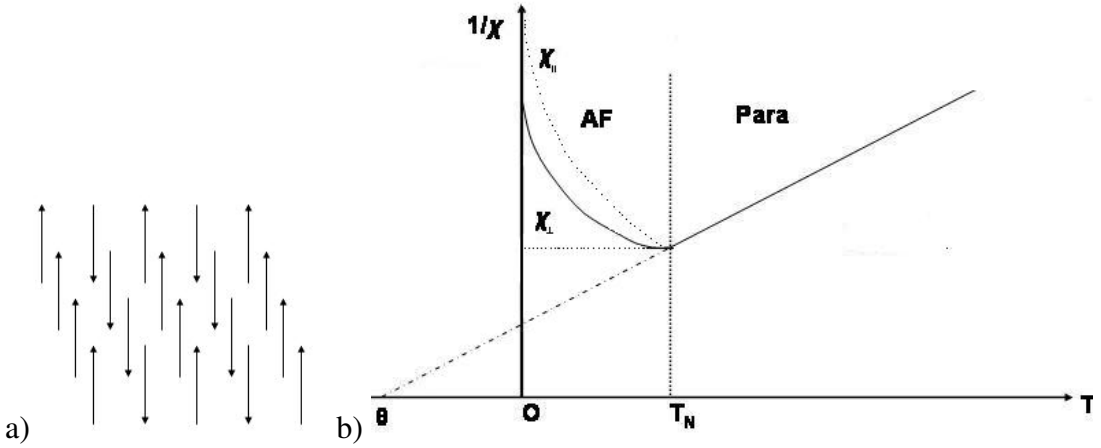

Figure 1.4 a) Antiferromagnetic order, b) Inverse susceptibility dependence with temperature

1.5 Ferrimagnetism

The ferrimagnetic order is very similar to the antiferromagnetic at the atomic level: the adjacent magnetic moments are locked in opposite directions, but with distinctive magnitudes (figure1.5). There is a certain temperature called compensation temperature, T_{comp}, where the opposed magnetic moment will cancel each other and the net magnetization for the system is zero. The behavior in an external applied field of the

ferrimagnetic substances is similar with the ferromagnetic substances: M(H) shows hysteresis and above Curie temperature the magnetic order disappear.

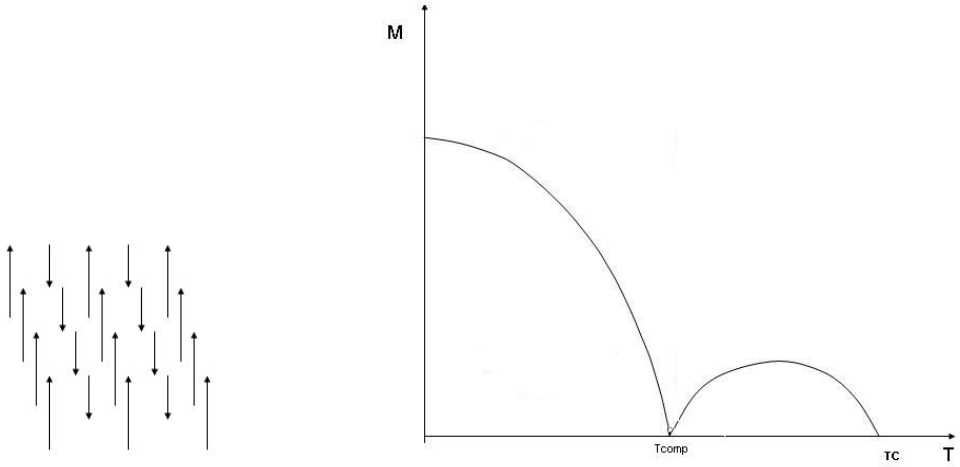

a) b)

Figure 1.5 a) Ferrimagnetic order, b) Magnetization dependence with temperature for a ferrimagnetic system

1.6 Magnetic interactions theories

To explain main properties of ferromagnetic materials like: magnetic order below Tc, but also zero magnetization in zero magnetic field, we introduce the magnetic interactions theories and the existence of magnetic domains.

Classical theory of magnetic order is based on the Molecular Mean Field and it was introduced by Weiss in 1907 [1, 2]. This is the mean field of the dipoles as a result of their strong interaction with all surrounding neighbors. The main assumption of this theory is that this molecular field H_m is proportional to the magnetization M.

$$H_m = N_m M \tag{1.6}$$

N_m –molecular field constant, independent of temperature

The interaction between magnetic dipoles leads to the creation of this field. Considering N atoms per unit volume that have angular momentum quantum number J, orbital quantum number L, and spin quantum number S, the spontaneous magnetization at T=0 and H=0 is:

$$M(0) = Ng\mu_B J \tag{1.7}$$

where $g = 1 + \frac{[(J+1) + S(S+1) - L(L+1)]}{2J(J+1)}$ is the splitting factor.

Along with spontaneous magnetization M(0), the theory explains also the temperature dependence of magnetization for $T<T_C$:

$$M(T) = M(0)B_J(x) \tag{1.8}$$

Where

$$x = \frac{Jg\mu_B H_m}{kT}, \tag{1.9}$$

with k- Boltzman constant and $B_J(x)$ - Brillouin function [1].

$$T_C = \frac{NJ(J+1)g^2\mu_B{}^2 N_m}{3k} \tag{1.10}$$

is the ferromagnetic Curie temperature.

At very low temperatures, close to 0K the approximation of $x \to \infty$ into Brillouin function will give:

$$M(T) = M(0)(1 - 2e^{-\frac{2T_C}{T}}),$$

For the paramagnetic regime above T_C, with $x \to 0$, the equation 1.8 becomes :

$$M = (Ng^2\mu_B 2J(J+1)/(3kBT)(H + \lambda M) \tag{1.11}$$

and the susceptibility is given by Curie-Weiss law:

$$\chi = \frac{C}{(T-\theta)} \tag{1.12}$$

$\theta = T_C$ is the paramagnetic or Curie temperature, and C the Curie constant, as shown in figure 1.3

There is disagreement with the experimental data for this theory in the ferromagnetic region and also around Tc. In reality Tc and θ are two different temperature: for Fe T_C=1043 K and θ= 1093K.

Weiss theory is amended by the exchange interaction theory, developed by Heisenberg, based on quantum mechanics.

1.6.1 Exchange Interaction

The molecular field is replaced by exchange interaction based on the following Heisenberg's Hamiltonian [1]:

$$H = -2J_{ij}S_iS_j\cos\alpha_{ij} \tag{1.13}$$

J_{ij} is the exchange integral between i^{th} and j^{th} spins and the summations extends over all spin pairs in the system.

For J_{ij} positive, the equilibrium of the system corresponding to minimum energy is obtained when α_{ij} the angle between i and j spins is zero, i.e. the spins are aligned parallel with each other.

J_{ij} depends on the extent and overlap between magnetic orbitals and on the interatomic separation. Thus the exchange interaction is a short range interaction.

Assuming identical atoms this interaction can be compared with the molecular field $J_{ij}=J_{ex}$:

$$N = \frac{Hm}{M} = \frac{(2xJ_{ex})}{Ng^2\mu_B{}^2} \tag{1.14}$$

And

$$J_{ex} = \frac{3k_BT_C}{2xJ(J+1)} \tag{1.15}$$

The exchange interaction calculated from Curie temperature is of the order of 10^3K in ferromagnetic materials like 3d metals and alloys.

If we consider an average moment <μ> of Z nearest neighbor atoms the molecular field proportional with magnetization is obtained in equation (1.6), as postulated by Weiss, with and M=N<μ>.

The spin wave theory at very low temperature T<<Tc gives the following magnetization – temperature dependence (Bloch's law), in good agreement with experimental data.

$$\text{is a } M = M(0)(1-aT^{3/2}) \tag{1.16}$$

where - a - is a constant dependent on exchange coefficient and lattice structure.

The spin wave is the propagation of a reverse spin through the crystal. The spin waves can also be considered as particles (magnons) obeying Bose Einstein statistics with energy and momentum associated with them.

The theory of clusters formation (Bethe-Peierls-Weiss theory) at high temperatures around transition temperature gives a good agreement with experimental results: the small concave curvature of $1/\chi$ around Tc and thus paramagnetic temperature θ different than Tc due to the following magnetization – temperature dependence figure 1.6 [1].

$$M = M(0)(T_C - T)^{\beta} \tag{1.17}$$

β =0.33 critical exponent describing the system

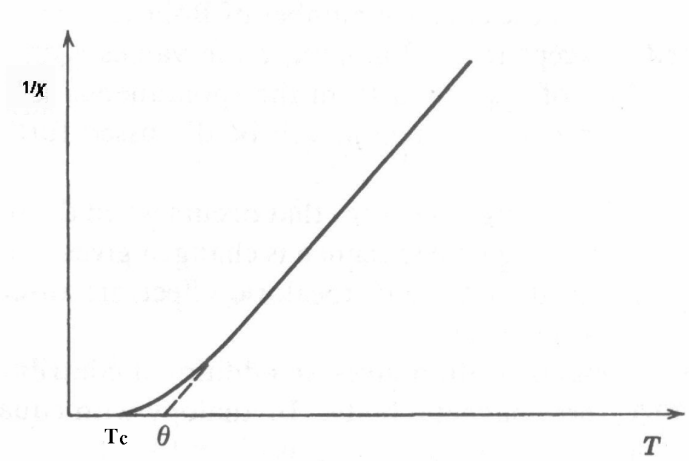

Figure 1.6 Inverse susceptibility of ferromagnetism above Curie temperature

This theory (used in alloys) considers a cluster of atoms that consists of a central atom and its Z nearest neighbors. The interaction of the neighbor atoms with each other and with the central atom is treated then by using the Heisenberg interaction.

It seems there is no theory to explain the complex behavior of ferromagnetism over the whole range of temperature [2].

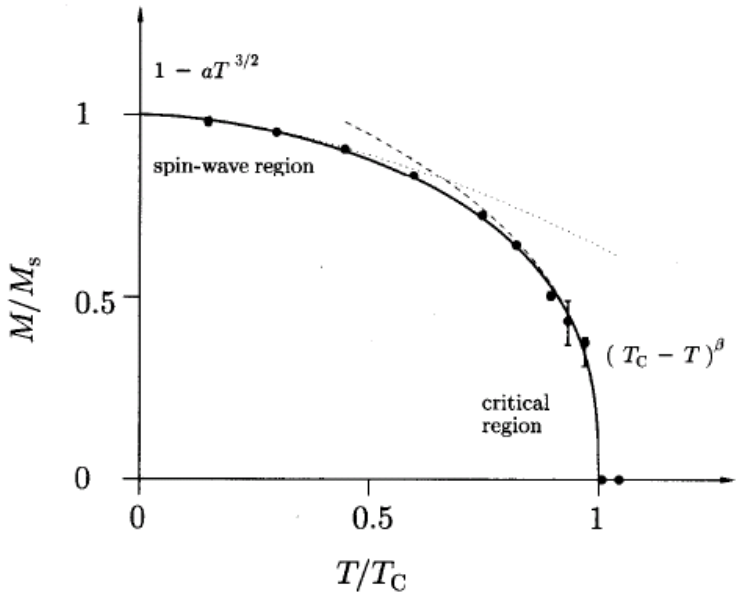

Figure 1.7 Magnetization as a function of temperature in a ferromagnetic system as a result of quantum theories

1.6.2 The Heisenberg exchange interaction

The Heisenberg exchange interaction applied to ferrimagnetism has to consider different interactions. If A and B are the atoms of two sublattices with antiferromagnetic alignment, the exchange Hamiltonian will be:

$$H_{exch} = -\sum J_{AB} S_A S_B \ , \tag{1.18}$$

J_{AB} intersublattice exchange interaction, $J_{AB}<0$ will describe the interaction in ferrimagnetic substances between two different sublattices with antiparallel orientation

J_{AA} and J_{BB} intrasublatttice exchange interaction, J_{AA}, $J_{BB}>0$ in general, will describe the interaction in ferromagnetic substances: identical magnetic moments are oriented parallel.

M_A and M_B, the magnetization of the two sublattices, will decrease differently toward zero due to different $M_A(0)$ and $M_B(0)$, and also due to different intraasublattices interaction strength. Eventually, both become zero at the Curie temperature T_C and the system becomes paramagnetic.

Different configurations will result as a function of the applied field and temperature. The larger of the two moments will align with the applied field, while the smaller will align opposite to the field direction.

The magnetization of the system

$$M(T) = \left| M_A(T) - M_B(T) \right| \tag{1.19}$$

will be zero at compensation temperature where there is also a reversal in direction.

Close to the transition temperature between paramagnetic and ferrimagnetic regions it was observed a very rapid change in $1/\chi$, figure 1.8 [1],which makes the paramagnetic temperature $\theta \neq Tc$ [1].

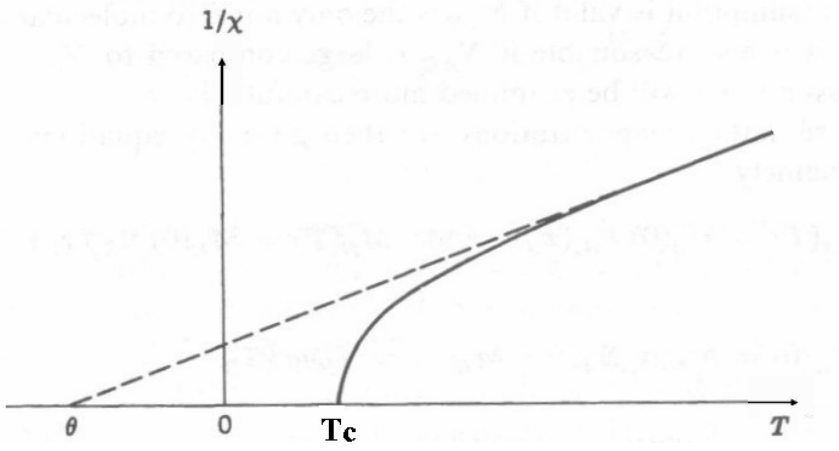

Figure 1.8 Inverse susceptibility of ferrimagnetism above Curie temperature

1.6.3 Magnetic Dipolar Interaction

Magnetic Dipolar Interaction is not quantum phenomenon in origin. It is a long range interaction between magnetic moments that can be accounted just for 0.1 K energy. As it is too small to be responsible for the ferromagnetism, dipolar energy is important in domain formation.

Domains are small regions where within each magnetization is uniform and reaches the saturation value, but the vector sum of all domains, i.e. the net magnetization of the system is zero. The zone between domains, where the magnetization changes direction is called domain wall.

Domain formation is energetically favored by the reduction of the dipolar energy in balance with the cost of creating and maintaining a domain wall. The type of domain wall can vary based on material. Some of the common domain walls are: Bloch

domain wall where the change in direction between two adjacent domains is done through a 180^0 in plane rotation, or Nell domain wall where the change in direction between two adjacent domains is through a 90^0 rotation perpendicular to the plane.

1.6.4 Hysteresis

The magnetization of ferromagnetic materials depends nonlinearly on the external field, is saturated (M_s) and has remanent magnetization (M_r) dependent on the history of the system. This dependence of M(H) is called hysteresis loop. Figure 1.9 presents magnetic moment response for a ferromagnetic sample to the applied magnetic field H. M(H) shows hysteresis as the external magnetic field changes direction.

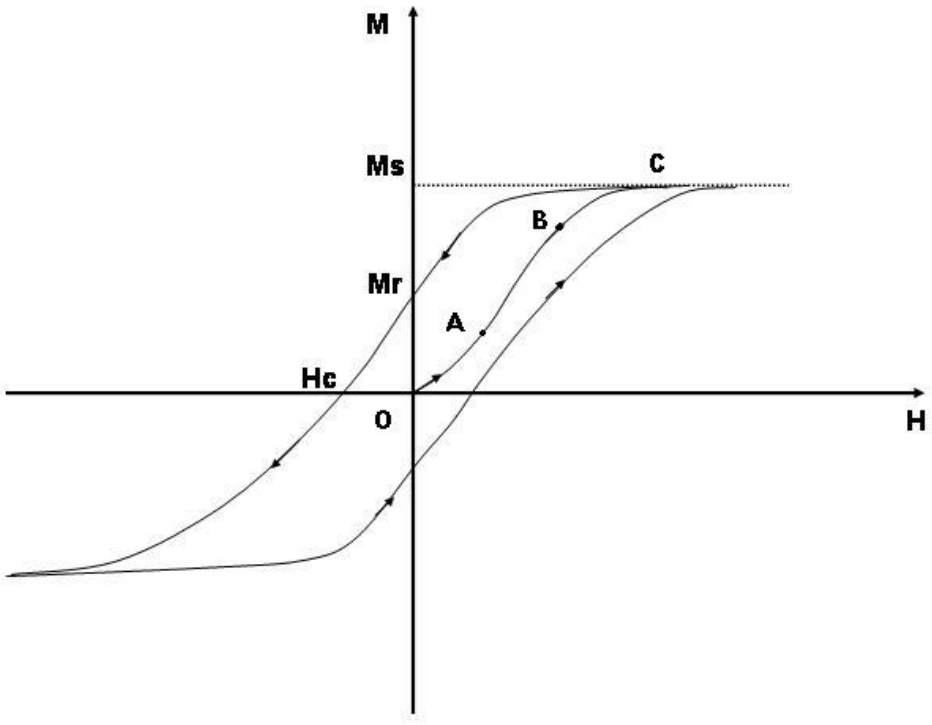

Figure 1.9 Hysteresis loop

Starting from demagnetized state M=0, H=0 ,the magnetization along the direction of applied field increases OABC curve, until reaches the saturation value, Ms. The OABC curve can be explained by domains volume change and magnetization rotation [3]. At weak applied field the volume of the domains favorably oriented with respect to the field increases at the expense of unfavorably oriented domains. This is OA region of reversible domain wall motion. Then, the irreversible domain wall motion region, AB and at strong applied field the domain magnetization rotates toward the direction of the field, the region BC.

As the field is reduced to zero, the moments will rotate first to the preferred crystallographic direction, the domain of reverse magnetization will reform, but the process will depend on the properties of the material defects, grain boundaries, surfaces and impurities. This will cause the irreversibility in ferro and ferrimagnet materials leading to the specific characteristics: remanence, and coercivity.

1.6.5 Remanent Magnetization

M_r, the remanent magnetization is the value obtained after the large field that produced the saturation magnetization of the sample is removed. The magnitude of the remanent magnetization is influenced by the saturation magnetization and the number and orientation of the easy axes. In figure 1.10 hysteresis loops are presented for different angle θ between anisotropy axis and applied field based on a Stoner Wolhfarth model for a single domain particle [3].

When the alignment of the anisotropy axis is perfect to the applied magnetic field (figure 1.10 a) θ=0, the hysteresis loop is square and Ms ≅ Mr. If the anisotropy

axis is perpendicular oriented with respect of the applied field direction (figure 1.10 c) the hysteresis loop will have an almost linear behavior portion and Mr ≅0. A case with $\theta=45^0$ is also presented (figure 1.10 b). Hc, the coercive field is the magnetic field required to reduce the remanent magnetization to zero.

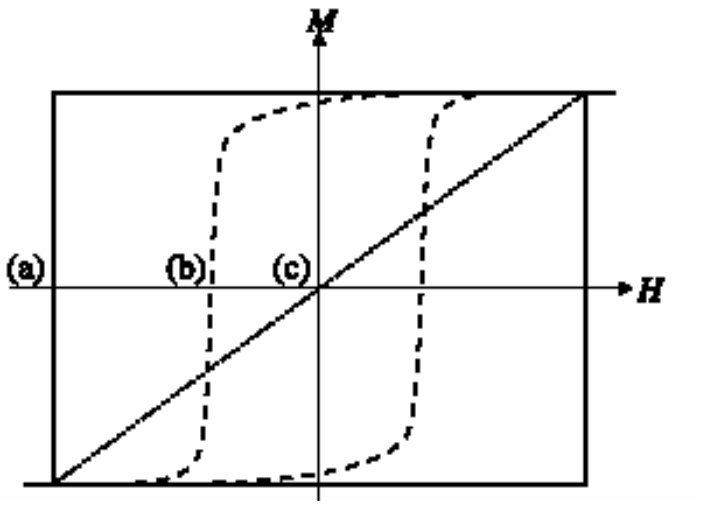

Figure 1.10 Hysteresis loops as a function of θ, the angle between anisotropy axis and applied filed a) θ=0, b) $\theta=45^0$, c) $\theta=90^0$

Materials with a low number of domains, or no domains, where a high energy is required to reverse the magnetization in a large volume will have a high coercive field. Materials with a large number of domains where the applied field will reverse magnetization through the movement of domain walls will have in general a low coercive field.

In figure 1.10 we observe how the magnitude of the Hc varies with θ. The extreme hysteresis loops presented, a) θ=0 with Hc=max and b) $\theta=90^0$ with Hc=0, suggest the importance of the orientation of the samples with strong anisotropy for the hysteresis loops measurements and magnetic properties investigations.

CHAPTER 2

MAGNETIC MULTILAYERS OF TRANSITION METALS / RARE EARTHS, ARTIFICIAL FERRIMAGNETIC STRUCTURES

Magnetic multilayer systems demonstrate interesting properties, both from fundamental, academic point of view and because of their applications in magnetic storage devices and sensors, magnetic and magneto-optical recording media.

In particular, multilayers with antiferromagnetic (AF) coupling are attractive systems to study not only for their magnetic properties, but also for interface coupling effects, or phase transitions' mechanisms. Transition Metals (TM) and Rare Earths (RE) are two distinct ferromagnetic materials with antiferromagnetic (AF) interlayer coupling. Due to this alignment TM/RE multilayers or alloys are artificial ferrimagnets.

$CoGd_5$ alloy were first studied as materials with better magnetic properties: higher magnetic moment and lower Curie temperature. Then in 1973 sputtered ferrimagnetic CoGd alloys were studied and used in applications as bubble domain materials and to thermomagnetic writing [4]. Similar sputtered ferrimagnetic alloys containing Fe, Co, Tb and Gd [5] have been studied as materials for magnetic and magneto-optical recording media. Thin films of these alloys exhibit preferred axis of magnetization perpendicular to the film plane and have compensation temperature associated with a large coercivity close to room temperature. More recently, TM/RE bilayers, multilayers and alloys have been studied [6-12] because of their ferrimagnetic

structure. Different experimental techniques investigating the total magnetic moment or element specific magnetic moment as a function of applied magnetic field and temperature, associated with structure analysis are used to reveal the multilayers' properties.

The materials used, the layering pattern, the films thicknesses and growth techniques can continuously change the structure of TM/RE magnetic multilayers. Additionally, the properties of the multilayers can be strongly tailored by the temperature and the values of external magnetic fields applied. The magnetic properties of multilayers including coercive fields, saturation magnetization, and compensation temperature can be different from those of any of the components. There are also differences between magnetic properties of bulk materials and of the thin films of the same materials leading to new phenomena that are appealing to investigate at the nanostructure level.

Some of the reasons responsible for these differences [13] are: interface effects that extend over more layers and thus influence the entire film, collective contributions due to the periodicity of the thin layers affecting fundamental excitations of the structure, and the layering pattern which with small changes can induce significant (controllable) variation in properties of the entire system.

2.1 Ferromagnetism of TM and RE

The ferromagnetism occurs in 3d Transition Metals (TM) (Fe, Co, Ni) and heavy Rare Earths (RE) (Gd, Tb, Dy) through different mechanisms.

The 3d electrons of transition metals are relatively far-from-the-core electrons and they are considered to form a band structure. The exchange field (proportional with the magnetic moment) of ferromagnetic metals is strong and causes a +spin and a -spin split band [2]. Exchange energy U, per pair of 3d electrons can be defined as the energy gained when switching from antiparallel to parallel spins. The imbalance between the numbers of spin up N↑ and spin down electrons N↓ will be seen (figure 2.1) as a shift of spin up and spin down bands relative to each other, leading to energy difference:

$$\delta E = E_F - E_2 = E_1 - E_F$$

and in the arise of non-integral magnetic moment :

$$M = (N_\downarrow - N_\uparrow)\mu_B$$

$$(N_\downarrow - N_\uparrow) = 2pn$$

where p is the fraction of electrons that moved from the spin-down to the spin-up band and

$$n = (N_\downarrow + N_\uparrow)$$

is the total number of 3d electrons per atom. E_F is energy at Fermi level.

The total change in the energy:

$$\Delta E = E_{KE} + E_{PE} = \frac{1}{2} g(E_F)(\delta E)^2 - \frac{1}{2} U(g(E_F)(\delta E))^2$$

$$\Delta E = \frac{1}{2} g(E_F)(\delta E)^2 (1 - Ug(E_F)) \tag{2.1}$$

is minimized when

$$Ug(E_F) > 1 \tag{2.2}$$

where density of states at the Fermi level, $g(E_F)$ is given by

$$g(E_F)\delta E = \frac{1}{2}(N_\uparrow - N_\downarrow) \tag{2.3}$$

Eq 2.2, proposed by Stoner, represents a criterion for the appearance of ferromagnetism [2]. It assumes that the density of states curve is unchanged even when the ferromagnetism appears. An alternative to this method is to consider electronic states of individual atoms when calculating the band structure. The result will show different shapes of density of states curves for + and – spins.

The density of states of the s and p electron bands is smaller that of the d band, which makes elements with incomplete d bands good candidates for ferromagnetism.

The 3d transition metals and their alloys have high Curie temperatures and show large spontaneous magnetization at room temperature being used in a wide range of practical applications. $2.22\mu_B$, $1.72\mu_B$, $0.61\ \mu_B$, are experimental values for magnetic moments of Fe, Co, and Ni respectively [14] and their Curie temperatures are: 1040 K for Fe, 1395K for Co and 629K for Ni.

The Co80Ni20 alloy is ferromagnetic below T_C=1406K and has a magnetic moment of $1.53\ \mu_B$. Co90Fe10 alloy is ferromagnetic below T_C =1308 K and has a magnetic moment of $2.66\ \mu_B$[15] .

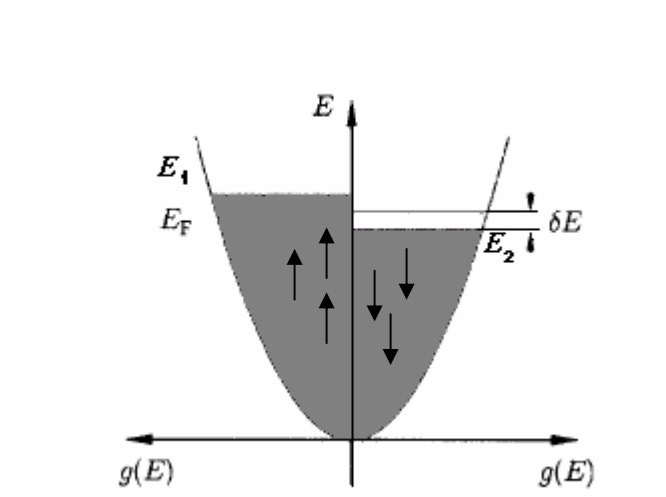

Figure 2.1 Density of states showing spontaneous splitting of energy bands

In rare earth elements the carriers of magnetism are the 4f electrons with wave functions well localized. The outer shells electrons ($5d^1$ and $6s^2$) provide a medium of exchange interaction which produces the ordered arrangement of 4f electrons.

The magnetic order for RE occurs below room temperature and they can not be used in applications as pure elements.

Gd (Gadolinium) is ferromagnetic and has a bulk Curie temperature, $T_C = 293$ K. The orbital angular momentum L=0, and the total angular momentum, J=L+S, is equal to the spin angular momentum S. The magnetocrystalline anisotropy of Gd is small and hence is easily magnetized. The theoretical magnetic moment is 7 μ_B and the experimental value, depending very much on the purity, may exceed 7 μ_B .

Tb (Terbium) has S=3, L=3 and J=6. The experimental value of magnetic moment at 0K is 9.34 μ_B, larger than the theoretical value of 9 μ_B. Ferromagnetism of Tb disappears above T_C = 215K, but hellimagnetism is observed up to 230K. In a

helimagnetic structure, like hcp (hexagonal closed packed) Tb, spins in a layered crystal are aligned within each c-plane, but the spin direction varies from plane to plane such that the tips of the spin vectors along the a line parallel to the c-axis describe a spiral or a helix [16].

2.2 Artificial Ferrimagnetic Structure

For multilayers and alloys of TM/ heavy RE (Gd, Tb, Dy, Ho) the net magnetic moment is the difference between the TM and the RE magnetic moment due to their antiparallel coupling . Unlike the typical antiferromagnetism, here the magnetizations of the two components are not equal; the system has a total magnetic moment that will be zero at a certain temperature, T_{comp}, the compensation temperature.

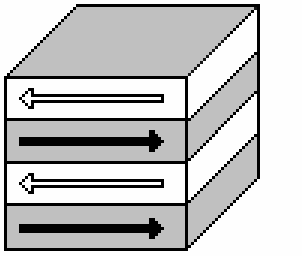

Figure 2.2 Model of TM /RE multilayer with magnetizations lying in the plane and antiparallel to each other

In the case of the TM / light RE (Ce to Eu) multilayers and alloys a ferromagnetic behavior was observed. The net magnetic moment of these systems is the sum between the TM and the RE magnetic moment due to their parallel coupling.

The exchange interaction between the rare earth spins and the transition metal moment combined with Hund's rule is presented the figure 2.3. The heavy rare earths

have a more than half-filled 4f shell and the spin S antiparallel with TM moment. Following Hund's rules the total electronic angular momentum, J=L+S, so J is antiparallel with TM moment, figure 2.3a. The light rare earths have S also antiparallel with the TM moment, however because 4f shell is less than half-filled, the value of J in the states of lowest energy is J=L – S. J is opposite to S and therefore in the same direction with TM atomic moment, figure2.3b.

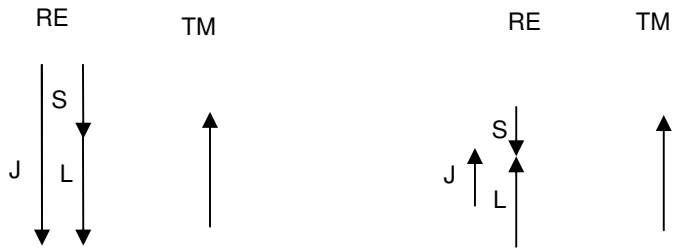

Figure 2.3 a) Heavy RE and TM exchange coupling, b) Light RE and TM exchange coupling

2.3 Magnetic States of TM/RE Multilayers

The total energy E for the antiferromagnetically coupled layers can be expressed in terms of Zeeman energy of the individual components, exchange coupling term dependent on the relative orientation of the two components moments, and the anisotropy energy .

2.3.1 Zeeman Energy

Zeeman energy is the magnetic potential energy of a system in a magnetic field:

$$E = -MH\cos\theta \tag{2.4}$$

θ is the angle between magnetic moment, and M the applied magnetic field H. Zeeman energy is minimized for a parallel alignment between applied field and magnetic moment.

2.3.2 Exchange Coupling Energy

Exchange energy is the interaction between spins in the same layer (the main interaction responsible for ferromagnetism) and also between the moment of adjacent layers or sublattices.

$$E = -2J_{ij} SiSj \cos \alpha_{ij} \tag{2.5}$$

A positive J_{ij} indicates ferromagnetic coupling and a negative J_{ij} indicates antiferromagnetic coupling.

2.3.3 Anisotropy Energy

In most of the magnetic ordered substances and systems the magnetic properties depend on the direction in which they are measured. This property, called magnetic anisotropy has different origins including: crystal anisotropy, shape anisotropy and stress anisotropy. Opposite to these intrinsic types of anisotropy, the induced magnetic anisotropy is the result of different methods of treatment like: annealing or plastic deformation. A very special case of induced anisotropy is the exchange bias or exchange anisotropy.

2.3.4 Magnetocrystalline Anisotropy

The magnetocrystalline anisotropy is the result of the spin-orbit interaction and the partial quenching of the orbital moment by the crystalline field. The magnetization

is not completely free to rotate but it is linked to distinct directions. The preferred magnetization axes or the easy axes are in most cases the same with the crystallographic directions.

The magnetocrystalline or anisotropy energy is defined as the work required to make the magnetization lie along a certain direction compared to an easy direction [1]. The magnetocrystalline energy is expressed as power series of cosθ, where θ is the angle between direction of magnetization and the principal axes of the crystal.

For a crystal with a single easy axis, referred as uniaxial crystal, the crystal anisotropy is given by:

$$E = K_1 \sin^2 \theta + K_2 \sin^4 \theta \tag{2.6}$$

K_1 and K_2 - anisotropy coefficients

The anisotropy coefficients (K_1 and K_2) are function of the crystal structure and are also temperature dependent. For Co, a hexagonal structure, the easy direction is the hexagonal c-axis at room temperature (figure 2.4). The anisotropy coefficients are K_1=5 10^5 J/m^3, K_2=1 10^6 J/m^3.

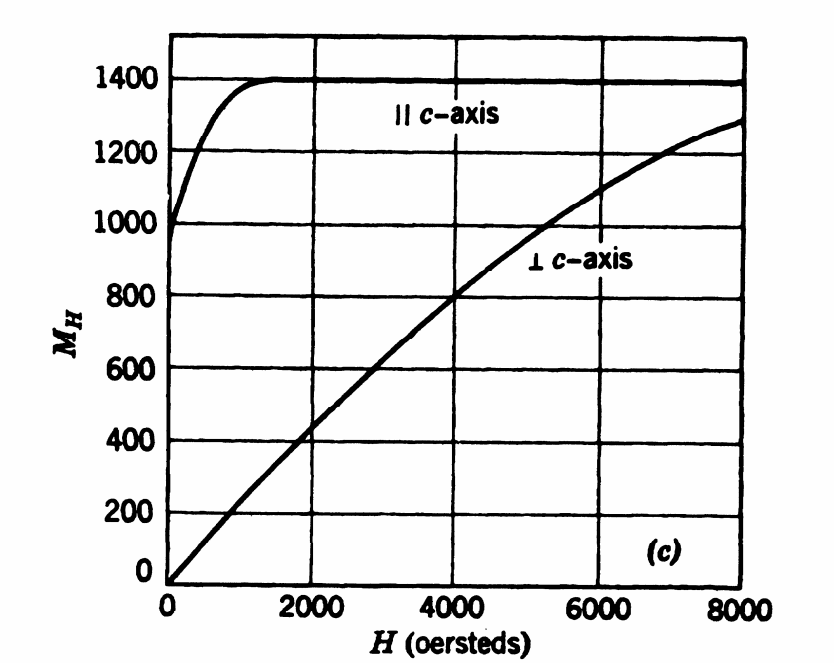

Figure 2.4 Magnetization curve of a single crystal of Co
for applied field along easy axis and hard axis

For a system with uniaxial symmetry, the competition between the anisotropy energy and the interaction energy with an external field E=-HM cosθ will give the coercive field: (Ms is the saturation magnetization)

$$H_C = \frac{2K_1}{M_s} \tag{2.7}$$

The magnetic properties of thin films compared with bulk material are different. The interface or surface anisotropy was predicted by Neel to results from the lowered symmetry at the surface or interface. The anisotropy constant can be phenomenological separated in two contributions: interface anisotropy K_s and volume anisotropy K_v [2].

$$K = \frac{2K_s}{t} + K_v \tag{2.8}$$

t is the layer thickness and the factor 2 arises from the two interfaces of the layer. As t decreases, the contribution of the surface term becomes important in thin films and multilayers.

Figure 2.5 shows a Co/Pd multilayer magnetic anisotropy energy MAE, dependence with the layer thickness, t [17]. A positive K describes a preferred direction of magnetization perpendicular to the thin film plane and the negative K indicates a negative dominant K_v favoring in plane magnetization orientation.

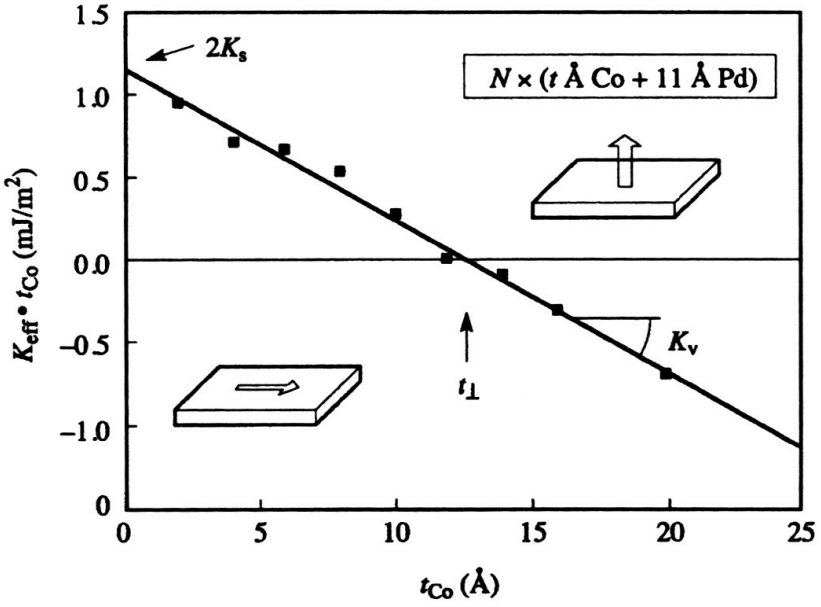

Figure 2.5 Magnetic anisotropy energy dependence with the layer thickness for Co/Pd multilayer

For polycrystalline materials, the anisotropy due to randomly orientated grains will average out and the system as a whole will have no crystal anisotropy.

2.3.5 Shape anisotropy

The energy associated with demagnetizing field of a sample is called magnetostatic energy.

$$H_d = -N_d M \tag{2.9}$$

This type of energy is due to the magnetic free poles that appear on the outside surface of a magnetic material. If the sample does not have a spherical shape, the magnetizing field along the longer axis is smaller than along shorter axis. N_d is the demagnetizing coefficient and is determined by the magnet shape.

$$E = \frac{1}{2} N_d M^2 \tag{2.10}$$

2.3.6 Strain anisotropy

If the lattice is changed by strain the distance between magnetic moments and energy interaction is altered and thus a magneto-elastic energy dependent on the angle between magnetization and stress direction should be considered. In thin films and multilayers strain can be produced by the growth conditions such as layers lattice mismatch.

The equilibrium states of the TM/RE multilayers will be presented using a theoretical model developed by R.E Camley [13, 18, 19], confirmed by experimental data for Fe/Gd multilayers [20-24].The spins within a single layer are considered parallel and equivalent. In addition, the spins lie in a plane parallel to the interfaces.

$$E = -H(m_1 t_1 \cos\theta_1 + m_2 t_2 \cos\theta_2) - J_{12} m_1 m_2 \cos(\theta_1 - \theta_2) - m_1 t_1 H_{1a} \cos^2\theta_1 - m_2 t_2 H_{2a} \cos^2\theta_2 \tag{2.11}$$

To have the stable magnetic state we have to impose the following conditions:

$$\frac{\partial E}{\partial \theta_1} = \frac{\partial E}{\partial \theta_2} = 0 \quad , \quad \frac{\partial E^2}{\partial \theta_1^{\,2}} > 0 \quad , \quad \frac{\partial E^2}{\partial \theta_2^{\,2}} > 0 \quad , \quad \left(\frac{\partial E^2}{\partial \theta_1^{\,2}}\right)\left(\frac{\partial E^2}{\partial \theta_2^{\,2}}\right) > \left(\frac{\partial E^2}{\partial \theta_1 \partial \theta_2}\right)^2 \tag{2.12}$$

H_{1a} is the anisotropy field of TM film assumed to be in the same direction as the applied field

J_{12} is the exchange coupling constant, negative for the antiferromagnetic coupling

m_1 is the magnetizations of TM,

H is the applied magnetic field.

t_1 is the TM film thickness

θ_1 is the angle between the m_1 and applied magnetic field and the same notations with the index 2 are used for the RE characteristics.

Neglecting the anisotropy effect, the exchange term contribution dominates over the Zeeman term at low fields. The magnetic moments are antiparallel to each other and, according to which moment is larger, the system will be in the RE aligned state at low, temperature (figure 2.5a) or in the TM aligned state at high temperature (figure 2.5b).

At higher fields, the Zeeman energy contribution will be comparable with the exchange coupling term and consequently will lead to a so-called spin-flop state (figure 2.5.c).The net moments are no more antiparallel, but twisted with respect of the applied field direction.

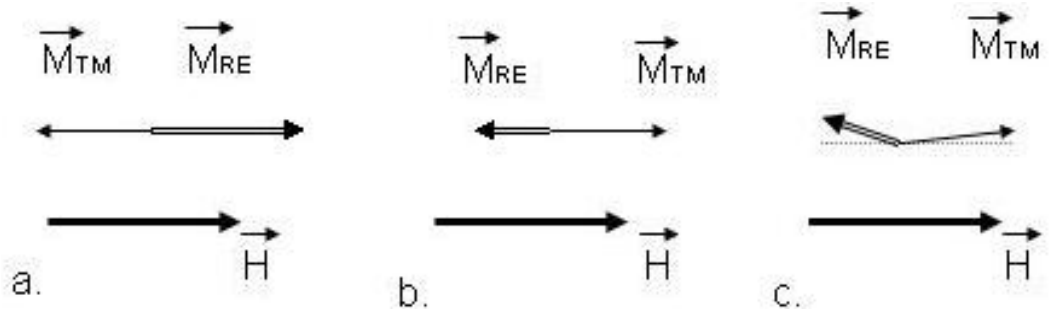

Figure 2.6 Model of three main phases in a TM/RE multilayer a) low temperature RE aligned phase, b) high temperature TM aligned phase, c) TM/RE twisted phase

CHAPTER 3

THERMODYNAMICS OF MAGNETIC PHASE TRANSITIONS

There are many systems in nature which have different microscopic order or symmetry states. The change in a system's behavior, independent of its symmetry type, driven by a parameter like force or temperature, is happening at a critical temperature. The transition between states is not gradual, but sharp, and is called phase transition. Some examples are: liquid to crystal, ferromagnetism to paramagnetism or normal metal to superconductor. The symmetry-breaking transitions are very common. Below a critical temperature, while cooling a liquid, the system's structure changes to that of a solid, with the atoms symmetrically arranged, but with the translational degree of freedom lost. The situation is similar for a ferromagnet: while cooling the system below Curie temperature, the transition is from the paramagnetic to ferromagnetic state. Above T_C, all directions are equivalent and magnetic moments can point in any direction, while below T_C the higher rotational symmetry is reduced as all the spins are pointing in the same direction. Not all the phase transitions involve a change in symmetry. The lowest energy state, the eigen state, gives the stable configuration of a system. The existence of a superposition of energy eingestates which are called metastable states is also possible. If the system is in a metastable state then the phase transition is the switch between one metastable state and the other metastable state.

When the transition is of first order, the property being measured near the transition temperature displays a sudden change in magnitude, thermal hysteresis and an associated latent heat, where first order derivative of Gibbs free energy (G) with temperature, the entropy (S), is discontinuous. The hysteresis effect, depending on the way the region of interest is investigated can be explained by the phases' coexistence in the studied system. The phase transitions in a magnetic system can be observed by measuring magnetization, magnetic susceptibility, and heat capacity, resistivity, while cycling the temperature or magnetic field. For a second order phase transition, the second derivative of G, the heat capacity (C), is discontinuous [25, 26].

The phase transitions in magnetic materials are continuously explored in connection with magnetocaloric effect, MCE, and alternative application to magnetic refrigeration. The MCE, discovered in iron by Warburg [27], is the heating or cooling of a magnetic material in a varying magnetic field. Magnetic refrigeration based on MCE was demonstrated in 1905 by Langevin [28] as a reversible temperature change caused by a paramagnet magnetization change. Later, Debye[29] and independently Giauque[30] proposed a cycle through which temperatures below 1K were obtained in paramagnetic salts. The reversible cooling process has two stages. The isothermal magnetization of a material decreases the entropy (ΔS_m vertical arrow in figure 3.1) while the adiabatically demagnetization leads to a temperature change (ΔT_{ad} - horizontal arrow in figure 3.1) [1, 31].

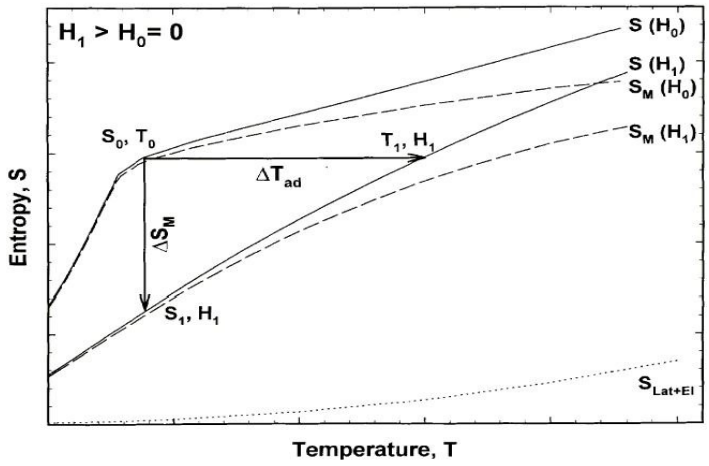

Figure 3.1 S-T diagram illustrating MCE

Interest for an alternate, efficient, nonpolluting cooling technology shifted the magnetic refrigeration research from low temperature to intermediate and room temperatures. All the magnetic materials show the magnetic caloric effect, but a good refrigerant material should have a high density of magnetic moments, and a strong temperature and/or field dependence of the magnetization. The studies on phase transitions in magnetic materials have mainly been focused on the order/disorder transitions such as ferromagnetic to paramagnetic. The entropy of a magnetic solid S(T,H) has magnetic (S_M), lattice, (S_L), and, electronic contributions (S_E). From these components just the magnetic contribution is field dependent.

$$S(T,H) = S_M(T,H) + S_L(T) + S_E(T)$$

Giant magnetocaloric effect is obtained by combining several contributions to the total entropy change. Coupling between electronic and magnetic transitions, or the

coupling between magnetic phase transition and structural phase transition are examples [32-37] of merged transitions where large entropy changes (ΔS) were achieved.

Basic thermodynamics review: S-entropy, T-temperature, V-volume, P-pressure, N-number of component in the system, μ-chemical potential.

(S, T), (V,-P), (M, H), (N, μ) fundamental variables

U-internal energy

$$dU = TdS - PdV + HdM + \mu dN$$

G-Gibbs' free energy

$$G = U - TS - HM$$

$$dG = -SdT - PdV - MdH + \mu dN$$

For magneto-caloric processes: N=const. and V=const.

$$dU = dQ + HdM = TdS + HdM$$

$TdS = dQ$ for a reversible process

E-Enthalpy

$$E = U - HM$$

$$dE = dQ - MdH = TdS - MdH$$

$$\left(\frac{\partial S(T,H)}{\partial H}\right)_T = \left(\frac{\partial M(T,H)}{\partial T}\right)_H$$ Maxwell relation

$$\Delta S_m = \int_{Hi}^{Hf} \left(\frac{\partial M(T,H)}{\partial T}\right)_H dH \qquad (3.1)$$

Following the thermodynamic relations:

$$dS(T,H) = \left(\frac{\partial S}{\partial T}\right)_H dT + \left(\frac{\partial S}{\partial H}\right)_T dH$$

$C_H = T\left(\frac{\partial S}{\partial T}\right)_H$ is the heat capacity at constant field.

Using eq.3.1 the infinitesimal adiabatic temperature change is given by:

$$(dT)_{ad} = -\left(\frac{T}{C_H}\right)_H \left(\frac{\partial M}{\partial T}\right)_H dH$$

Integrating, we get the temperature change:

$$\Delta T_{ad}(T,\Delta H) = -\int_{Hi}^{Hf}\left(\frac{T}{C_H}\right)_H \left(\frac{\partial M(T,H)}{\partial T}\right)_H dH \qquad (3.2)$$

The $\left(\frac{\partial M}{\partial T}\right)_H$ sign indicates whether the sample will be cooled or heated by magnetization process, while the size of the effect is determined by the field dependence of M and C_H .Considering a magnetization process, $\Delta H > 0$, and $\left(\frac{\partial M}{\partial T}\right)_H > 0$ $\Delta S_m(T,\Delta H)$ should be positive and $\Delta T_{ad}(T,\Delta H)$ should be negative. This represents the inverse magnetocaloric effect.

The first reports about cooling an antiferromagnet by adiabatic magnetization process were from 1961[38] based on theoretical calculations. Using the spin wave theory, Joenk [39] in 1963 investigated the magnetic field dependence of the thermodynamic properties of an antiferromagnet. A possible use of adiabatic magnetization on an antiferromagnet, other than the –coling per se- was suggested to be a sink for the heat generated when a paramagnetic is magnetized prior to cooling by

adiabatic magnetization. The inverse magnetocaloric effect, as $\Delta S > 0$ was experimentally observed when the magnetic field is adiabatically applied in NiMnSn and similar compounds [40] known as ferromagnetic shape memory alloy, due to martensitic transformations [41,42]. For one of this compounds a combined $\Delta S > 0$ and $\Delta S < 0$ was measured, suggesting that both the magnetizing demagnetizing processes can be employed for cooling [43].

Changes in the properties of materials due to magnetization or demagnetization of the sample were evaluated based on thermodynamics and statistics method through experimental measurements. Direct temperature measurements can be used to determine initial T_i and final temperature, T_f of a sample in magnetic field change $\Delta H = H_f - H_i$ under adiabatic conditions. Indirect methods of measuring heat capacity based on calorimeters can be used to determine both ΔS and ΔT. The indirect methods eliminate the critical adiabatic condition for the measurements and the errors of the temperature sensors in contact with the sample. But unfortunately, the calorimetric methods can not be used for samples with reduced size and mass. Most of the calorimeters mask the signals induced by nanostructures like thin films or nanoparticles phase transitions as they are mainly designed for bulk materials analysis.

Another indirect technique to determine the magnetic entropy change widely used and also suitable for nanostructures is based on magnetization measurements. M(H) curves are measured at different temperatures in magnetizing or demagnetizing process of the sample. For this method the accuracy of the result, depends on the accuracy of temperature, magnetic field and magnetic moment measurements.

Numerical integration is involved (eq.3.1) and the exact differentials dM, dT, dH are replaced by the measured ΔM, ΔT, ΔH.

The entropy can be calculated theoretically directly from the partition function, Z, and the average value of the magnetic energy $\langle \varepsilon \rangle$.

$$\Delta S(T) = S(T,H) - S(T,0)$$

where the entropy is given by:

$$S(T,H) = \frac{< \epsilon >}{T} + k_B \ln(Z)$$

TM aligned phase and RE aligned phase magnetic states presented in Chapter 2 for ferrimagnetic TM/RE multilayers are metastable states in certain temperature regions and in low applied magnetic fields. The magnetic entropy change associated with first order phase transitions is for the first time measured for these multilayers and the results are presented in Chapter 6.

CHAPTER 4

EXPERIMENTAL METHODS

The samples investigated are multilayers of CoNi/Gd, CoFe/Gd, NiFe/Gd, Ni/Gd, and Co/Tb obtained through sputtering using a DC magnetron deposition system. The magnetic properties were studied by using a SQUID magnetometer. Crystal and layer structure analysis was done using XRD in thin film configuration and surface quality of thin film was analyzed using an AFM. The general theory of these procedures is described subsequently.

4.1 The DC Magnetron Sputtering System

The sputtering system with the main components is presented in figure 4.1.

The system has tree guns, symmetrically positioned inside the main chamber at a distance of 17 cm from the substrate and tilted at 13 degrees with respect to the substrate normal. Inside of the sputtering gun there is a 1.5" diameter sputtering target, which is the material to be sputtered. In a parallel plate symmetry, with the target as cathode and the substrate as anode, an Ar discharge is establish at a pressure of 10^{-3} torr with a DC voltage of kV. High energy Ar^{+} ions hit the target material and transfer their energy dislocating material which then condenses onto substrate forming thin layer.

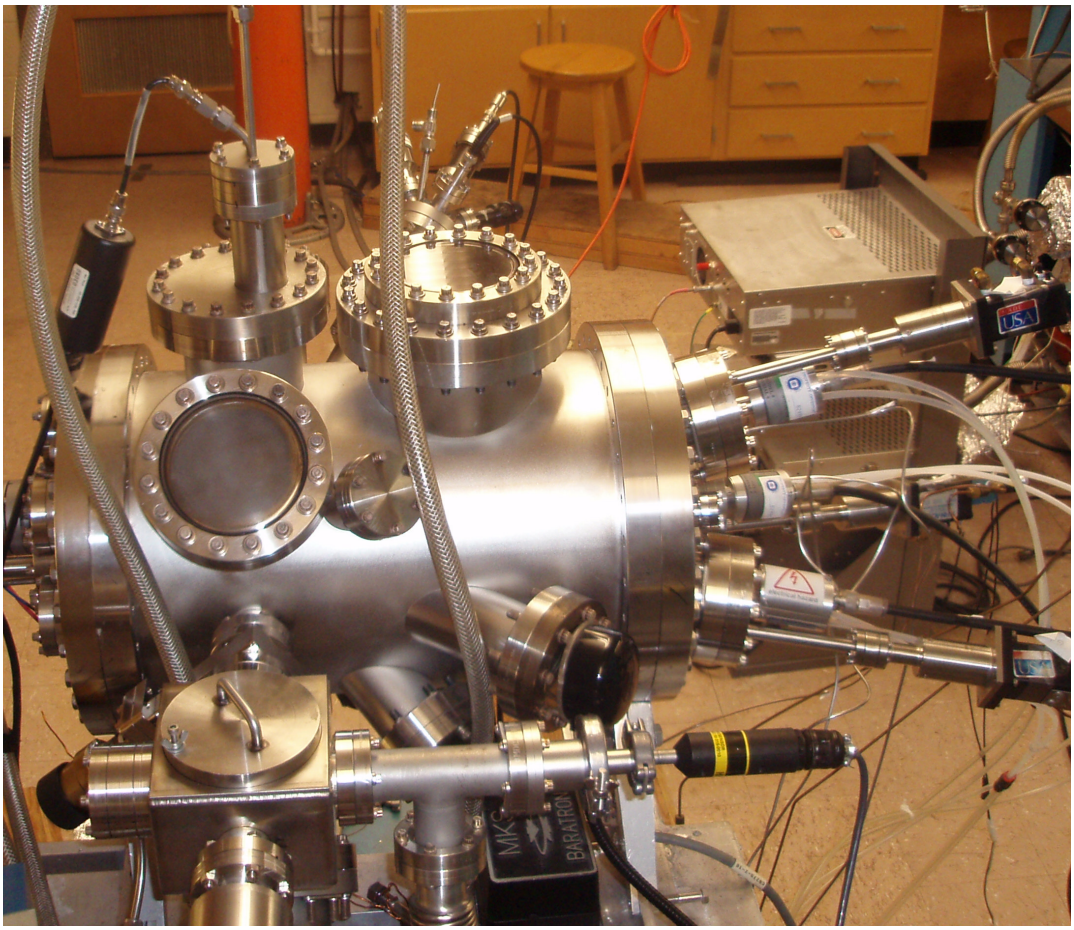

Figure 4.1 DC Magnetron Sputtering System

The target is placed on the magnets of a planar magnetron with a special geometry of electric and magnetic fields such that secondary electron motion is constrained near the target. This secondary electron trapping establishes denser plasma in the target region, equivalent to an increased bombardment of the target and leading to higher target sputtering and deposition rates on the substrate. The higher deposition

rates lead to a flat layer with few grain boundaries or pinholes on μm scale, but favors interdiffusion at the interfaces (nm scale).

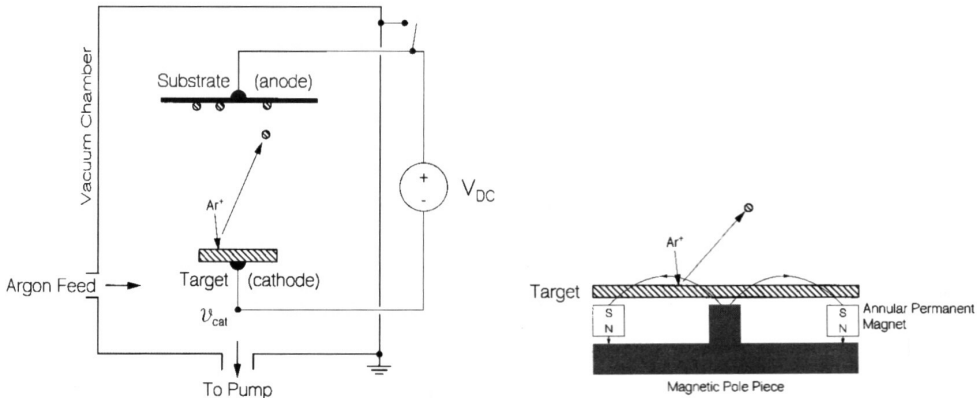

a) b)

Figure 4.2 a) DC sputtering with a parallel plate discharge, b) the magnetron

Deposition of the film thickness uniformity can be changed with the distance between the target and substrate, target to substrate diameter ratio and emission profile of the sputtered atoms. The emission profile is a cosine distribution, but can deviate from it depending on the target structure and the sputtering ion energy [44].

4.2 The SQUID

A SQUID is a Superconducting QUantum Interference Device. The system makes extremely sensitive measurements of magnetic moment. It is actually used as a very sensitive magnetic flux – voltage converter. The SQUID is integrated into a Quantum Design Magnetic Property Measurement System (MPMS).

The functioning of a SQUID is based on superconductivity, Josephson tunneling through a weak link and flux quantization into a superconducting ring.

4.2.1 Superconductivity

Superconductivity is a quantum phenomenon observed when certain substances are cooled below a critical temperature, T_c, where the electrical resistance becomes very small and the material becomes a perfect diamagnetic material. For most metals T_c is of the order of a few Kelvin.

In a superconductor two electrons near the Fermi level could couple to form an effective new "particle". This particle is called Cooper pair, in which each electron has the same energy, momentum and invariant phase relationship. The pair behaves as a separate entity and is in a very coherent state. The mechanism is explained [14] by a virtual phonon exchange produced due to the lattice dynamics. The dispersion rate of the `phonon wave` is very slow and consequently the attraction can be felt over distances of 10^{-6}m (200 times the interatomic distance).

4.2.2 Flux quantization

An important phenomenon in the development of SQUIDs is the flux quantization. This process happens in a superconducting ring with a magnetic field oriented perpendicular to the ring. Due to the quantum restrictions, the Cooper pair wave function integrated over a closed loop only differs in phase factors of $2n\pi$, where n is any integer (including zero). As a direct consequence, the magnetic flux will be quantified according to:

$$\Phi = n\Phi_0 \tag{4.1}$$

where $\Phi_0 = \frac{h}{2e}$ =2.07 10^{-15}Wb is the quantum flux and n is an integer.

In a low magnetic field, flux quantization is maintained by a circulating current in the ring [14].

4.2.3 Josephson junction

The Josephson junction is composed of two superconductors separated by a thin insulating layer which is also referred to as a "weak link" [45]. This small enough junction between the superconductors allows pairs of electrons to tunnel across with zero resistance. The current is dependent only on the phase difference between wave function of the Cooper pairs in the two regions:

$$J = J_0 \sin \delta \tag{4.2}$$

In addition, an applied voltage across the Josephson junction causes the "supercurrent" to alternate with a frequency equal to $\frac{2eV}{h}$.

4.2.4 RF – SQUID

There are basically two types of squid: with one Josephson junction – the RF-SQUID, and with two junctions – the DC-SQUID. The MPMS-Quantum Design magnetometer has a RF-SQUID, as described below.

The superconducting current (I_S) in a single junction ring placed in a magnetic field can be shown to have the form [46, 47]:

$$I_S = I_C [\sin 2\pi(1 - \frac{\Phi_i}{\Phi_o})], \tag{4.3}$$

Where I_C is the critical current, Φ_0 is a flux quantum and Φ_i is the incident flux on the ring. The incident flux on the ring, Φ_i is the sum of the external applied flux to be measured Φ_X, and the flux from the coupling to the resonant circuit formed by the ring: LI_s. The equation (4.3) is a non-linear due to the appearance of I_s in the term

$$\Phi_i = \Phi_x + LI_S . \tag{4.4}$$

Therefore, there is no general analytic solution for either I_s or Φ_i. However, it can be shown that the equation has a unique solution for the parameter $\frac{2\pi LI_C}{\Phi_o} < 1$ and that if there is a transition of state, a voltage pulse appears across the junction as the internal flux changes by $n\Phi_0$, with n an integer. It is this transition that will absorb the energy $\frac{\Phi_0^{\,2}}{2L}$ from an external LC circuit (tank) that feeds the superconducting ring with a convenient resonant radio wave and it can be detected by an external electronic circuit. Thus the SQUID can detect changes in magnetic field as small as the quantum change of flux Φ_0.

4.3 MPMS

The system used to collect experimental data was a Quantum Design Magnetic Property Measurement System (MPMS) XL SQUID magnetometer. The MPMS main parts are: the SQUID, the magnetometer, the probe assembly, the dewar and the electronic control system.

Even though a SQUID is capable of detecting changes in magnetic flux without any extra equipment, this is not practical because the superconducting material present within the SQUID would effectively screen out the field that is being measured and, to block out any influences from external fields, the SQUID must be operated within a magnetic shield. Therefore, the measurements are obtained by linking the SQUID through a flux transformer to a detecting magnetometer as shown schematically in figure 4.2.

The MPMS magnetometer is configured to detect the magnetic moment of a sample from which the magnetization and susceptibility can be determined. The MPMS can measure magnetic moment within a range of 10^{-8} emu to 2 emu. The sample is placed in a uniform magnetic field and moved slowly in a 3 cm length through a set of superconducting detection coils. Using a second order gradiometer coil arrangement, the detecting system is insensitive to the uniform field applied. Thus, only the magnetic moment of the sample induces the electric current in the detection coils.

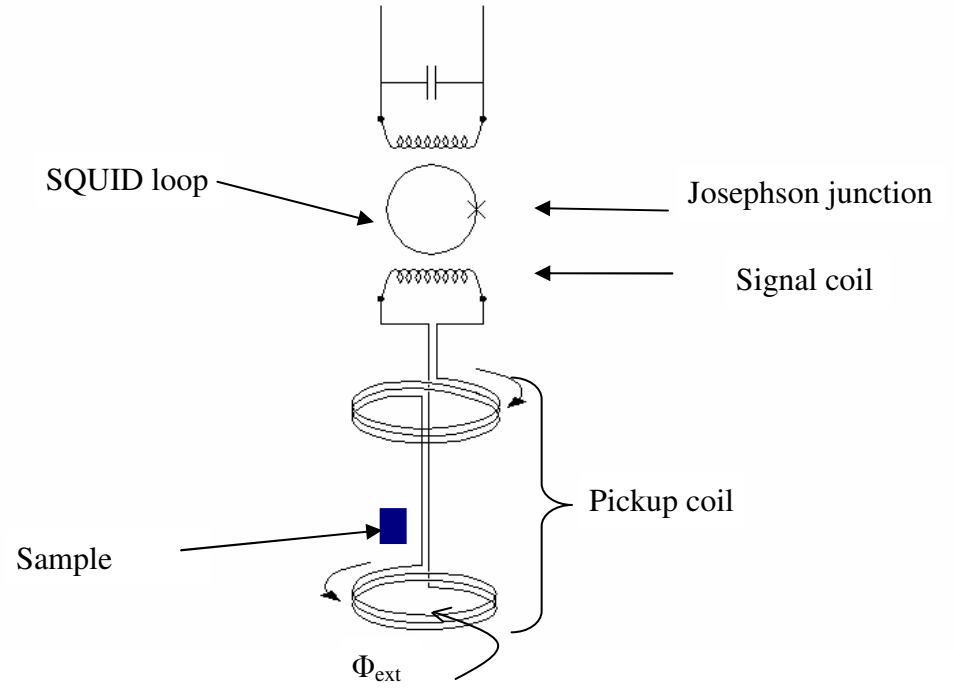

Figure 4.3 Schematic representation of RF-SQUID

The detection coils and the signal coil form a closed superconducting loop, so any change of magnetic flux in the detection coils produces a change in the signal circuit. This will be applied to the SQUID and detected trough the electronics associated with the RF circuit coupled with the SQUID.

All of these circuits are superconducting and therefore need to be cooled. The temperature control system provides control over the sample temperature in the range of 4.2 K to 400 K and over the superconducting state, by using the liquid helium. Taking advantage of the integrated superconductivity circuits the static field of magnetometer and the SQUID shield are also superconductors. Thus, the superconducting magnet of the magnetometer, wound in a solenoidal configuration, is charged up to a specific

current, and then it is operated during the measurements in persistent mode without benefit of an external current source or power supply, providing magnetic fields up to 7T. The magnetic shield surrounding the SQUID is also a superconducting one, providing a constant and very stable field inside the shield rather than a small field. The stability aspect is very important considering the magnetic flux produced by a typical small sample is of the order of 1/1000 of a flux quantum (Φ_0) [48, 49].

4.4 General procedure

The magnetic properties of the multilayers such as compensation temperature, coercivity, and saturation moment will be studied in relation with the materials used and layer thicknesses.

The sample is obtained by deposition on a glass substrate under controlled conditions. The Corning 7059 glass substrate is mechanically cleaned by blowing the dust with Nitrogen gas, brushing the substrate with a nylon brush using a solution of deionized water and Micron cleaner (International product Corporation), rinsing it with deionized water and drying it with Nitrogen gas.

TM and RE layers were deposited consecutively at room temperature, on the glass substrate, starting with Gd or Tb at 3 mTorr in ultra high purity Ar gas. To prevent contamination an Ultra High Vacuum was achieved in the deposition chamber (10^{-9}torr base pressure) and to prevent sample from oxidation a 20nm of Ag was sputtered as buffer and cap layers in all samples. The sample thickness was controlled “in situ” with a quartz monitor calibrated by a stylus profilometer.

It was shown, using structural analysis techniques and magnetic measurements, that the growth order influences interface alloying and magnetic properties of Fe/Tb [50] and Co/Gd multilayers and alloys [51-54]. However, the main characteristic of the antiparallel coupling between TM and heavy RE is maintained.

In the CoNi/Gd case the experimental results [55-57] show an increase in the coercivity when CoNi was deposited on Gd layer, compared with the reverse order. Due to the strong diffusion of Co and Ni into Gd a ferrimagnetic alloy of 20-30 Å is developed at the interface.

Interdifussion effects have been investigated in NiFe/Gd/NiFe trilayers and NiFe/Gd multilayers [58-61].A weak coupling of the trilayers was observed due to Ni difussion into Gd. Fe concentration into Gd layer was insignificant as was previously observed for Fe/Gd multilayers.

The Ag and the glass substrate have a diamagnetic contribution into the total magnetic of the sample, adding a linear magnetization with the applied field, independent of temperature.

The measurement of the background was performed in order to verify its contribution to the total magnetization (figure 4.4). It was confirmed that the diamagnetic effect can be observed and may be significant at high fields.

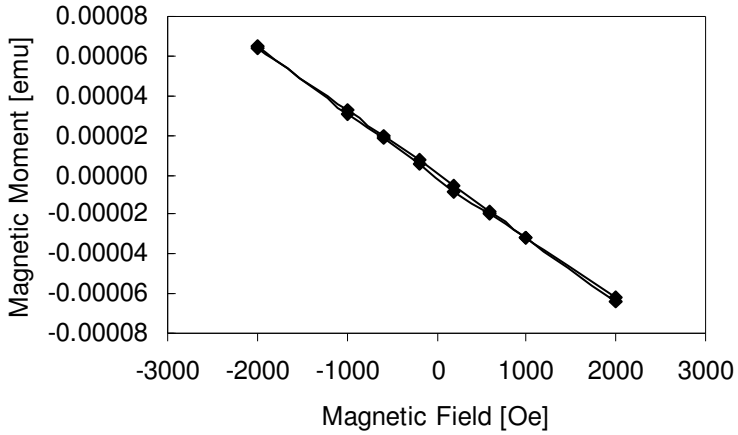

Figure 4.4 Diamagnetic contributions of the glass and Ag layers as background to magnetic measurements

Figure 4.5 presents the temperature dependence of magnetization for various transition metals and alloys (20nm), Gadolinium (50nm) and Terbium (20nm) thin films. It can be see that the TM magnetization is almost constant, while the RE (Gd) and (Tb) magnetization decreases rapidly when the temperature is varied from 10 to 300 K. The Curie temperature for Gd thin film is around 290K and for Tb is around 200K.

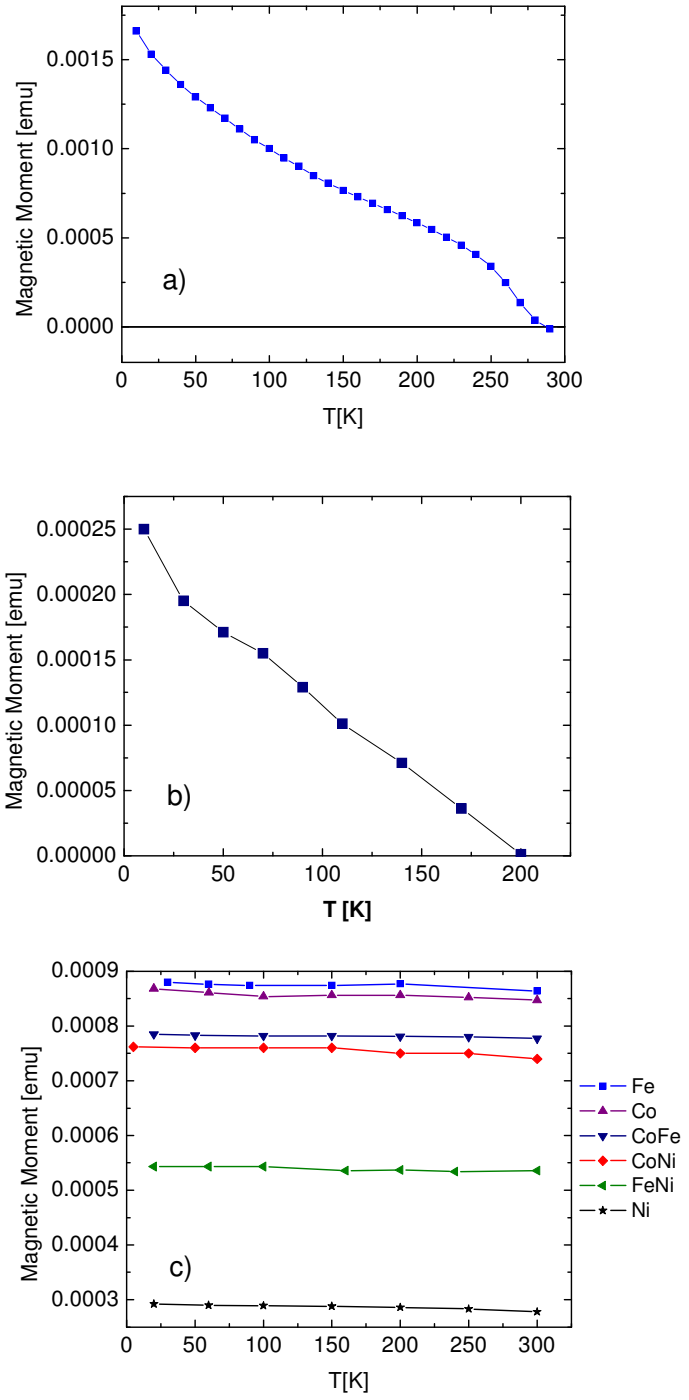

Figure 4.5 Magnetization as a function of temperature for a) 50nm Gd thin films, b) 20nm Tb thin film, c) 20nm different TM and alloys thin films

CHAPTER 5

FERRIMAGNETIC SYTEMS AND THERMAL HYSTERESIS

Stable states of TM/RE multilayers have been presented in Chapter 2 as the result of Zeeman energy and exchange interaction energy competition. Taking into consideration the anisotropy energy other properties like thermal hysteresis may be explained.

For the TM/RE multilayers, calculations with anisotropy field Ha, that is temperature independent and in the same direction with the applied field, demonstrate the existence of both aligned phases (TM and RE) stable over a certain range of temperature. This stability correlates with the different behavior of the two components when the temperature changes and gives thermal hysteresis [62]. Gd and Tb magnetic moment have a strong temperature dependence between 10 and 300K, in contrast with almost constant value for TM (figure 4.5).

At high temperature and small fields, the antiferromagnetically coupled system is in the TM aligned state: TM moments aligned with the field dominates the RE moment, which are small and aligned antiparallel to the field. As the temperature decreases the RE moment increases. However, due to the anisotropy, the TM moments are held parallel with the external field. Therefore, the net moment is antiparallel aligned to the field until the configuration leaves the stability region and the moments

are reversed to the RE aligned phase. A similar situation occurs as the temperature of the system is increased from the RE aligned phase, but the phase transition occurs at a different temperature. As the applied field increases the stability region decreases leading to the decrease of the thermal hysteresis width also. A critical field for which the thermal hysteresis can be still observed was found to be dependent on the exchange coupling: a weaker exchange coupling allows the canting of spins at the interface at lower applied field and the aligned state becomes instable. The thermal hysteresis effect was first measured for Fe magnetization as a function of temperature by neutron scattering measurements in a multilayer of Fe/Gd [62].

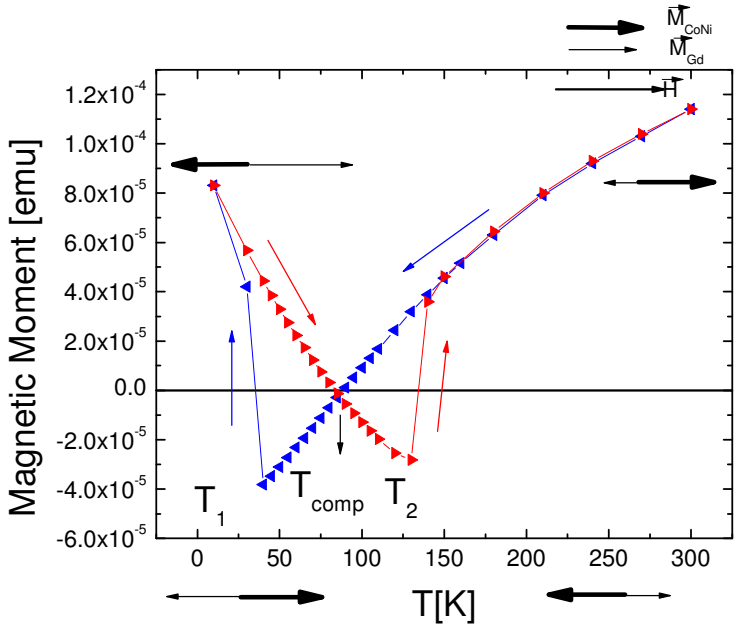

Figure 5.1 Thermal hysteresis

In different TM/RE (Co, CoNi, Fe/Gd,) multilayers and alloys (CoGd), the total magnetic moment was measured as a function of temperature and experimental results are in good agreement with the theoretical calculations [63, 64]. The measurements of total magnetic moment in TM/RE multilayer as a function of temperature during both cooling and heating the sample in moderate fields give rise to a characteristic "bow-tie" shape. A typical M(T) curve is shown in figure 5.1 .

Thermal hysteresis was experimentally investigated for ferromagnetic-antiferromagnetic exchange bias structure [65], or theoretically for thin films of Fe/Dy/Fe, or Gd/Dy/Gd [66] and ferromagnetic dots [67] exchange coupled with uncompensated AFM substrate system proving that anisotropy represents an important aspect in nanostructured samples.

Thermal hysteresis, as M(T) measurements, is investigated in Co/Tb [68], Ni/Gd and NiFe/Gd multilayers and the results are shown in the following sections along with M(H) measurements which illustrate the ferrimagnetic behavior of these multilayers.

5.1 Co/Tb multilayers

In order to reveal the importance of H_a in the coupling of individual sublayers in Co/Tb multilayers, the total magnetic moment as a function of temperature was investigated for layer thicknesses between 3-7 nm. The results presented are for multilayers of (Co 3nm /Tb 4.5 nm) $_8$ and (Co 4nm /Tb 6 nm) $_{8.}$ The multilayers were cooled at a rate of 10K/min from 300 K to 10 K, followed by the heating process, back to 300 K under a constant in plane applied magnetic field with different values (1000-

9000 Oe). The hysteresis loops M (H) were measured between 10-300 K with an in plane applied field to estimate the temperature dependence of the remanent moment and the coercivity field magnitude.

The layers thickness (less than 10nm for Co and Tb) and also the sputtering conditions have determined polycrystalline structure of the multilayers. X-ray diffraction (θ-2θ) is shown for $(Co3nm/Tb4.5nm)_8$ if figure 5.2.

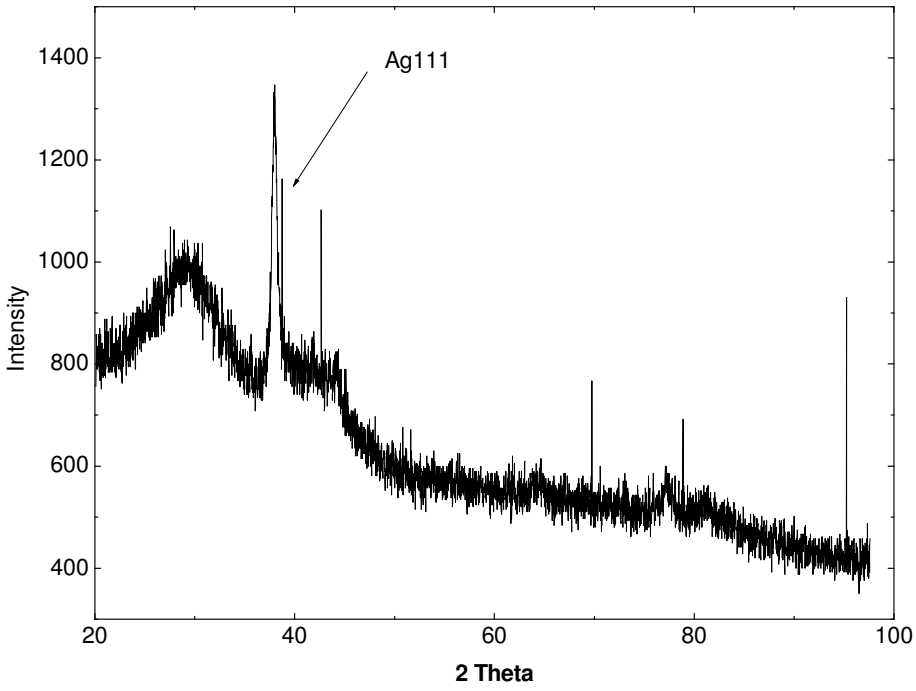

Figure 5.2 X-ray diffraction for $(Co3nm/Tb4.5nm)_8$

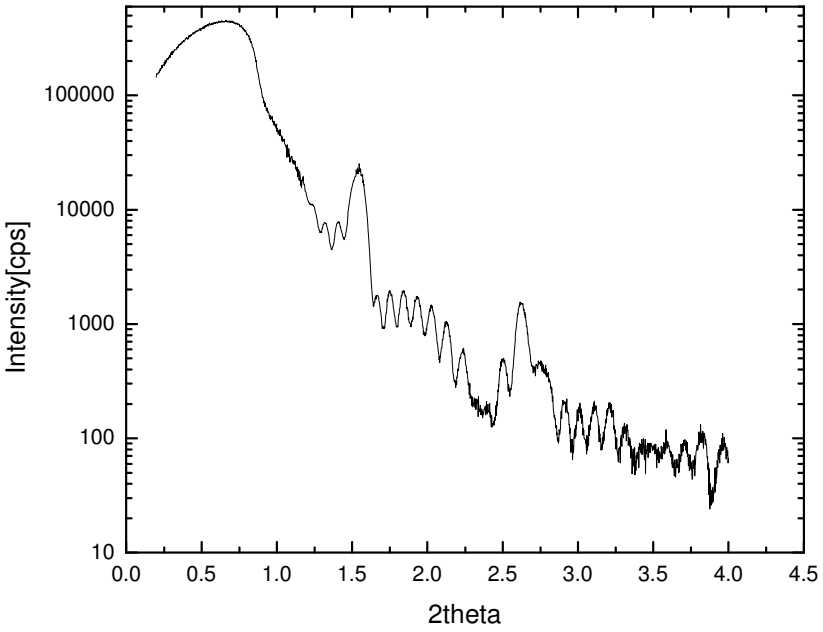

Figure 5.3 Reflectivity diffraction for $(Co3nm/Tb4.5nm)_8$

A reflectometry configuration with a Co source was used to check the quality of the layered structure. In figure 5.3, just 2 Bragg orders are observed, indicating high interface roughness. The additional fringes in between Bragg peaks arise from periodic bilayer (Co3nm/Tb4.5nm) repetition.

Figure 5.4 presents the remanent moment of the multilayers vs temperature, for $(Co\ 3nm\ /Tb\ 4.5\ nm)_8$ and $(Co\ 4nm\ /Tb\ 6\ nm\ )_8$.The temperature dependence of the magnetic moment with a minimum at compensation temperature, T_{comp}, is a typical behavior for ferrimagnetic systems. The antiferromagnetically coupled moments of Co and Tb compensate each other around 210K for $(Co\ 3nm\ /Tb\ 4.5\ nm)_8$ and around 140 K for $(Co\ 4nm\ /Tb\ 6\ nm\ )_8$.

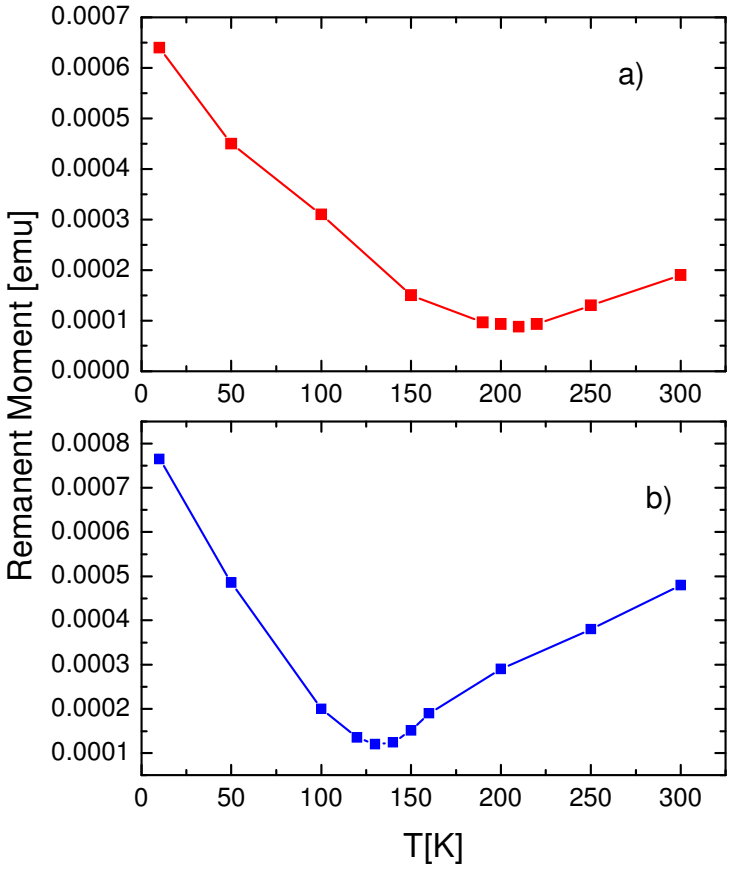

Figure 5.4 Remanent moment temperature dependence for a) $(Co3nm/Tb4.5nm)_8$, b)$(Co4nm/Tb\ 6nm)_8$

Figure 5.5 shows the coercive field temperature dependence. There is a small increase in coercivity near compensation temperature for both multilayers. Hysteresis loops for $(Co3nm/Tb4.5nm)_8$ are shown in figure 5.6 and in figure 5.7 for $(Co4nm/Tb6nm)_8$.

High coercivity and saturation moment observed at 50K and 100 K figure5.6 are due to Tb moment which is aligned with the magnetic field direction below T_{comp}=210K. After T_{comp}, Co magnetic moment is aligned with the magnetic field

direction, the moment gradually increases and coercivity decreases. At 300K H_c=500 Oe and M_r =1.92 10^{-4} emu.

The same trend is observed for the (Co 4nm/Tb 6nm)$_8$ multilayer. At 300K, H_c=340 Oe and M_r= 4.58 10^{-4} emu. The effect of the background is observed in the saturation regions at high fields were the magnetization shows a negative diamagnetic slope.

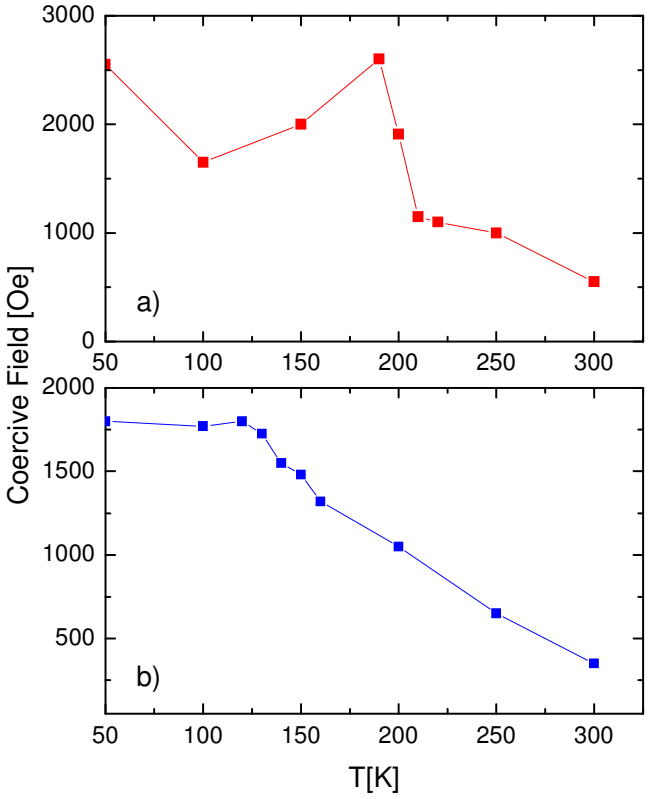

Figure 5.5 Coercive field temperature dependence for a) (Co3nm/Tb4.5nm)$_8$, b) (Co4nm/Tb6nm)$_8$

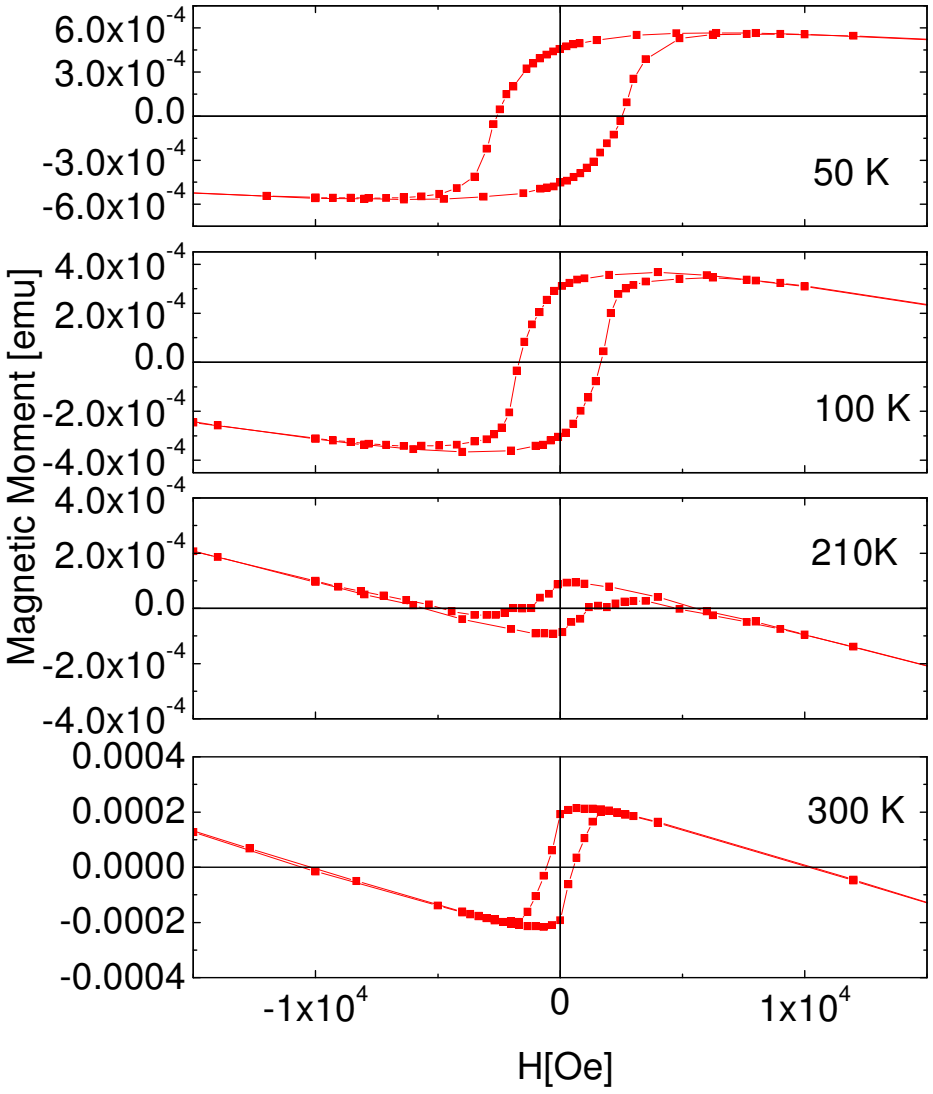

Figure 5.6 Field hysteresis loops at different temperatures for $(Co3nm/Tb4.5nm)_8$ multilayer

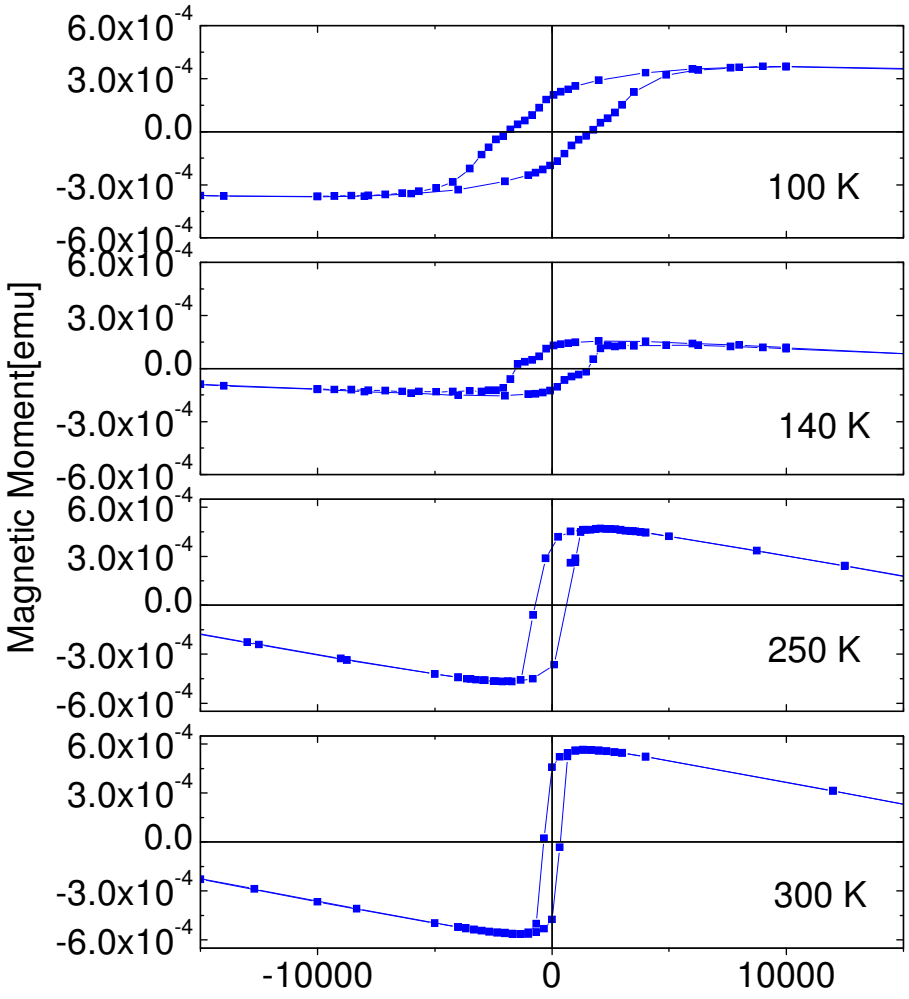

Figure 5.7 Field hysteresis loops at different temperatures for $(Co4nm/Tb6nm)_8$ multilayer

Figure 5.8 shows the magnetic thermal hysteresis results at different values of applied external magnetic fields for $(Co\ 3nm\ /Tb\ 4.5\ nm)_8$. In figure 5.8 (a), at 1000 Oe, as the temperature is reduced from 300 K, the Tb moment increases and dominates over the Co moment, but the anisotropy keeps the system in the Co aligned state through the

entire temperature range. As a result of this we measure negative moment below 200 K and also a small increase in magnetization below 50 K.

Between 2000-4000 Oe the M (T) graph has a" bow-tie" shape as presented in Figure 5.8 (b), (c), (d)and (e) respectively . The two minima observed in the measurement of magnetic moment as a function of temperature during the heating and cooling cycles correspond to magnetic phase transitions. The system will switch from the Co aligned state to the Tb aligned state during the cooling cycle at $T_1<T_{comp}$, and back to the Co aligned state at $T_2 >T_{comp}$ during the heating cycle. The "width" of the thermal hysteresis ($\Delta T=T_2-T_1$) is around 90 K for 2000 Oe and 40K for 4000 Oe. As shown in figure 5.8 (f), at 6000 Oe and higher applied magnetic fields the M (T) looses the "bow-tie "characteristic. The system goes through the same states on the heating and cooling cycles, the only minimum indicating the compensation temperature.

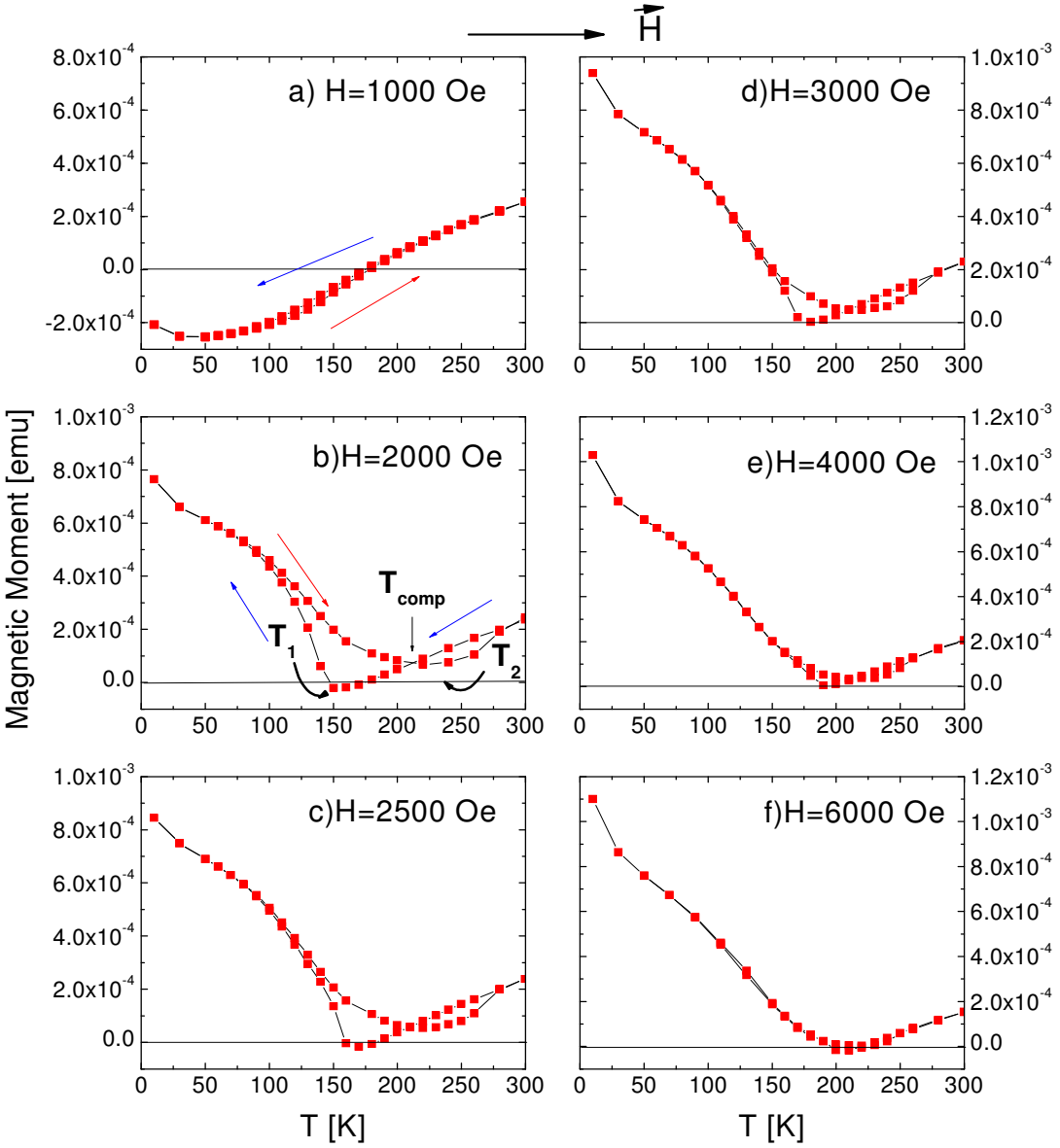

Figure 5.8 Thermal hysteresis loops for different applied magnetic fields for $(Co3nm/Tb4.5nm)_8$ multilayer

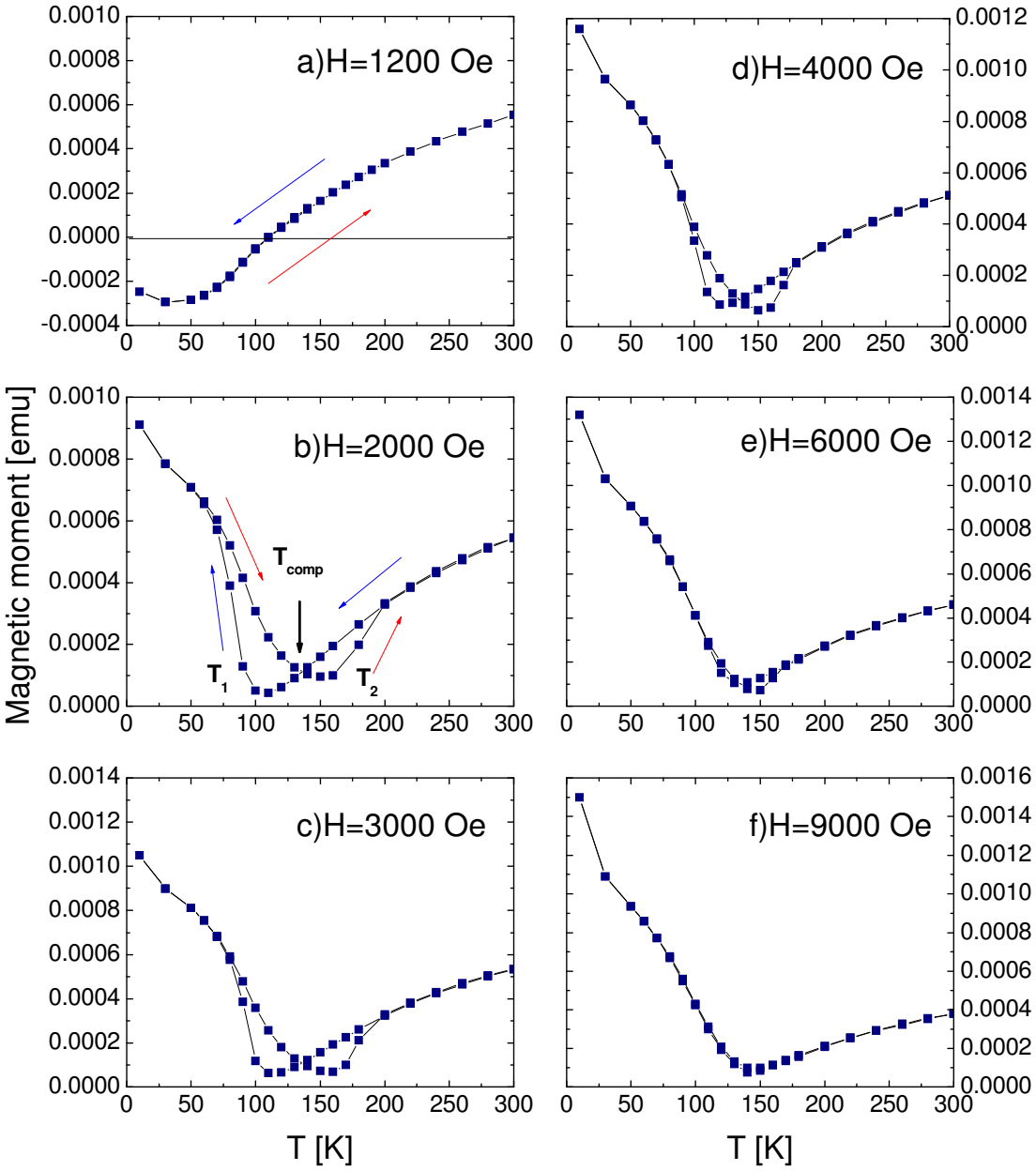

Figure 5.9 Thermal hysteresis loops for different applied magnetic fields for $(Co4nm/Tb6nm)_8$ multilayer

Figure 5.9 shows the magnetic moment vs temperature for a thicker multilayer (Co 4nm/Tb 6nm)$_8$ for different values of applied magnetic field. Negative moment is observed just at 1200 Oe, below 125 K, as shown in figure 5.9 (a), which corresponds to the Co aligned state for the entire temperature range measured. For this multilayer, more symmetric "bow-tie" curves are measured for 3000- 4000 Oe external fields, as shown in figure 5.9 (b), (c), and (d) respectively. As the external magnetic field increases we observe again a decrease in the thermal hysteresis "width". ΔT= 50 K at 3000Oe, 30K at 4000Oe, and 10K at 6000Oe. The "width" of the thermal hysteresis is zero at 9000 Oe as shown in figure 8(f).

Shown in figure 5.10 is the thermal hysteresis width dependence with applied field. The decrease of ΔT with external magnetic field:90 K at 2000 Oe , 12 K at 6000 Oe for (Co3nm/Tb4.5nm)$_8$, 60 K at 2000 Oe, 10 K at 6000 Oe for (Co4nm/Tb6nm)$_8$.The thinner multilayer gives larger thermal hysteresis, for the same external magnetic field.

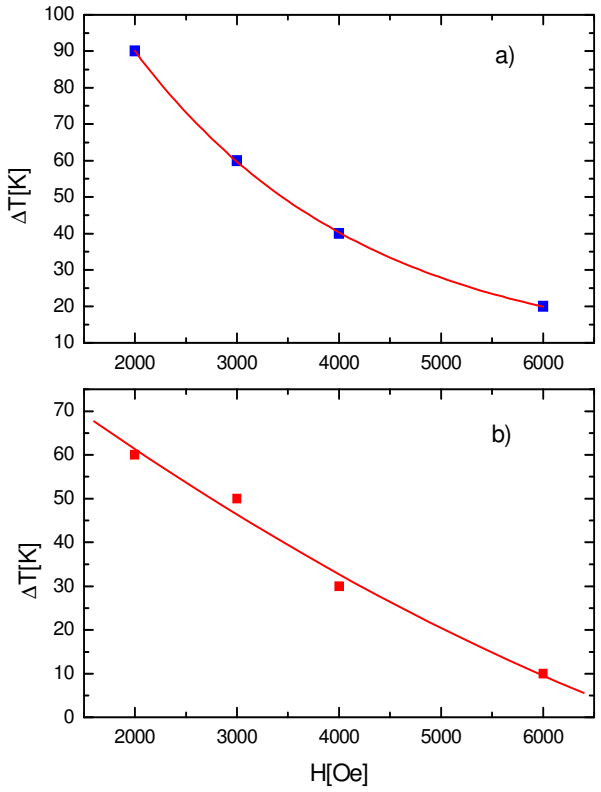

Figure 5.10 Thermal hysteresis width dependence with applied magnetic field for a) $(Co3nm/Tb4.5nm)_8$, b) $(Co4nm/Tb6nm)_8$ multilayers

Co/Tb multilayers are hard ferrimagnetic systems. There is a clear minimum in Mr(T),but with incomplete compensation. This point indicates the compensation temperature. The compensation temperature was defined also as the middle point of temperature hysteresis curves (crossing point of heating and cooling cycles).As compensation temperature of the multilayer, this temperature is field independent result proved by the measurements M(T) at different magnetic fields(figures 5.8 and 5.9). But again we can observe from the thermal hysteresis loops the incomplete compensation

of the antiparallel coupled moments. The Terbium moments present a spread of their directions because of the strong local anisotropy.

The phase transitions between Co and Tb aligned states are not as sharp as observed in M(T) measurements for CoNi or Co/Gd multilayers. An anisotropy term for Tb layers and more complex than uniaxial form (as assumed for Co) has to be included in the model.

For Co/Tb multilayers, tunability of thermal width over 0-80K can be achieved with large magnetic fields (1-9) kOe. The large constant magnetic fields that can give the thermal hysteresis behavior is direct related with large coercivity of the multilayer.

5.2 NiFe/Gd multilayers

A series of $(NiFe2nm/Gdxnm)_4$ multilayers with x=2,3,4nm were investigated. NiFe/Gd multilayer combines a soft transition metal alloy, Permalloy (Ni80Fe20), with a low anisotropy rare earth , Gadolinium.

Figure 5.11 presents magnetic moment as a function of temperature for $(NiFe2nm/Gdxnm)_4$ multilayers. The applied field was 200 Oe for except for $(NiFe2nm/Gd4nm)_4$ for which the applied field was 500 Oe. Due to the antiparallel alignment between the TM and the RE moments and the strong temperature dependence of the Gd moment between 10-300K, the multilayers present compensation temperature for x=2, 3 nm. For x=4nm M(T) has a broad minimum that can be accounted for compensation temperature. NiFe/Gd bilayers and multilayers have been previously

investigated. The existence of an alloy due to Ni diffusion into Gd was proved by different experimental techniques [61].

The compensation temperature increases as the amount of Gd is increased .The multilayer with smaller Gd magnetic moment requires a smaller Py for the moments to compensate. Therefore T_{comp} increase as Gd thicknesses is increased.

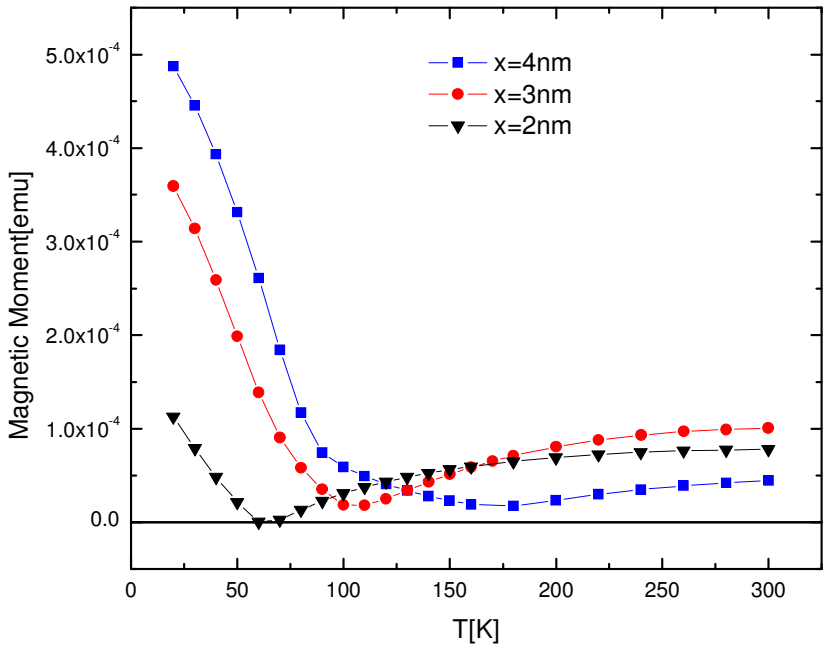

Figure 5.11 Magnetic moment as a function of temperature for $(NiFe2nm/Gdxnm)_4$ multilayers, with x=2,3,4nm.

The thermal hysteresis, M(T), at constant field are presented in figure 5.12 for $(NiFe2nm/Gd3nm)_4$ multilayer.

The thermal hysteresis width is 40K at 50 Oe and 30K at 100Oe and the bow tie characteristics is disappearing above 300 Oe.

The field hysteresis M(H) are presented in figure 5.13. The shape is changing very much around compensation temperature. M(H) at T_{comp}= 80K illustrates the typical moment decrease at compensation temperature in ferrimagnetic systems.

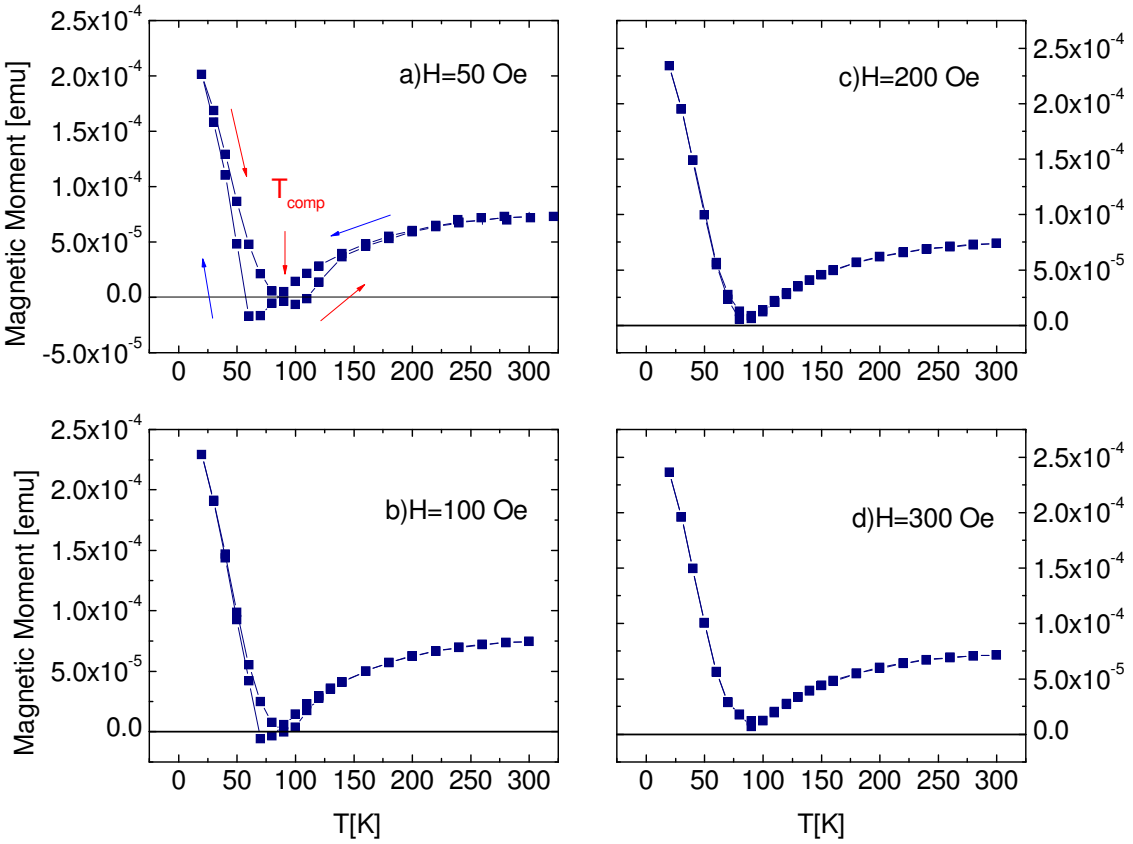

Figure 5.12 M(T) at different magnetic fields for $(NiFe2nm/Gd3nm)_4$

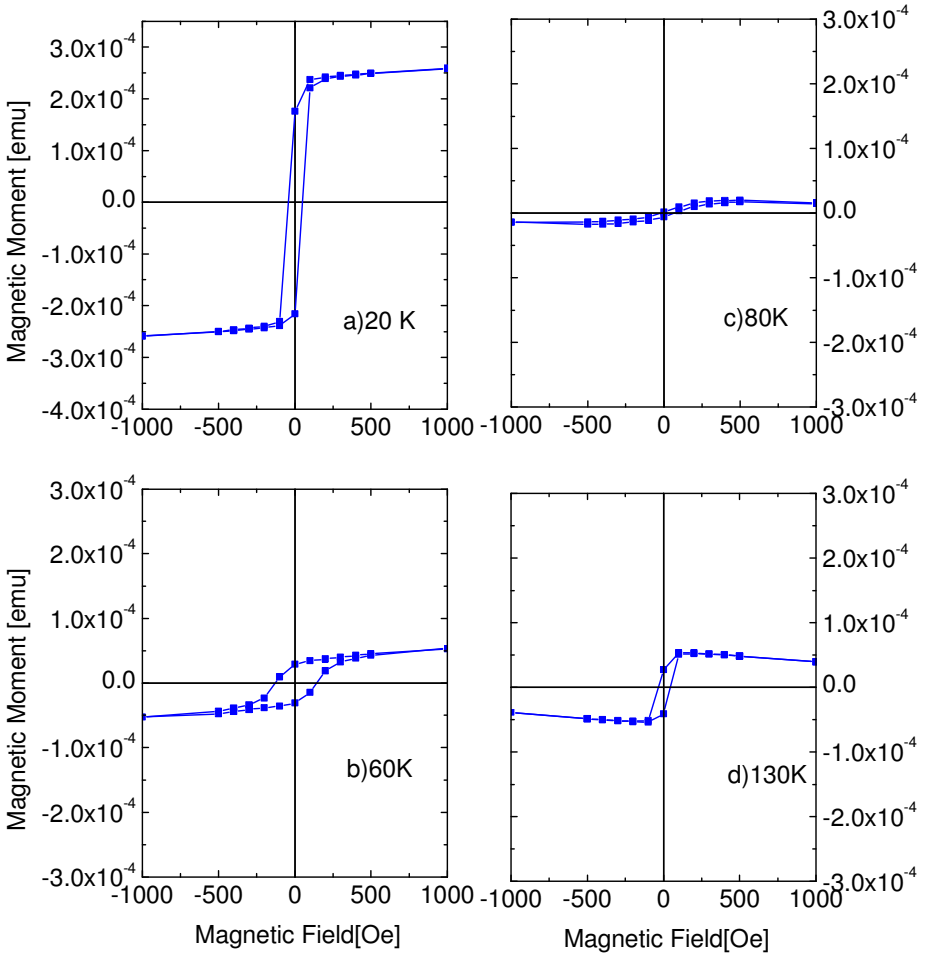

Figure 5.13 M(H) at different temperatures for $(NiFe2nm/Gd3nm)_4$

A different series is also investigated $(NiFex/Gdx)_4$ with x=2,4,6nm. Figure 5.14 presents the magnetic moment temperature dependence M(T) for the multilayers at 500nm applied magnetic field. The compensation temperatures are 40K, 50K and 60K for the multilayers with x = 6nm, 4 nm and 2nm respectively. The incomplete compensation is observed for the thicker multilayer.

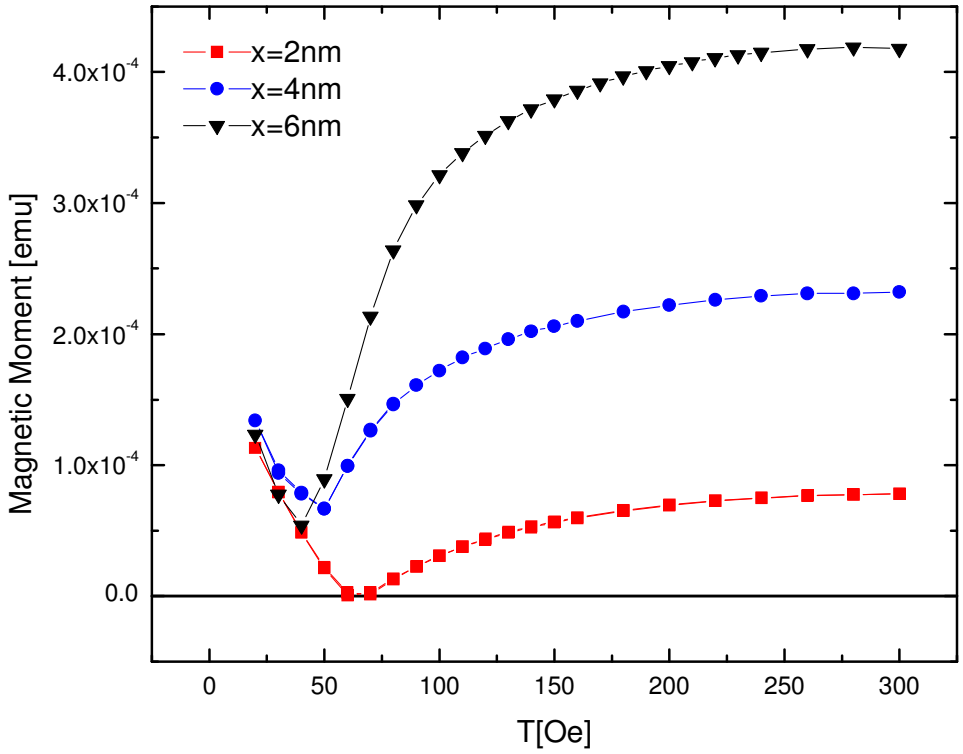

Figure 5.14 M(T) for $(NiFex/Gdx)_4$ with x=2,4,6nm at 500 Oe applied magnetic field

As the amount of NiFe in increased, the anisotpropy of the alloy due to the Fe becomes important. Thicker layers of NiFe may not have a perfect parallel in plane alignment of the magnetic moments. Lower applied field of 100 Oe will keep the multilayers in the TM aligned phase, and fields above the anisotropy values will not induce thermal hysteresis, the switch from TM to Gd aligned phases will be around the same temperatures.

Figure 5.15 shows Mr(T) and Hc(T) for $(NiFe2nm/Gd2nm)_4$. Remanent moment and coercive field were measured from magnetic field hysteresis loops. The multilayer

displays an ideal ferrimagnetic behavior, with almost zero magnetic moment at T_{comp}=60K.

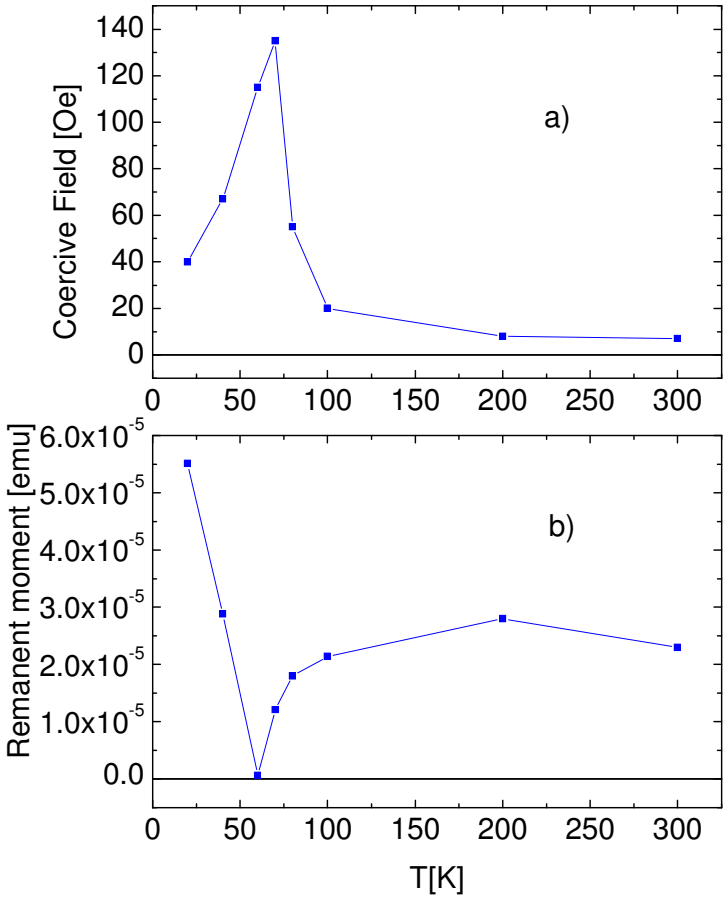

Figure 5.15 a) Hc(T), b) Mr(T) for $(NiFe2nm/Gd2nm)_4$

Figure 5.16 shows M(T) for $(NiFe2nm/Gd2nm)_4$ at different applied magnetic fields. The features associated with the thermal hysteresis measurements are identified also for this multilayer.

At 20 Oe, figure 5.16(a), the system is in the TM aligned state for the entire measuring temperature range. The Gd moment increases at low temperature and so does the Zeeman energy, but anisotropy energy dominates and keeps the multilayer in NiFe

aligned state. $\Delta T=T_2-T_1$, of just 20 K is controlled by 50 or 100 Oe applied magnetic field as seen in figures 5.16 b and 5.16 c. Above 300 Oe, figure 5.16 d, thermal hysteresis disappear.

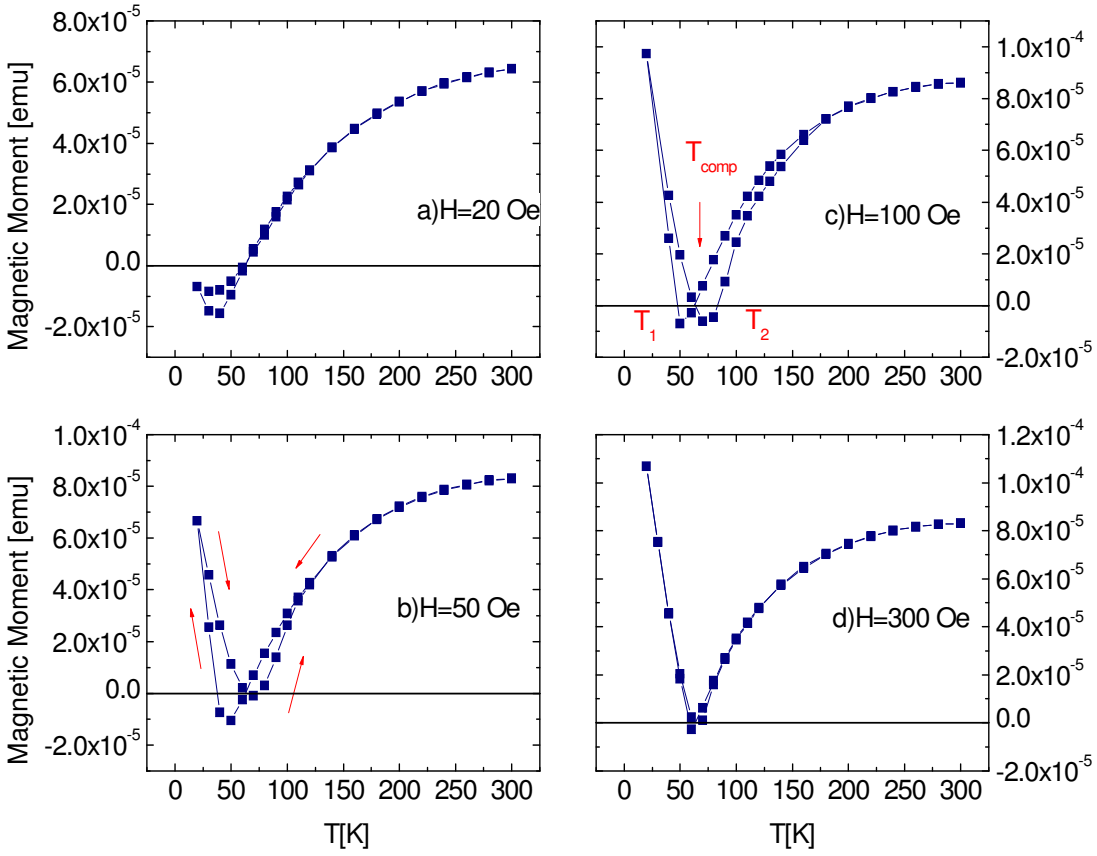

Figure 5.16 Thermal hysteresis for $(NiFe2nm/Gd2nm)_4$ at different applied magnetic fields

Field hysteresis loops are presented in figure 5.17 at different temperatures. At T=60K there is a typical increase in coercivity as the net magnetic moment decreases. Above compensation temperature total moment continuously increases, coercivity decreases and the hysteresis loop become square.

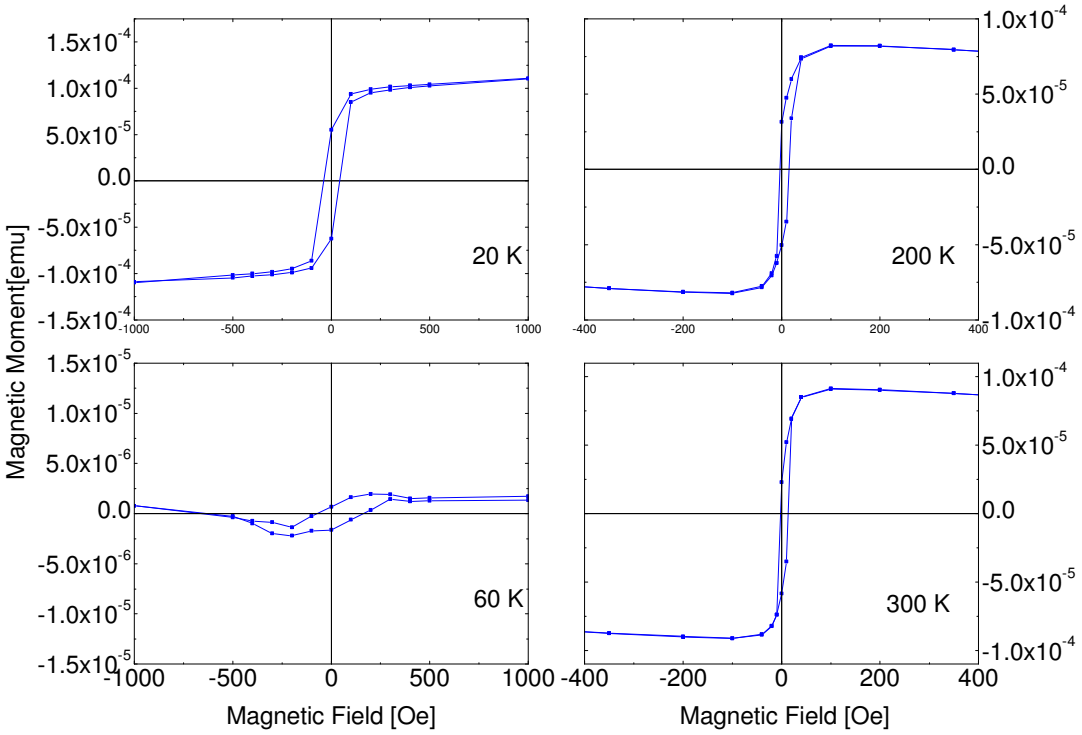

Figure 5.17 Field hysteresis for $(NiFe2nm/Gd2nm)_4$

5.3 Ni/Gd multilayers

Field hysteresis measured at different temperatures in (20-300 K) temperature interval and temperature hysteresis at constant in plane magnetic field (50-300 Oe) have been measured for $(Ni4nm/Gdxnm)_4$ multilayers with x=2,4,6nm. Figure 5.18 presents M(T) at 200 Oe applied magnetic field .Compensation temperatures are:40K,60K and 70K for x=2,4and 6nm respectively.

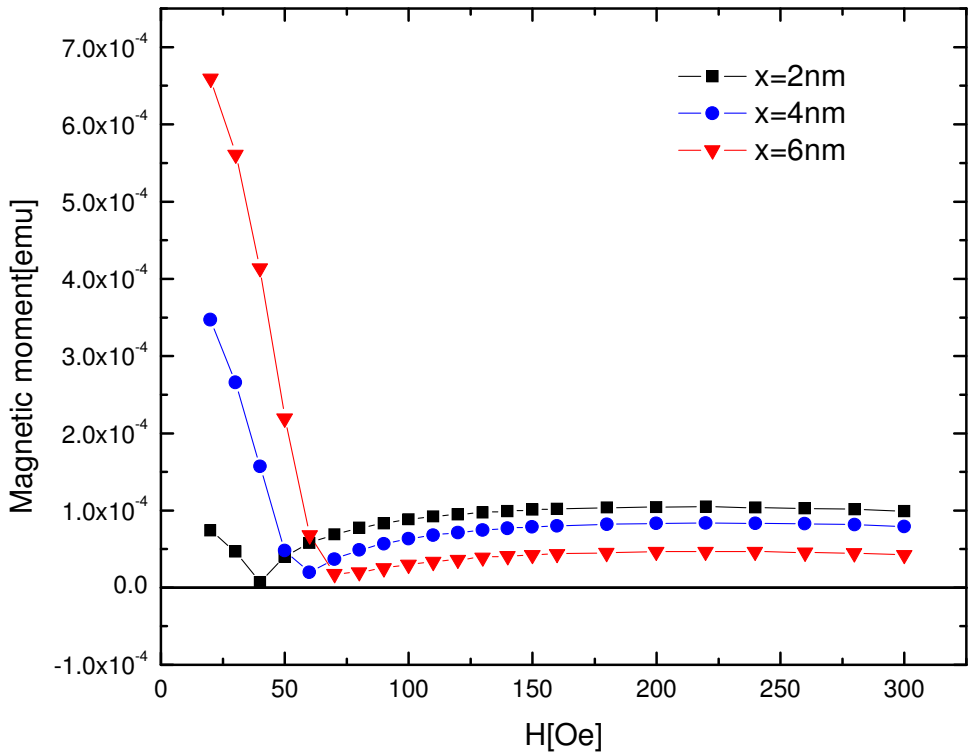

Figure 5.18 M(T) for $(Ni4nm/Gdxnm)_4$ with x=2,4,6nm multilayers at 200 Oe applied magnetic field

Thermal hysteresis characteristics are observed in M(T) for all the multilayers between 50-300 Oe. The multilayers have small anisotropy energy, around 20-50 Oe.

Field hysteresis loops and thermal hysteresis loops are presented for $(Ni4nm/Gd4nm)_4$ multilayer.

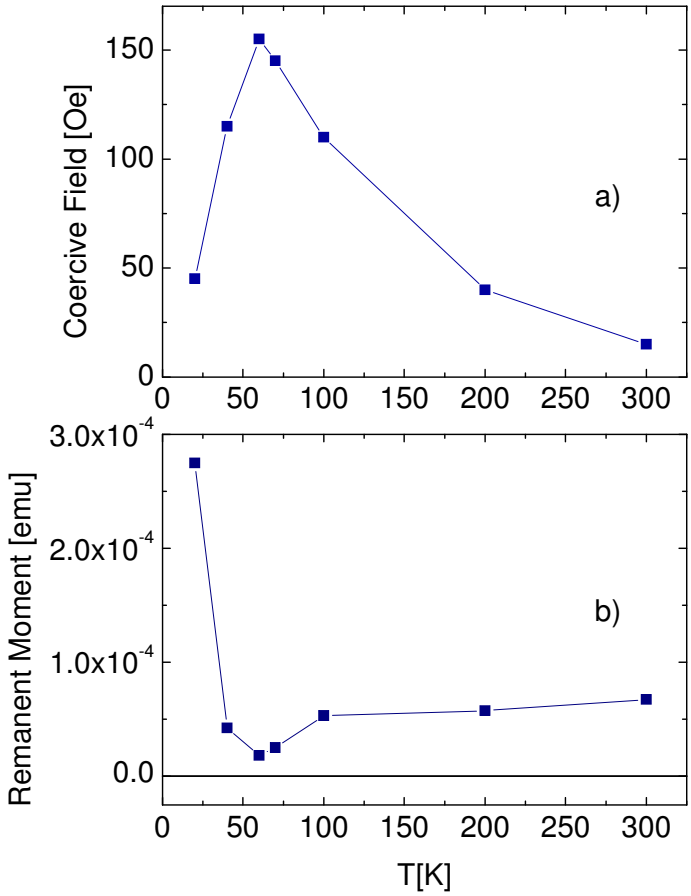

Figure 5.19 a) Hc(T), b) Mr(T) for $(Ni4nm/Gd4nm)_4$ multilayer

The coercive field as a function of temperature is shown in figure 5.19 a). The coercive field increases near the compensation temperature. Because the coercive field is dominated by the anisotropy and Ha is proportional with 1/Ms, as the magnetization decreases to zero (around T_{comp}), a high field will be required to reverse the magnetization.

The remanent moment as a function of temperature Mr(T) is presented in figure 5.19 b) for $(Ni4nm/Gd4nm)_4$

The Mr(T) graph shows a minimum that is a typical behavior for ferrimagnetic systems. The antiferomagnetically coupled moments of Ni and Gd compensate each other at 60K.As the temperature is increased from 5 K the system switches between the Gd aligned state below T_{comp} to Ni aligned state above T_{comp}.

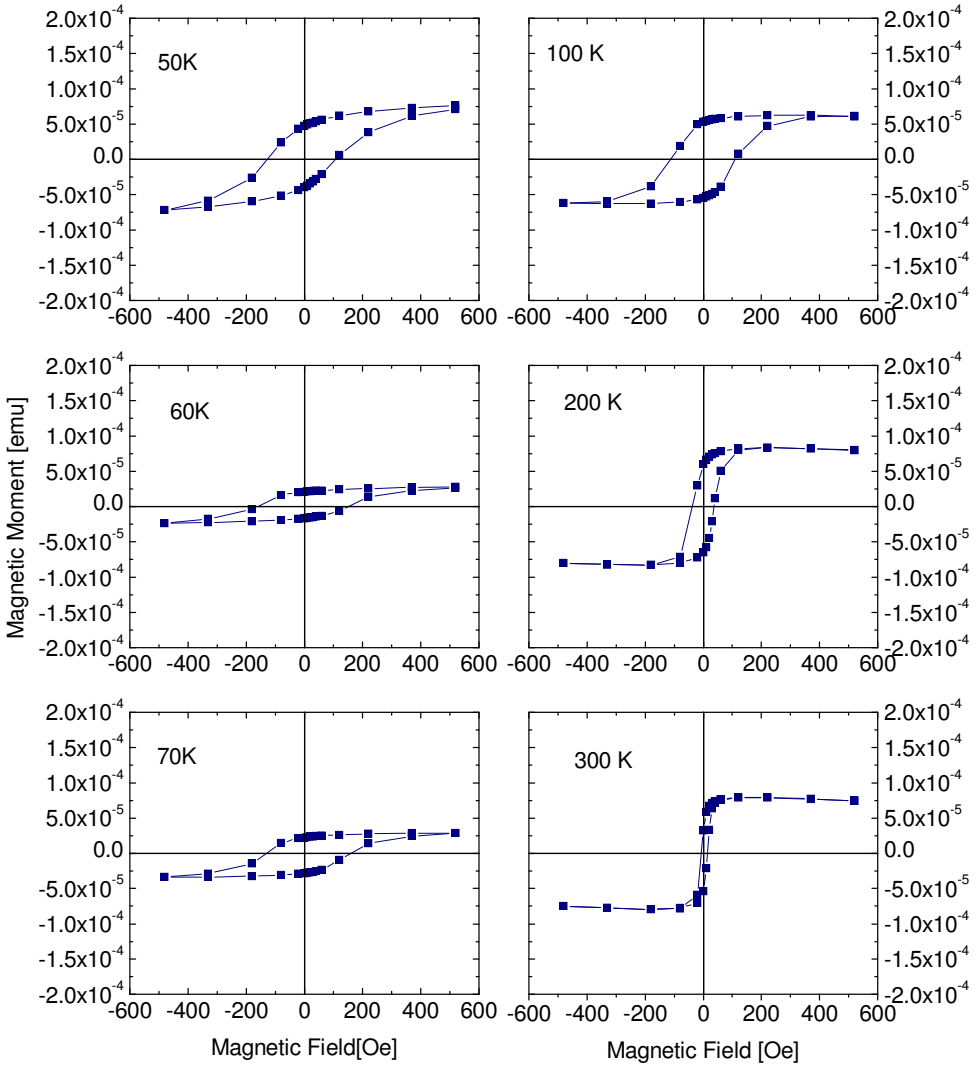

Figure 5.20 Hysteresis loops of the $(Ni4nm/Gd4nm)_4$ multilayer

In figure 5.20 the hysteresis loops of the $(Ni4nm/Gd4nm)_4$ multilayer at temperatures below and above the T_{comp} (60K) are shown by comparison, just to demonstrate the change in coercive field and total magnetic moment around the compensation temperature. The sample is cooled under zero field to low temperature, and after that hysteresis loops were measured increasing the temperature.

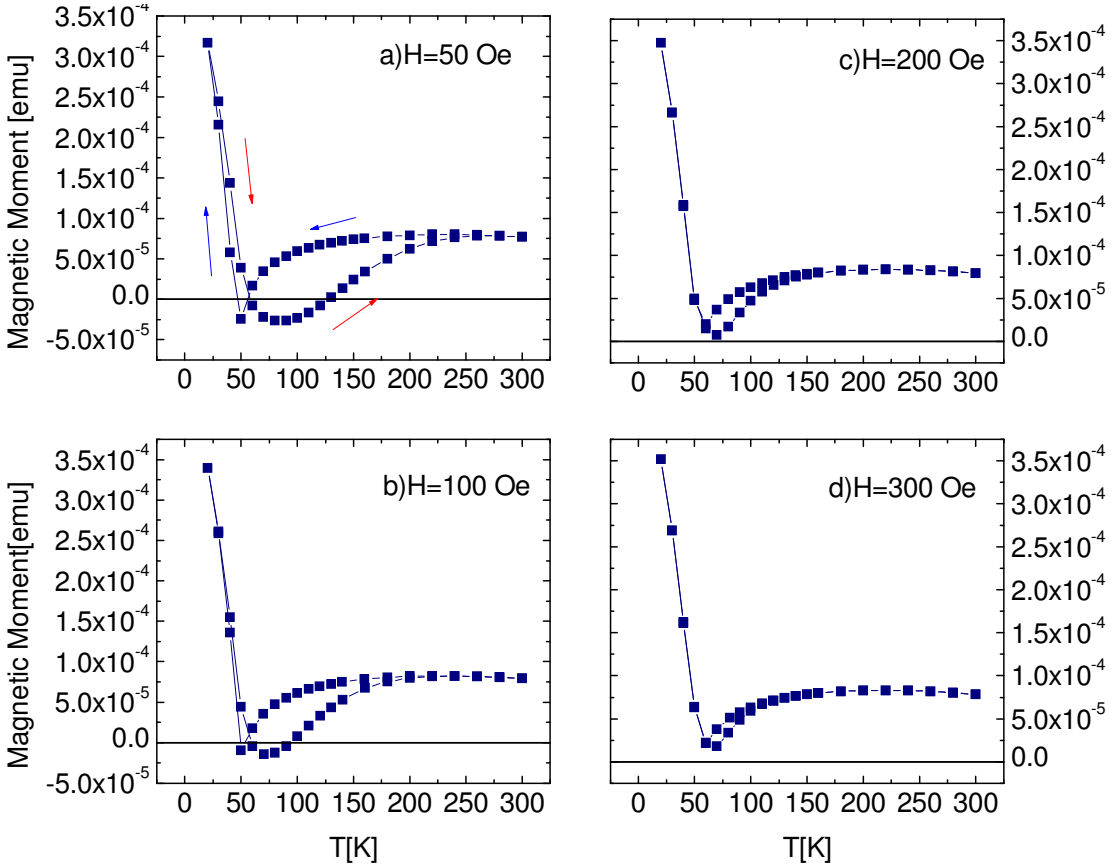

Figure 5.21 Thermal hysteresis loops for $(Ni4nm/Gd4nm)_4$ multilayer

M(T) graphs are shown in figure 5.21 for $(Ni4nm/Gd4nm)_4$.Very small fields (50-300Oe)control the thermal hysteresis behavior. Two distinct transition temperatures

during the cooling and the heating are observed for 50 Oe and 100 Oe, but with a difference of just $\Delta T=30K$ and 20K respectively. For 200 Oe and 300 Oe, the phase transition temperatures are 10K apart. A strong asymmetry is observed for all the applied fields. The switch from Ni aligned phase to Gd aligned phase at temperatures below compensation temperature is sharp, during the cooling cycle. The switch from Gd aligned to Ni aligned phase is gradual, during the heating cycle.

Diffusion of Ni into Gd layer may be responsible for the gradual rotation as the interface has an NiGd alloy and a Gd layer which will rotate differently as the temperature is increased.

The presence of a compensation temperature where the net magnetic moment of the system is minimum and the presence of a maximum in coercivity around T_{comp} for the multilayers studied support the assumption that NiFe/Gd and Ni/Gd are soft ferrimagnetic systems.

The compensation temperature from M(T) measurements is near the same with the one measured from field hysteresis as minimum in Mr (T) curve. The anisotropy of Gd is weak due to the 4f electrons. Gd moments are antiparallel to Ni or NiFe moments and the multilayers have an easy axis in the film plane.

Temperature difference of 20, 30 K between the phase transition temperatures can be controlled by small magnetic field (50-300 Oe).Above a certain value the thermal hysteresis, predicted theoretically, disappear and this is observed experimentally for both systems Ni/Gd and NiFe/Gd.

The Ni diffusion into Gd layer during the sputtering process may be different from a pure Ni target compared to a NiFe target. The existence of an alloy changes the interface coupling (weaken the exchange coupling) and the mechanism of the phase transition during the cooling and the heating cycles. Also a temperature dependent anisotropy and more complex than uniaxial form may be considered for explaining the thermal hysteresis.

The experimental data for both hard and soft ferrimagnetic systems are far from the theoretical models where perfect interfaces are considered, but M(T) measurements reflect the anisotropy contribution in magnetic stable states of TM/RE at moderate magnetic fields.

CHAPTER 6

MAGNETIC ENTROPY CHANGE IN CoNi/Gd, CoFe/Gd AND Co/Tb NANOLAYERS

Theoretical and experimental investigations of phase transitions, as well as their practical applications, have been conducted in many different systems.

The studies on phase transitions in magnetic materials have mainly been focused on the order/disorder transitions such as ferromagnetic to paramagnetic. The isothermal magnetization of a material decreases the entropy and subsequent adiabatic demagnetization can lead to a temperature decrease. The inverse effect, entropy increase, was also observed in first order phase transitions near the ordering temperatures when the magnetic field is adiabatically applied. Direct or indirect entropy change (ΔS)calculations on bulk materials have been done in pure Gd, Tb, Dy, Ho, Er or Tm and in their alloys [69-71] in large external magnetic fields. Phase transitions appear next to the Curie temperature and at lower temperatures when the spin structure changes [72-74]

Recently, interest in the use of nanoparticles and thin films for MCE has grown [75-77]. These nanostructures offer several advantages, including: 1. magnetic properties are easier to be tuned in nanostructured materials than in bulk materials. 2. the entropy change can be achieved across a broader temperature interval with external magnetic fields on the order of kOe or even lower. Due to these small applied magnetic

fields, magnetic anisotropy becomes an important factor in determining the entropy change [78].

The nanolayers of (CoNi, CoFe) /Gd presented here have additional advantages: the first order magnetic phase transition temperatures can be easily tuned with external magnetic fields. In addition, both $\Delta S<0$ and $\Delta S>0$ for cooling and heating cycles respectively can be measured for the same sample.

In this paper, we present magnetic entropy change, ΔS, due to magnetic first order phase transitions in ultrathin multilayers of CoNi/Gd [78] and CoFe/Gd. Thermal hysteresis in transitions between two ordered states were observed in measurements of magnetic moment versus temperature, M (T), in constant external magnetic field, leading to change in magnetic entropy. Among the systems that have shown thermal hysteresis CoNi/Gd and CoFe/Gd multilayers were chosen because of their sharp transition and also large temperature interval for which the thermal hysteresis is observed.

6.1 CoNi/Gd multilayers

Figure 6.1 presents M(T) curves for $(CoNi1.5nm/Gd2nm)_4$. The two minima observed in figure 6.1 a) at T_1 and T_2 in the measurement of magnetic moment as a function of temperature during the cooling and heating cycles correspond to first order magnetic phase transition temperatures.

CoNi and Gd moments are antiferromagnetically aligned in small external fields (50-300 Oe) where the interaction is dominated by the exchange and anisotropy energy

values. In figure 6.1a) the sample will switch from the CoNi aligned state to the Gd aligned state during the cooling cycle (supercooling) at T_1, and back to the CoNi aligned state at T_2 during the heating cycle (superheating) under an external magnetic field of 50 Oe. On the top of the figure, the thin and thick arrows indicate the Gd and CoNi magnetic moments respectively. As the temperature is reduced from 300 K, the Gd moment increases and dominates over the CoNi moment (assumed constant in 10-300K temperature interval), however the anisotropy keeps the system in the CoNi aligned state through supercooling. As a result negative moments are measured between 165K, (crossing point of cooling and heating curves) and T_1=100K (the transition temperature). Similarly negative moments were measured between 165K and T_2 = 230 K as the system is kept in the Gd aligned state through superheating. The thermal hysteresis width $\Delta T=T_2 - T_1$, represents the coexistence temperature interval for the two magnetically ordered CoNi and Gd aligned phases. At H=50 Oe (as shown in figure 6.1a) ΔT=130 K and at H=100 Oe (as shown in figure.6.1 b)) ΔT=60K. With higher external magnetic fields, the difference in transition temperature becomes smaller and above a critical external magnetic field, it is reduced to zero. An H= 200 Oe external magnetic field reduces ΔT to 20K, (as shown in figure 6.1c)) and for H=500Oe (as shown in figure 6.1d)) the M (T) shows just the typical T_{comp} of ferrimagnetic systems with no thermal hysteresis. At 500 Oe, M (T) is reversible for the heating and cooling cycles, the only minimum indicating the unique T_{comp}.

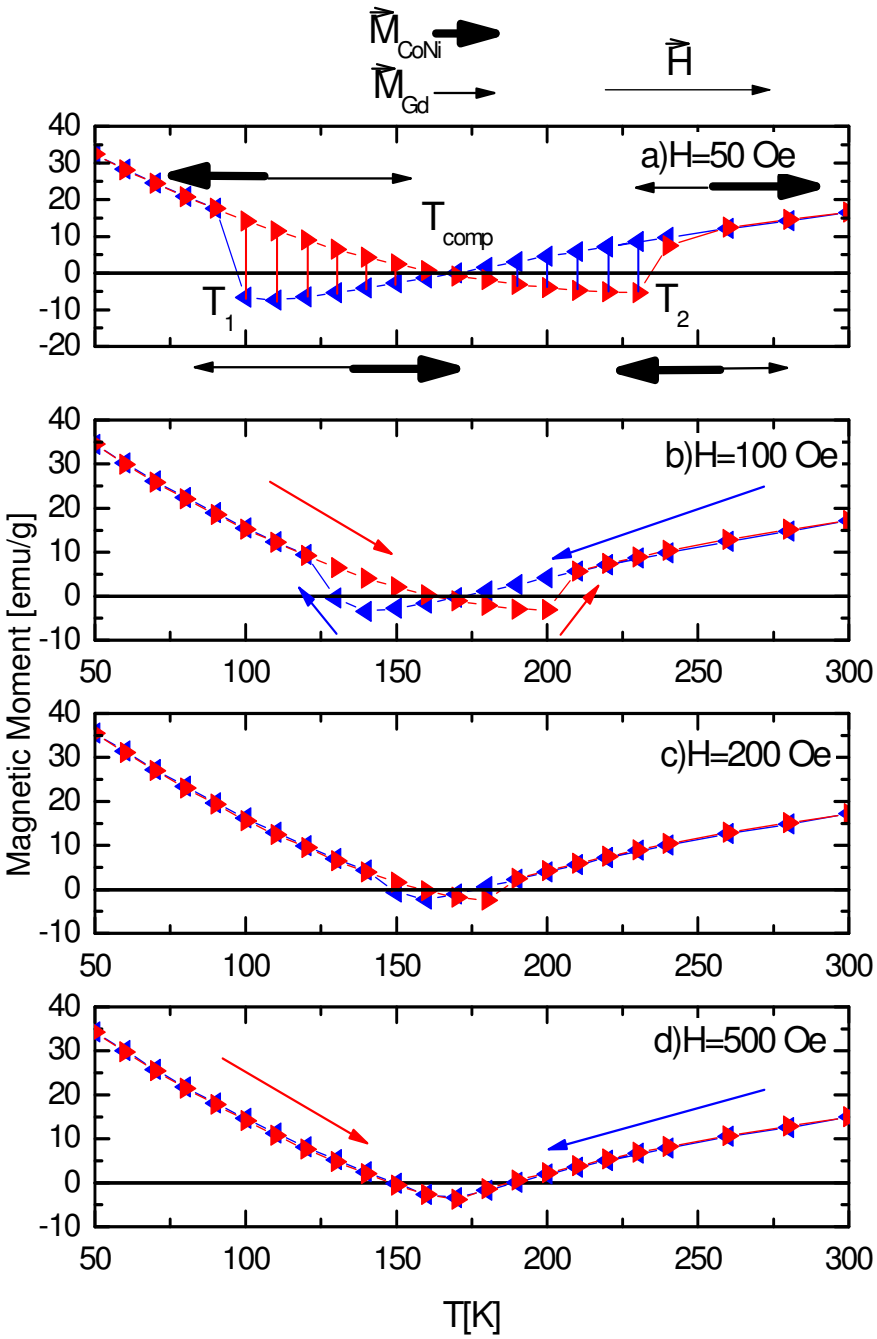

Figure 6.1 Thermal hysteresis loops for $(CoNi1.5nm/Gd2nm)_4$.

The thermal hysteresis width decreases as a function of the applied field. The experimental data ΔT (H) shown in figure 6.2) has an exponential fit.

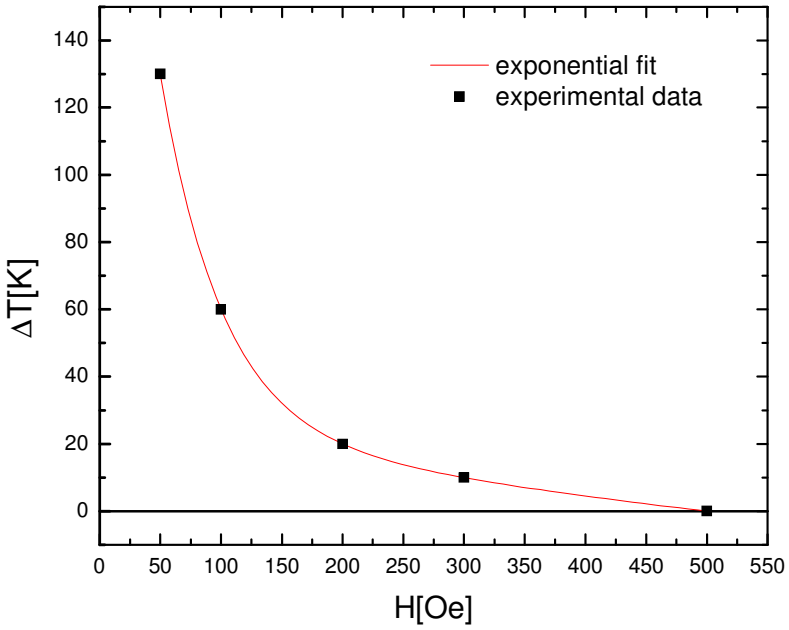

Figure.6.2 Thermal hysteresis width as a function of the applied field

The integration of Maxwell relation for an isothermal hysteresis indicates that entropy change is directly proportional to the magnetization derivative with respect to temperature at constant magnetic field and scales with the applied magnetic field value. The sign of ΔS as determined from eq.6.1 is dependent on the sign of ΔM during the heating or cooling cycle of the measurement.

$$\Delta S_m = \int_{Hi}^{Hf} \left(\frac{\partial M}{\partial T} \right)_H dH \qquad (6.1)$$

The entropy change ΔS, as function of temperature is shown in figure 6.3. ΔS is calculated by numerically evaluating the integral in eq. 6.1 using the isothermal hysteresis data. As the model for magnetic thermal hysteresis predicts [62], the temperature stability interval of the two phases is controlled by the magnetic field. The sudden change in magnetic moment with temperature gives a discontinuity to ΔS(T) in a narrow temperature range.

On either side of the transition temperatures, the two phases have similar symmetries. The CoNi and Gd moments are coupled antiparallel to each other; the larger of the moments aligns parallel to the external magnetic field while the smaller moment aligns opposite to the magnetic field. There is an abrupt change between these two stable states at two critical temperatures (T_1 and T_2). During the cooling, the system undergoes a phase transition from CoNi to Gd aligned state: the multilayer switches magnetization 180^0 and hence magnetic moment changes from negative to positive at 100K. The anisotropy holds the system in the CoNi aligned state down to T_1 (figure 6.1a) through a supercooling process**.** This transition determines the decrease in entropy observed below 100K (figure 6.3 a)).

Similarly, when the system is heated up, the anisotropy holds the system in the Gd aligned state after the system passes through T_{comp} and reaches T_2 as shown in (figure 6.1(a)(superheating). The system reverses the phase to the CoNi aligned phase, with a second abrupt 180^0 switching of the magnetic moment, reaching the favorable energetic state for high temperatures**.** The transition will now determine a second discontinuity in ΔS(T) around 250K, while the system is heated back to 300K as shown in figure 6.3

(a). In figure 6.3(b) for H=100 Oe similar minimum and maximum values of ΔS(T) are related with magnetic phase transitions temperatures at T_1=130K and T_2=200K respectively. ΔS (T) for H=200 Oe is shown in figure 6.3(c).The minimum and maximum of ΔS are around 150K and 180 K respectively.

The absolute value of ΔS(T) increases slightly with the external magnetic field value (H= 0-200 Oe), and the phase transitions collapse to a single temperature above the critical field of H=500 Oe. In this case, the Zeeman energy will dominate the anisotropy energy at all the temperatures. This shows that the thermal hysteresis in the magnetic phase transitions is temperature controlled under small external magnetic fields. In figure 6.1(d) for H=500 Oe, the system shows no hysteresis in M(T) measurements and correspondingly no peaks are observed in ΔS(T) shown in figure 6.3 (d).

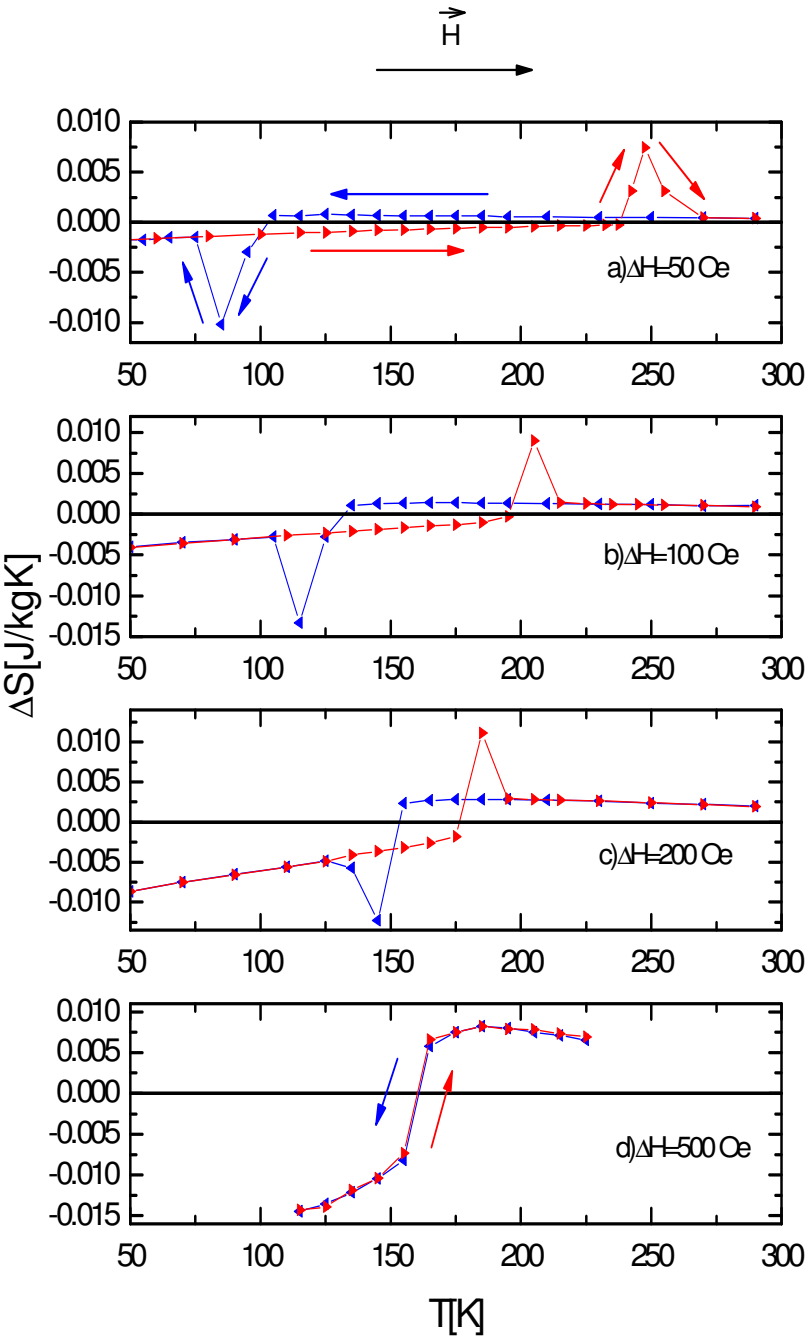

Figure 6.3 Entropy change as a function of temperature of $(CoNi1.5nm/Gd2nm)_4$ for different external magnetic fields

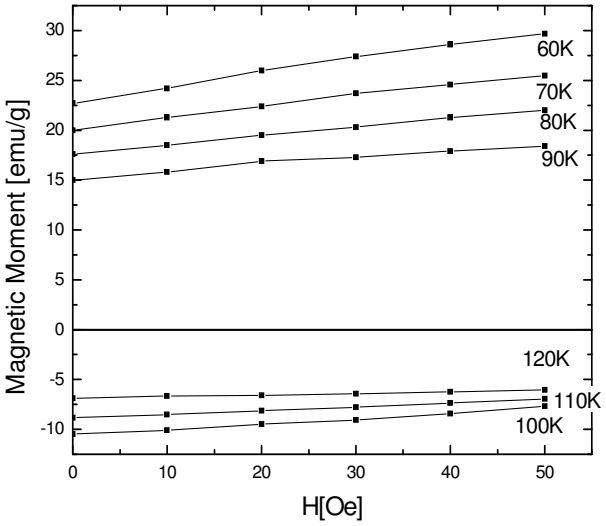

a)

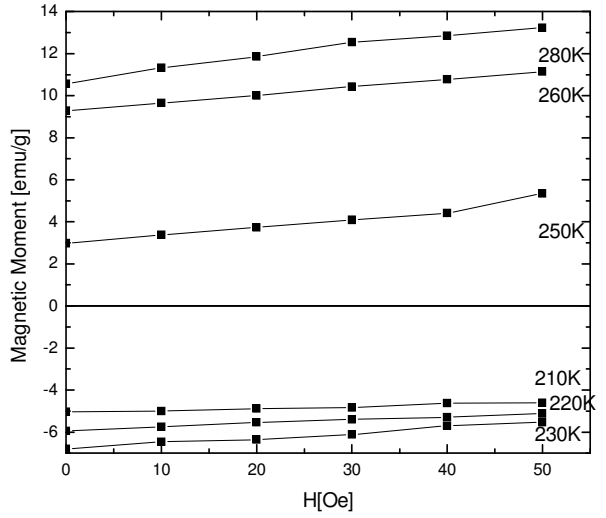

b)

Figure.6.4 Selected hysteresis loops for (CoNi1.5nm/Gd2nm) $_4$ multilayer around transition temperatures a) T_1=100K, b) T_2=230K

Figure 6.4 a) shows the magnetic hysteresis loops, M(H), of (CoNi1.5nm / Gd2nm)$_4$ for temperatures around the transition temperature T_1=100K. It can be seen that the magnetic moment does not change significantly with the applied field from 0-

50 Oe, but it does change sign with temperature. Magnetic moment has the same negative sign observed in the thermal hysteresis between (120-100) K and then becomes positive in the lower temperature interval (90-60) K. Figure 6.4 b) shows the magnetic hysteresis loops, M(H), of $(CoNi1.5nm/Gd2nm)_4$ for temperatures around the transition temperature T_1=240K with the same characteristics: no saturation, but strong temperature dependence. For temperatures between (210-230)K negative magnetic moment is measured corresponding to the metastable Gd aligned phase. Positive magnetic moment is measured then measured between (250-280)K as a result of moments reversal into CoNi aligned phase.

The change in energy between CoNi and Gd aligned phases is calculated at T_1 and T_2 based on eq. (2.11) and Ref.13.

$$\Delta E_{T1} = E_{CoNi} - E_{Gd} = 2H(M^{T1}{}_{Gd} - M_{CoNi}) > 0\,,\ (M^{T1}{}_{Gd} > M_{CoNi}) \quad (6.2)$$

$$\Delta E_{T2} = E_{CoNi} - E_{Gd} = 2H(M^{T2}{}_{Gd} - M_{CoNi}) < 0\,,\ (M^{T2}{}_{Gd} < M_{CoNi}) \quad (6.3)$$

$M^{T1}{}_{Gd}$ and $M^{T2}{}_{Gd}$ are Gd magnetic moments at the two transition temperatures respectively. M_{CoNi} is the CoNi magnetic moment, which is temperature independent to a good approximation in the 20-300 K interval and H is the applied magnetic field. The anisotropy term and exchange coupling terms were considered temperature independent and they canceled out in the difference.

It should be pointed out that ΔE_{T1} and ΔE_{T2} have opposite signs, which is in agreement with the signs of $\Delta S(T)$ from experimental data. At H=100 Oe applied field, ΔS_{T1}= -13.33mJ/KgK and ΔS_{T2}=9.02mJ/KgK as shown in table 6.1. The trend $|\Delta S_{T1}| > 1\Delta S_{T2}1$ is observed in figure 6.2 and presented in table 6.1 for all the fields. At low

temperature, more energy is required to switch larger magnetic moments even if the net magnetic moments at the transition temperatures have the same magnitude. This is due to the Gd moment temperature dependence and it is shown in figure 6.1a) using the arrows. The magnitude of entropy change does not scale with the applied field like in second order phase transitions. The nature of the transition is different in this case and the value of the applied field controls just the phase transition temperatures - figure 6.1 e).

Table 6.1 Entropy Change (ΔS) at the first-order phase transitions for $(CoNi1.5nm/Gd2nm)_4$ for different applied magnetic fields.

ΔH[Oe]	ΔS_{T1}[mJ/kgK]	ΔS_{T2}[mJ/kgK]
50	-10.22	7.46
100	-13.33	9.02
200	-12.30	11.10

$(CoNi2nm/Gd2nm)_4$ with lower T_{comp} was also investigated. The addition of more CoNi to the system makes the compensation temperature lower, T_{comp}= 65K. The magnetic moment as a function of temperature is shown for this multilayer in figure 6.5. The vertical lines show the region where the two phases coexist.

A difference in behavior is observed at applied magnetic field of 50 Oe. This multilayer can have no phase transition or one phase transition depending on the

starting point (300 K or 10 K respectively). The multilayer stays in the CoNi aligned phase during cooling from 300K to 10K and follows the same path while heating back to 300K.This is due to the fact that the_the anisotropy of the multilayer is now higher than the Zeeman energy (figure 6.5 a)). If the initial state is at low temperature, the Gd aligned phase, during heating to 300K, the system undergoes a very sharp phase transition at T_2=140K as shown in figure 6.5 b). On contrary, the first multilayer studied has 2 phase transitions for this applied field of 50 Oe independent of the starting point. In figure 6.5 c), under a 100 Oe applied field, two-phase transitions are observed. One at T_1=40K and one at T_2=100K, during the cooling and heating cycles respectively.

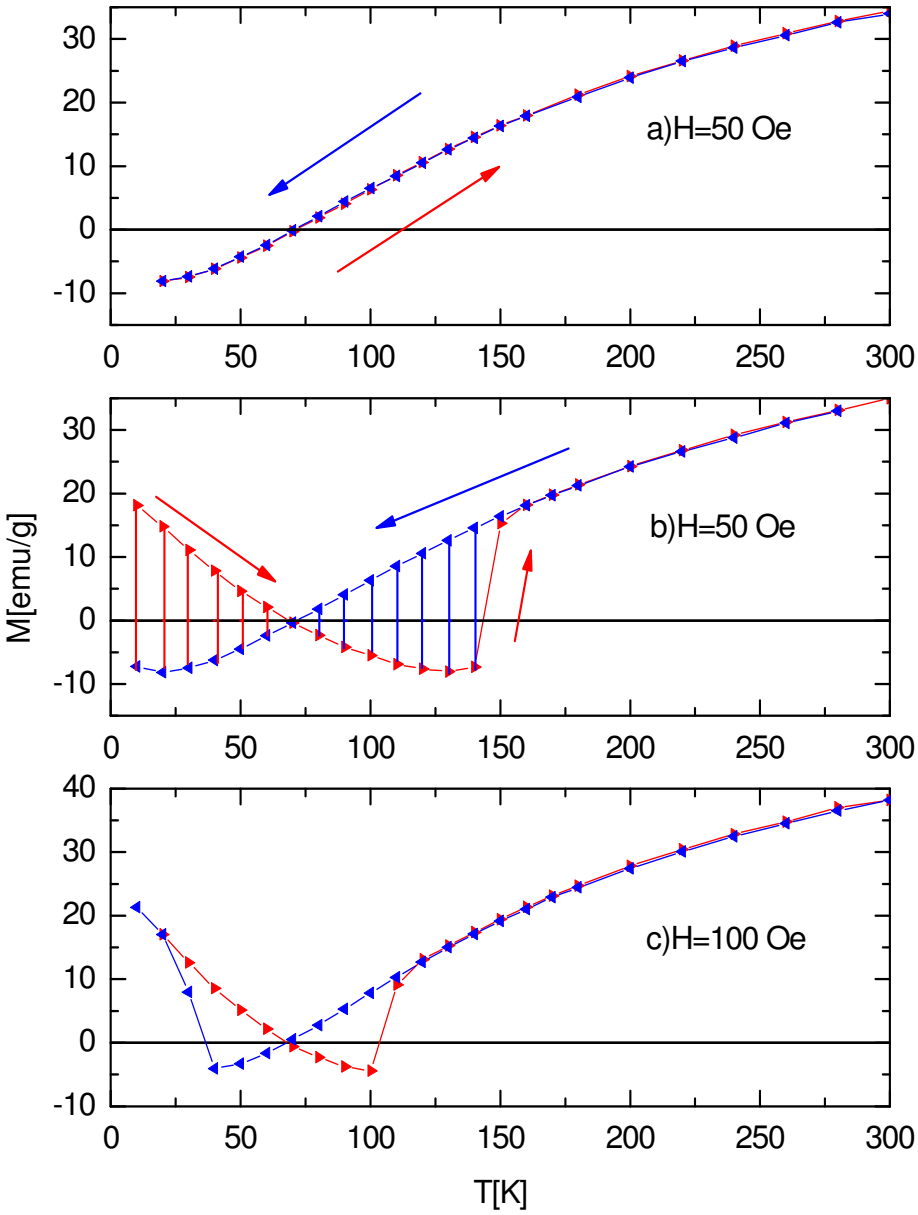

Figure 6.5 Temperature dependence of magnetic moment for (CoNi2nm/Gd2nm) $_4$ for different external magnetic fields.

The entropy change as a function of temperature, ΔS (T), is presented for this sample in figure 6.6. In figure 6.6 a), H=50Oe, starting from 20K,and heating the sample toward 300K, just a maximum in entropy change around 150K is observed as

the system switches from Gd to the CoNi aligned phase. For the cooling cycle ΔS(T) has a monotonic temperature dependence. In figure 6.6 b), at H=100 Oe, starting from 300K, a minimum corresponding to the first phase transition around 40K, and a maximum corresponding to the second phase transition around 100K are observed in ΔS (T). These results demonstrate that at low fields one can observe no transition or one transition only depending on the starting point of M (T) measurements.

Table 6.2 Entropy Change (ΔS) at the first-order phase transitions for $(CoNi2nm/Gd2nm)_4$ for different applied magnetic fields.

ΔH[Oe]	ΔS_{T1}[mJ/kgK]	ΔS_{T2}[mJ/kgK]
50	-	12.2
100	-22.5	22.2

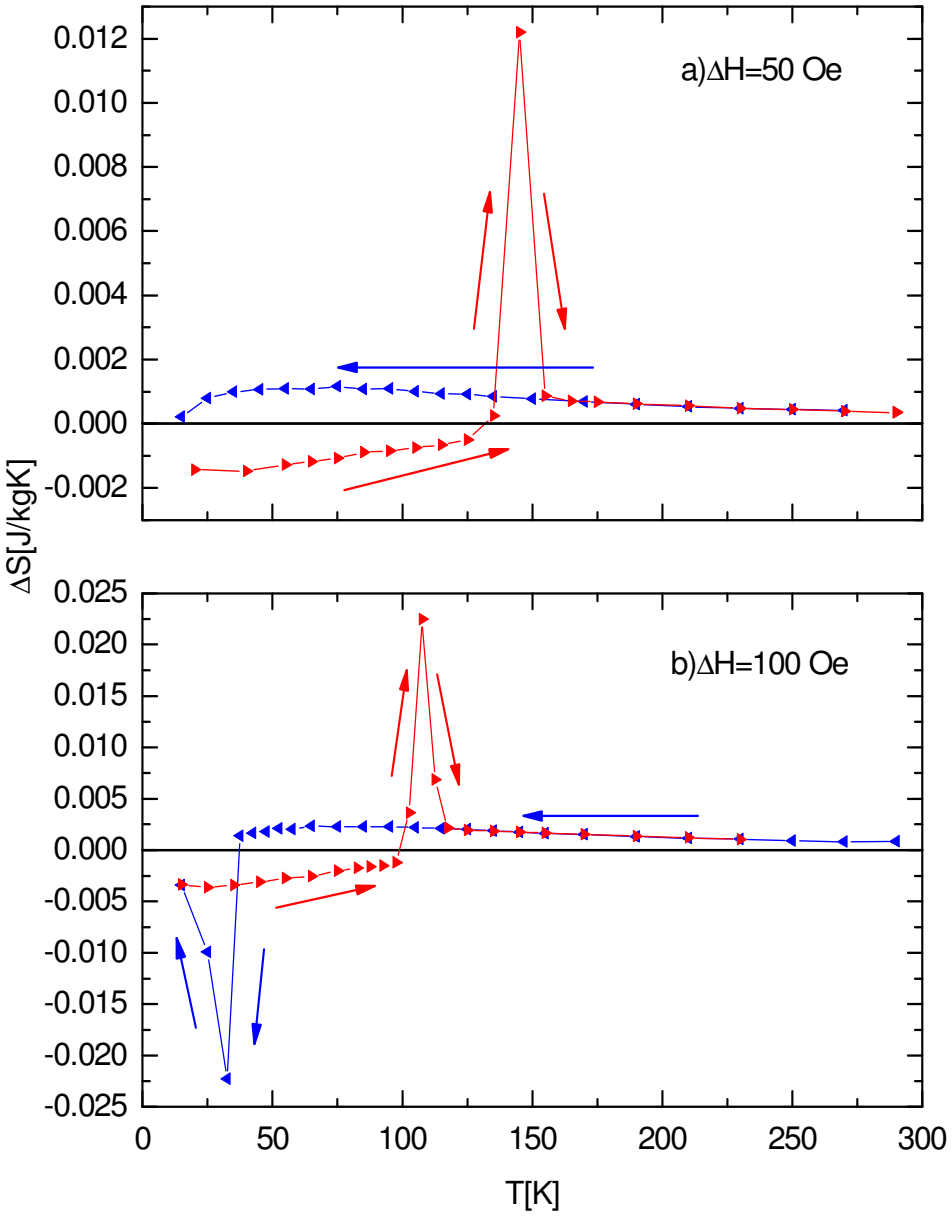

Figure 6.6 Entropy change as a function of temperature $(CoNi2nm/Gd2nm)_4$ for different external magnetic fields

A different way to change the multilayer compensation temperature and also the transition temperatures is changing the bylayer repetition number. $(CoNi2/Gd2nm)_8$ has

T_{comp} = 310K. M(T) and corresponding S(T) are presented in figure 6.7 for 100 Oe applied field.

There is an almost constant entropy change of 1mJ/kgKin a large temperature interval (360-280K) followed by the minimum of ΔS= - 4.5mJ/kgK around 260K. On the heating cycle, a continuous, small rate decrease of ΔS for 200-320K temperature interval, followed by the maximum of 2.46mJ/kgK at around 350K.

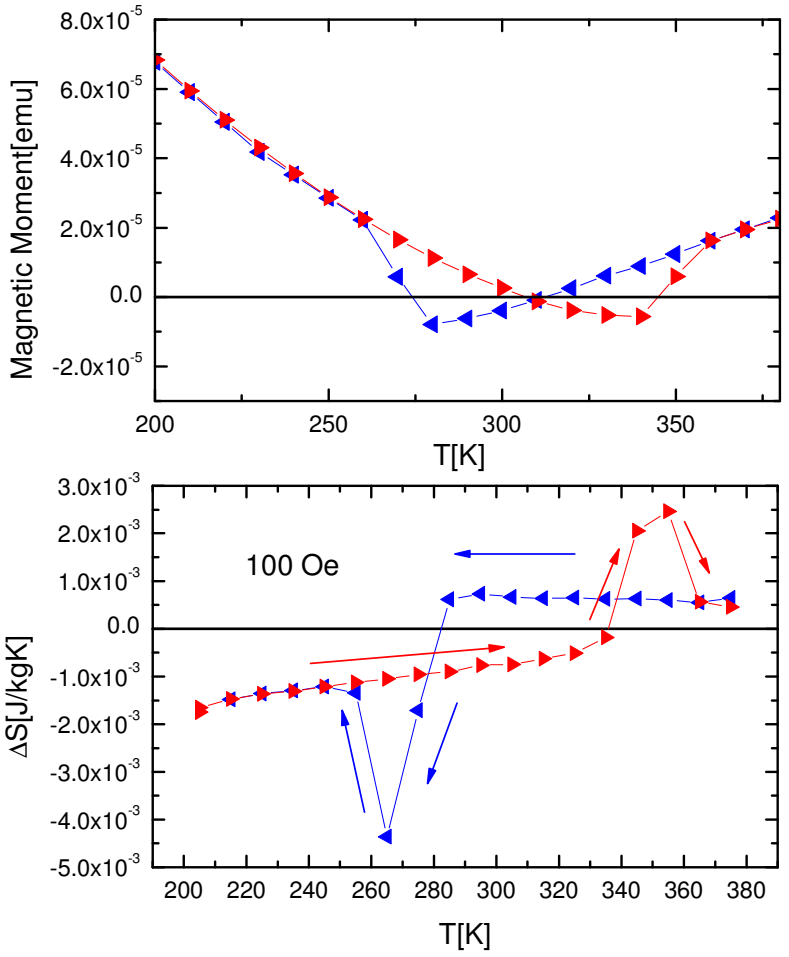

Figure 6.7 Temperature dependence of magnetic moment and entropy change as a function of temperature $(CoNi2nm/Gd2nm)_8$ for H=100 Oe external magnetic field

6.2 $(CoFe2nm/Gd2nm)_8$ multilayer

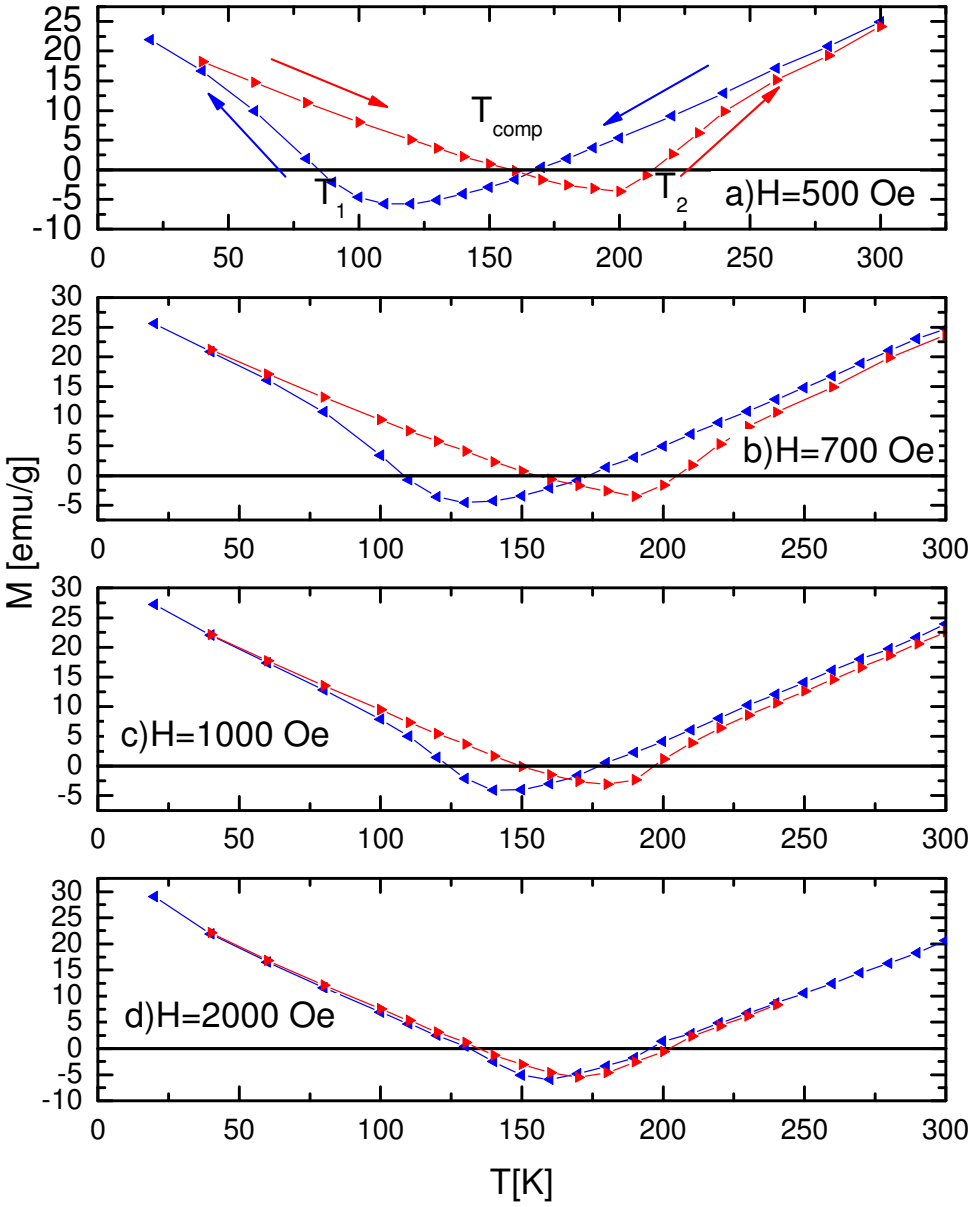

Figure 6.8 Temperature dependence of magnetic moment for $(CoFe2nm/Gd2nm)_8$ multilayer

Figure 6.8(a) shows the magnetic moment as a function of temperature for $(CoFe2nm/Gd2nm)_8$ multilayer under different external magnetic fields, from 500 to 2000 Oe. CoFe and Gd moments are antiferromagnetically aligned and the interaction is dominated by the exchange and anisotropy energy values. The sample will switch from the CoFe aligned state to the Gd aligned state during the cooling cycle at T_1, and back to the CoFe aligned state at T_2 during the heating cycle. The thermal hysteresis width, $\Delta T=T_2 - T_1$, represents the coexistence temperature interval for the two magnetically ordered CoFe and Gd aligned phases. As predicted by the theoretical model [62], the thermal hysteresis width becomes narrower by applying higher external magnetic fields as shown in figure 6.9. The thermal hysteresis width as function of applied magnetic field $\Delta T(H)$ is presented in figure 6.9. ΔT = 90K is reduced to 10K when the applied field changes from 500Oe to 2000 Oe.

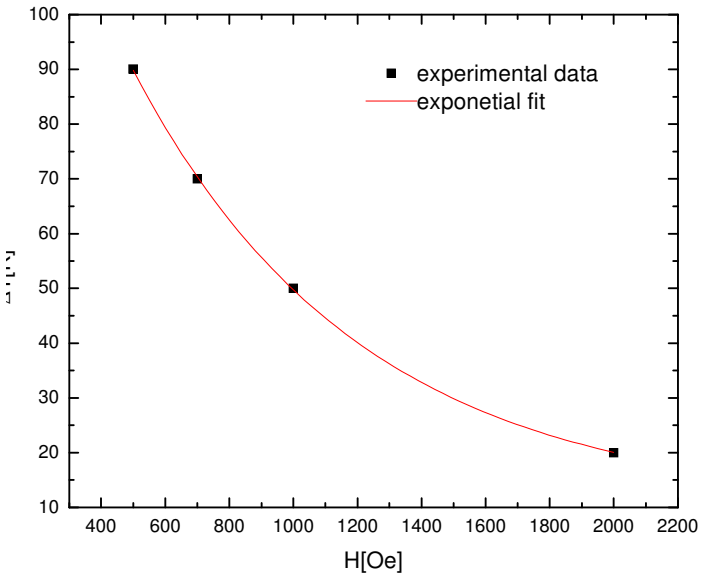

Figure 6.9 Thermal hysteresis width dependence on applied magnetic field for $(CoFe2nm/Gd2nm)_8$ multilayer

Figure 6.10 shows ΔS(T) measured while magnetizing the sample, as determined from the Maxwell equation. The magnetic entropy change has a strong temperature dependence. A minimum during the cooling cycle and a maximum during the heating cycle connected with the magnetic phase transitions temperatures at T_1 and T_2 respectively. Starting at 300K, ΔS is positive and almost constant for a large temperature range. This is due to a continuous decrease of the magnetic moment with temperature. Around transition temperature $T_{1,}$ where there is 180^0 switch of magnetization, ΔS changes sign and has a drop in magnitude. As the temperature is increased from 20K, ΔS is negative as the magnetization decreases monotonically with increasing temperature. Around $T_{2,}$ where there is the second 180^0 switch of magnetization to the CoFe aligned state, ΔS changes sign again and has an increase in magnitude. As shown in figure 6.10.thermal hysteresis in ΔS(T) is observed at different applied fields, but in a different temperature interval. The absolute value of ΔS(T) ~10^{-1} J/kg K can be obtained in a 235-185 K interval as the applied field (500- 2000 Oe) controls the phase transition temperatures.

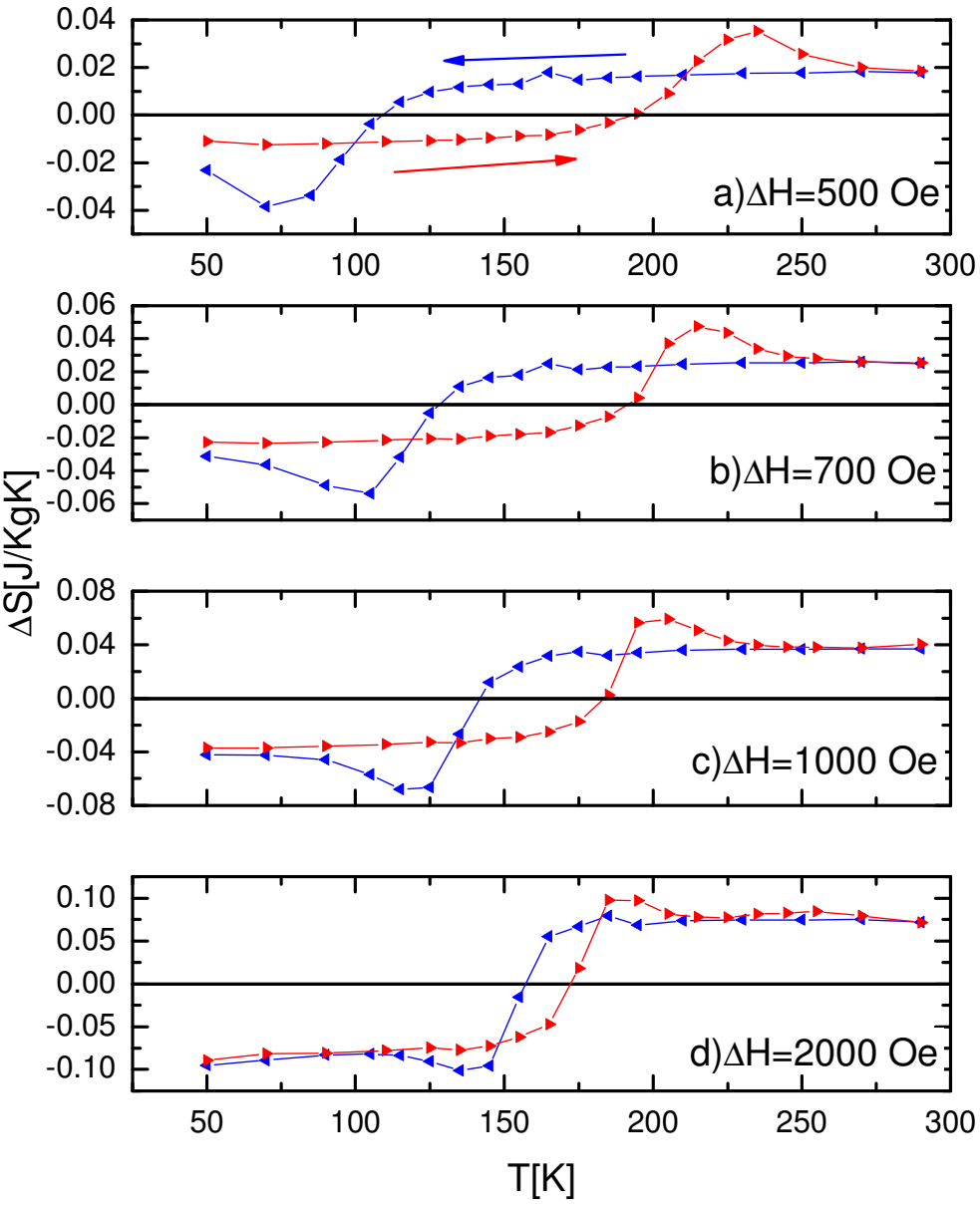

Figure 6.10 Entropy change as a function of temperature $(CoFe2nm/Gd2nm)_8$

Table 6.3 shows the entropy change at the first-order phase transitions for $(CoFe2nm/Gd2nm)_8$ for different applied magnetic fields.

Figure 6.11 shows the M(T) measurements at H=200 Oe when the applied field value is comparable with the anisotropy field. As shown in figure 6.11 a), if the starting point is room temperature, the anisotropy energy dominates the Zeeman energy and the system is kept in the CoFe aligned phase. As shown in figure 6.11 b) starting at low temperature, the system has one phase transition around 200K from the Gd aligned phase to the CoFe aligned phase. Accordingly the entropy change decrease monotonic during the cooling cycle and has a peak during the heating cycle, as shown in figure 6.12. The thermal hysteresis is eliminated in this case and the positive or inverse entropy change obtained during the magnetization process can be used for cooling. Inverse magnetocaloric effect, which has $\Delta S>0$, unlike cooling by adiabatic demagnetization which requires $\Delta S<0$, is measured in this case. Considering the small applied magnetic field values, the magnitude of ΔS measured for CoFe/Gd multilayer becomes an important result.

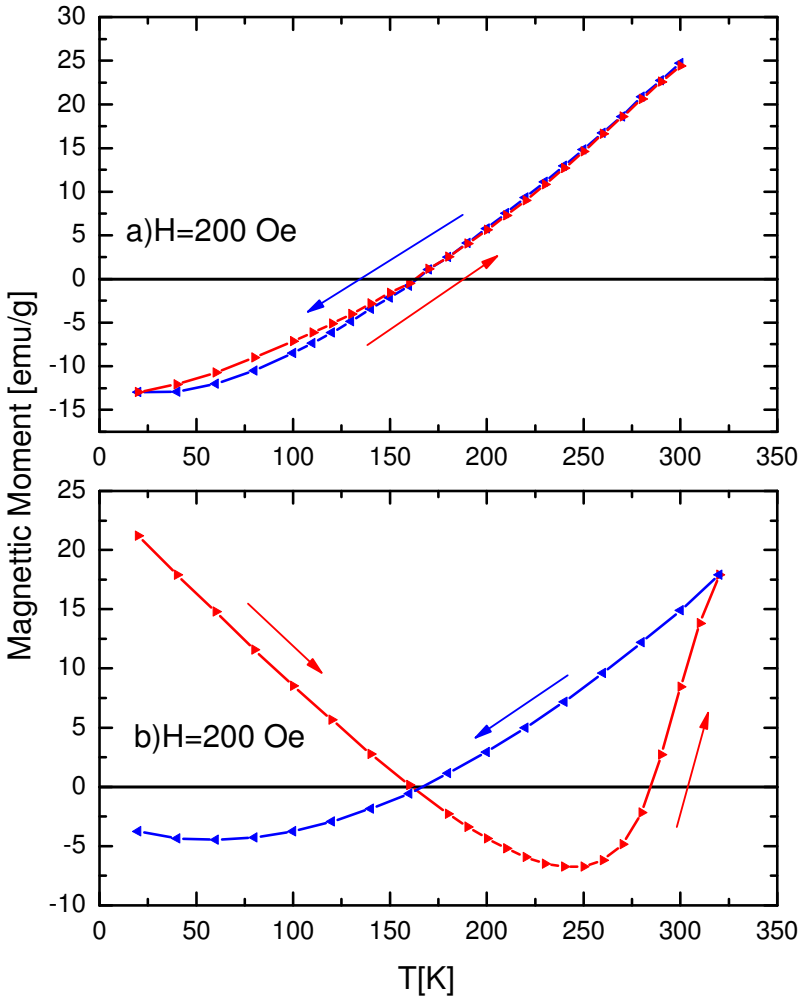

Figure 6.11 Entropy change as a function of temperature $(CoFe2nm/Gd2nm)_8$ at H=200 Oe with different starting points: a) room temperature, b) low temperature

The following M(T) cycle was repeated a few times with identical results. Cooling in 200 Oe magnetic field from 300K to 20K, applying 3000 Oe for short time to switch from CoFe aligned phase to Gd align phase, followed by heating from 20 to 300 K under the 200 Oe applied field that will give now the phase transition around 300K.The results are similar with the data shown in figure 6.11b).The purpose of this

induced transition is to eliminate the hysteresis and have just one discontinuity in ΔS(T).

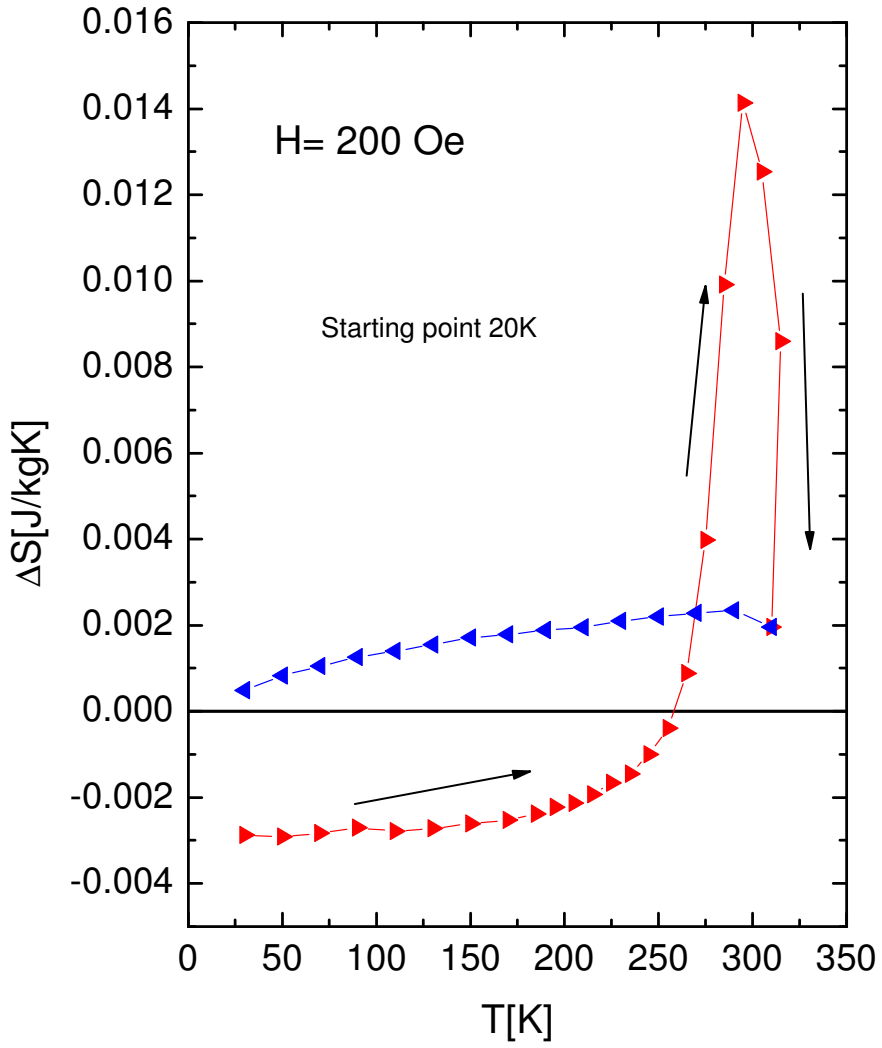

Figure 6.12 Entropy change as a function of temperature for $(CoFe2nm/Gd2nm)_8$ for ΔH=200 Oe.

Table 6.3 Entropy Change (ΔS) at the first-order phase transitions for $(CoFe2nm/Gd2nm)_8$ for different applied magnetic fields.

ΔH[Oe]	ΔS_{T1}[mJ/kgK]	ΔS_{T2}[mJ/kgK]
200	-	14.13
500	-38.46	35.37
700	-53.95	47.41
1000	-67.80	59.34
2000	-101.64	97.45

Figure 6.13 shows field hysteresis loops for CoFe/Gd multilayer. The increase in coercivity associated with the decrease in remanent and saturation moment observed in measurements at 100 and 200K proves the antiferromagnetic coupling of CoFe and Gd.

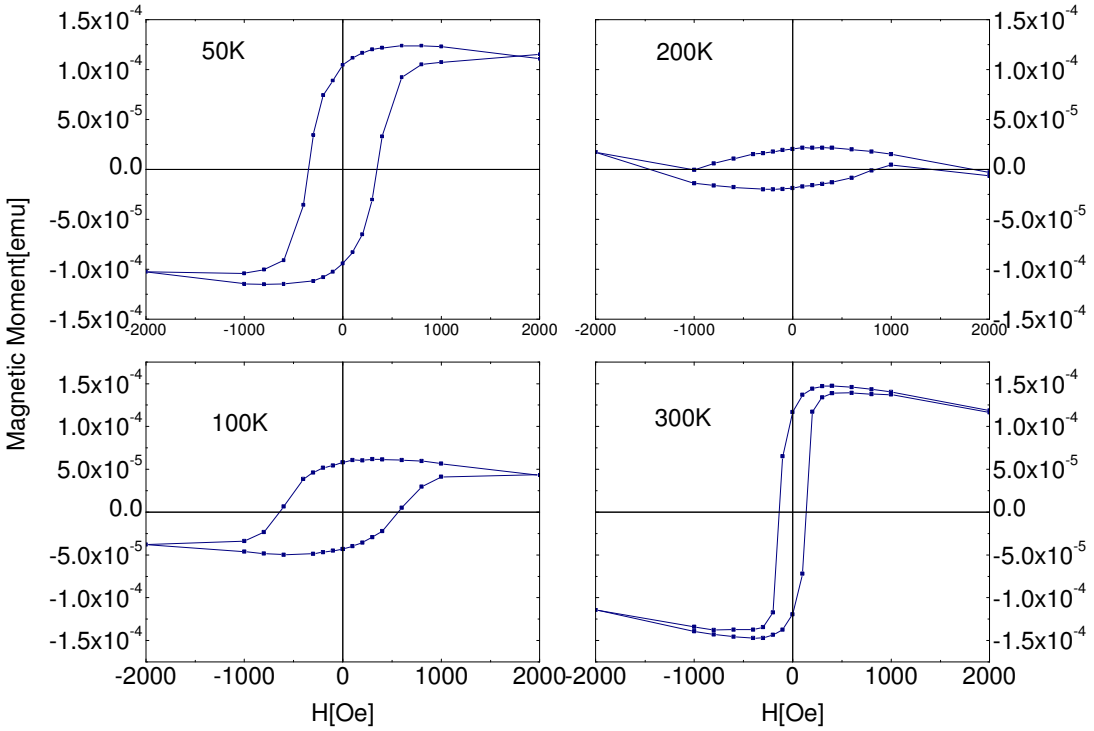

Figure 6.13 Hysteresis loops for $(CoFe2nm/Gd2nm)_8$ multilayer

For CoFe/Gd multilayer, the phase transitions follow the same trend, as for the CoNi/Gd multilayer, but they are less abrupt. This behavior may be due to a better, in plane, ferromagnetic alignment inside the CoNi than the CoFe alloy. The applied fields at which the phase transitions occur are higher (500-2000Oe) than for the CoNi/Gd system (50-500Oe). This is an indication that higher anisotropy field is responsible for thermal hysteresis: H_a may be around 200Oe for CoFe and around 50Oe for CoNi. The entropy change values of mJ/kgK can be measured at different temperatures over a 40K temperature interval for CoFe/Gd, and over a 70K for CoNi/Gd during the heating or cooling of the sample.

Magnetic entropy change has been measured for artificial ferrimagnetic systems of CoFe /Gd and CoNi/Gd nanolayers. ΔS (T) associated with first order magnetic phase transitions, has a minimum during the cooling cycle and a maximum during the heating cycle. The magnetic phase transitions with entropy change can be controlled over 20-300K interval with small applied magnetic fields. The order-order magnetic phase transitions observed in M (T) and ΔS (T) are explained due to the temperature dependence of the Gd moment associated with the existence of an anisotropy field in the TM layers. The same multilayer can show none, one, or two-phase transitions by varying an external magnetic field in a small range and by changing the starting point in the cooling/heating cycles. The positive entropy change during an adiabatically magnetization process can find applications in materials cooling.

6.3 $(Co4nm/Tb6nm)_8$ multilayer

Entropy change was calculated for the hard ferrimagnetic system $(Co4nm/Tb6nm)_8$

Figure 6.14 shows ΔS(T) and M(T) for $(Co4nm/Tb6nm)_8$ at 3000 Oe applied magnetic field ΔS= - 350mJ/kgK at 85K during the sample cooling. During the heating ΔS= - 290 mJ/kgK at 105K and ΔS=85mJ/kgK at 174K.

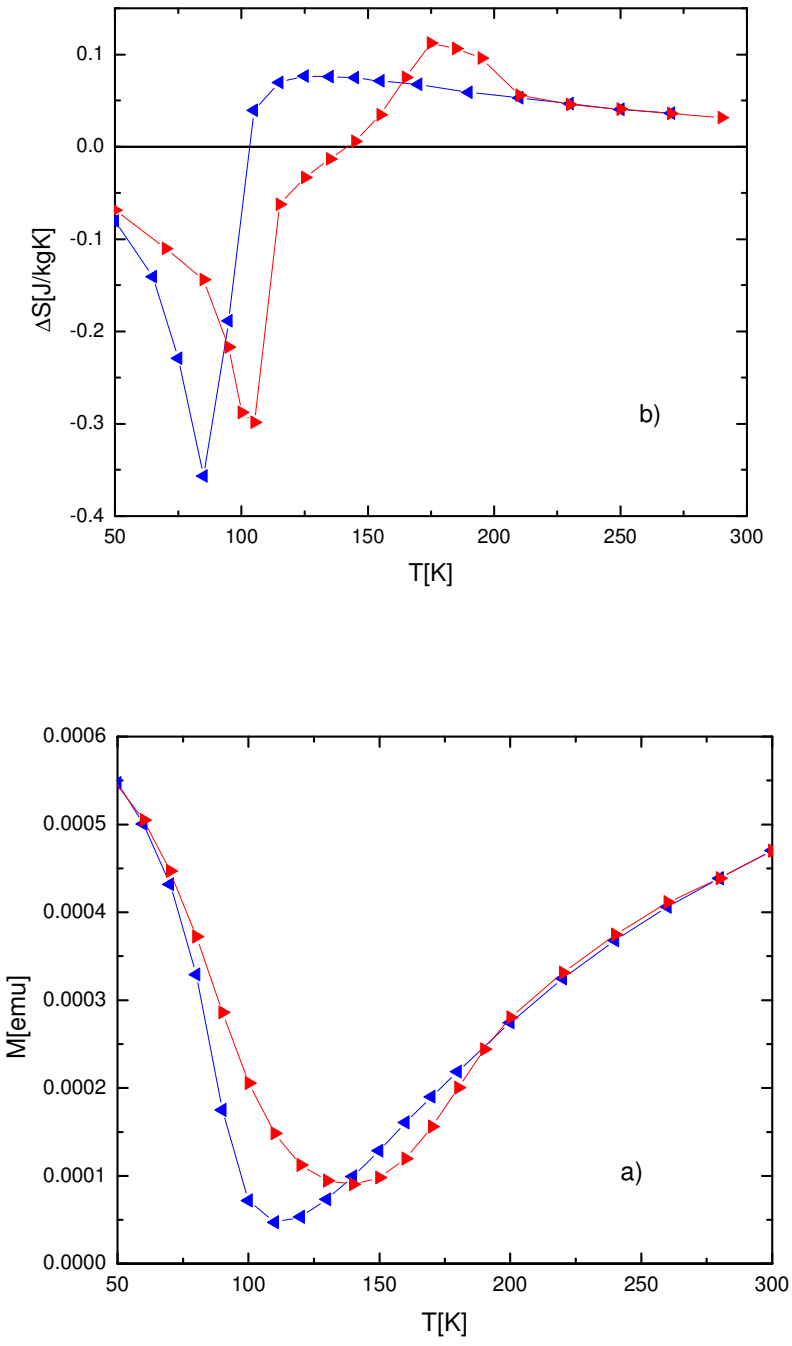

Figure 6.14 a) M(T), b)ΔS(T) for $(Co4nm/Tb6nm)_8$ at H=3000 Oe

Figure 6.15 shows ΔS(T) and M(T) for $(Co4nm/Tb6nm)_8$ at 4000 Oe. The entropy change ΔS= - 340mJ/kgK at 95K was measured during the cooling cycle and ΔS= - 240mJ/kgK at85 K and ΔS= - 150mJ/kgK at175K during the heating cycle. The entropy change does not have symmetric temperature dependence with just a minimum and a maximum like previously observed for CoNi or CoFe/Gd multilayers. Based on the measurement method, the entropy change follows the M(T) dependence. Due to the large thickness, the middle of Tb layer may not be very well pinned by the adjacent Co layers. The helical structure of Tb gives field dependent moment reorientations and hence the change in magnetic moment is gradual as there may be a continuous rotation of the moments from Co to Tb aligned phase.

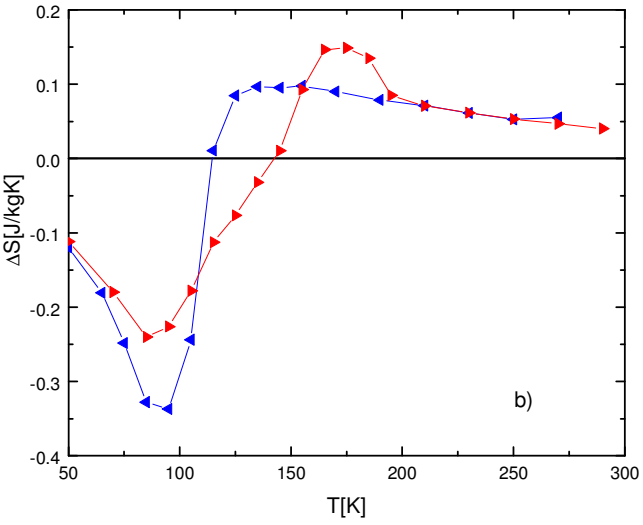

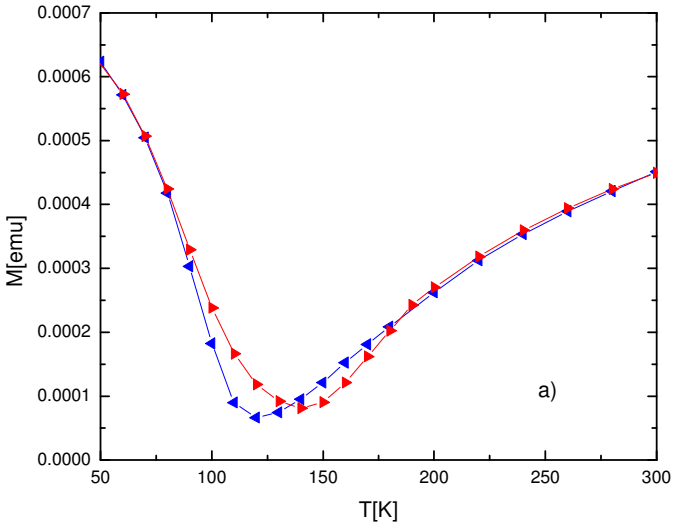

Figure 6.15 a) M(T), b)ΔS(T) for $(Co4nm/Tb6nm)_8$ at H=4000 Oe

.

CHAPTER 7

CONCLUSIONS

The presence of a compensation temperature where the net magnetic moment of the system is minimum and the presence of a maximum in coercivity around T_{comp} for the multilayers studied support the assumption that Co/Tb, NiFe/Gd and Ni/Gd are ferrimagnetic systems.

For the hard ferrimagnetic $(Co3.5nm/Tb4nm)_8$ and $(Co4nm/Tb6nm)_8$ multilayers a minimum in Mr(T) was measured at 210K and at 140 K respectively. These minimum temperatures indicate the compensation temperatures. The Terbium moments present a spread of their directions because of the strong local anisotropy and incomplete compensation is observed from hysteresis loops.

For $(NiFe2nm/Gdxnm)_4$ series with x=2,3,4 nm and also for $(Ni4nm/Gdxnm)_4$ multilayers with x=2,4,6nm, the compensation temperature increases as the amount of Gd is increased .The multilayer with smaller Gd magnetic moment requires a smaller NiFe or Ni for the moments to compensate. Therefore T_{comp} increase as Gd thicknesses is increased. As the Gd thicknesses is increased the minimum in M(T) becomes broader as a result of incomplete compensation.

Thermal hysteresis was measured in constant magnetic field for total magnetic moment (M). The M(T) graph has two minima corresponding to first order magnetic

phase transitions. As the external magnetic field increases the thermal hysteresis width decreases for all the studied multilayers. At lower fields the anisotropy contribution is dominant in the competition with Zeeman energy or with the exchange coupling term. The system is hold in the TM aligned phase for the entire temperature range and negative magnetization was measured in this case. At higher magnetic fields the M(T) measurements will show just one minimum which corresponds to compensation temperature.

The phase transitions between Co and Tb aligned states, observed at different temperatures during the cooling and heating of the sample in constant applied magnetic field, are not as sharp as predicted by the theory [62]. An anisotropy term for Tb layers and more complex than uniaxial form (as assumed for Co) has to be included in the model. Tunability of thermal hysteresis width over 0-80 K can be achieved with large magnetic fields (1-9) kOe. The thinner multilayer gives larger thermal hysteresis, for the isame external magnetic field. The large constant magnetic fields that can give the thermal hysteresis behavior is direct related with large coercivity of the multilayers.

For Ni/Gd and NiFe/Gd thermal hysteresis characteristics are observed in M(T) for all the multilayers. Temperature difference of 20, 30 K between the phase transition temperatures can be controlled by small magnetic field (50-300 Oe). Above a certain value the thermal hysteresis, predicted theoretically, disappear and this is observed experimentally for both systems Ni/Gd and NiFe/Gd.

For Ni/Gd a strong asymmetry is observed for all the applied fields The Ni diffusion into Gd layer during the sputtering process may be different from a pure Ni

target compared to a NiFe target. The existence of an alloy changes the interface coupling (weaken the exchange coupling) and the mechanism of the phase transition during the cooling and the heating cycles. Also a temperature dependent anisotropy and more complex than uniaxial form may be considered for explaining the thermal hysteresis.

The experimental data for both hard and soft ferrimagnetic systems are far from the theoretical models where perfect interfaces are considered, but M(T) measurements reflect the anisotropy contribution in magnetic stable states of TM/RE at moderate magnetic fields.

Magnetic entropy change has been measured for artificial ferrimagnetic systems of CoFe /Gd and CoNi/Gd nanolayers. ΔS (T) associated with first order magnetic phase transitions, has a minimum during the cooling cycle and a maximum during the heating cycle. The magnetic phase transitions with entropy change can be controlled over 20-300K interval with small applied magnetic fields. The order-order magnetic phase transitions observed in M (T) and ΔS (T) are explained due to the temperature dependence of the Gd moment associated with the existence of an anisotropy field in the TM layers.

For CoFe/Gd multilayer, the phase transitions are less abrupt than for CoNi/Gd. This behavior may be due to a better, in plane, ferromagnetic alignment inside the CoNi than the CoFe alloy. The applied fields at which the phase transitions occur are higher (500-2000Oe) than for the CoNi/Gd system (50-500Oe). This is an indication that higher anisotropy field is responsible for thermal hysteresis: H_a may be around 200Oe

for CoFe multilayer and around 50Oe for CoNi multilayer. The entropy change values of mJ/kgK can be measured at different temperatures over a 40K temperature interval for CoFe/Gd, and over a 70K for CoNi/Gd during the heating or cooling of the sample. The same multilayer can show none, one, or two-phase transitions by varying an external magnetic field in a small range and by changing the starting point in the cooling/heating cycles. A measurement cycle M(T) is designed starting from low temperature, such as the hysteresis is eliminated and just positive entropy change is measured . The positive entropy change during an adiabatically magnetization process can lead to temperature decrease and find applications in materials cooling.

REFERENCES

1. A. H. Morrish, The Physical Principles of Magnetism (IEEE Press, New York, 2001)

2. S. Blundell, Magnetism in Condensed Matter (Oxford University Press, New York, 2001)

3. G. Bertotti, Hysteresis in Magnetism (Academic Press, 2001)

4. P. Chaudhari, J.J. Cuomo, and R.J. Gambino, Apply. Phys. Lett. **22**, 337(1973)

5. M. H. Kryder, Annu. Rev. Matter. Sci, 411, (1993)

6. T. Morishita, Y. Togami, and K. Tsushima, J. Phys. Soc. Jpn. **54**, 37 (1985)

7. C. D. Stanciu, A. V. Kimel, F. Hansteen, A. Kiriluk, A. Itoh, and Th. Rasing, Phys. Rev. Letter **99**, 217204 (2007)

8. K. Cherifi, C. Dufour, Ph. Bauer, G. Marchal, and Ph. Mangin, Phys Rev B **44**,7733(1991)

9. J. P. Andres, L. Chico, J. Colino, and J. M. Riveiro Phys Rev B, **66**, 094424 (2002)

10. S. Demirtas, A.R Koymen, H Zeng, Journal of Physics: Condensed Matter **21,** L213 (2004)

11. O. S. Anilturk and A. R. Koymen, Phys Rev B **68**, 024430 (2003)

12. H. Nagura, K. Takanasi, S. Mitani, K. Saito, and T. Shima, Journal of Magnetism and Magn. Mat **240**,183(2002)

13. R.E. Camley and R.L. Stamps J. Phys.: Condens. Matter **5**, 3727 (1993)

14. Ch. Kittel, Introduction to Solid State Physics (Wiley, New York,1986)

15. R. M. Bozorth, Ferromagnetism (IEEE Press, New York, 1993)

16. S. Chikazumi, Physics of Ferromagnetism (Oxford University Press, New York,1997)

17. F. J. A. den Broeder, W. Hoing, P. J. H .Bloemen JMMM **93**, 562 (1991)

18. R.E. Camley and D.R. Tilley, Phys. Rev. B **37**, 3413 (1988)

19. R.E. Camley, Phys. Rev. B **39**,12316 (1989)

20. M. Sajieddine, Ph. Bauer, K. Cherifi, C. Dufour, G. Marchal and R. E. Camley, Phys. Rev. B **49**, 8815 (1994)

21. D. Haskel ,Y .Choi, D. R .Lee ,J.C. Lang ,G. Srajer , J. S .Jiang, S .D .Bader, Journal of Applied Phys **93**,6507 (2004)

22. W. Hanh, M. Lowenenhaupt, Y. Y. Huang, G. P. Felcher and S.S.P. Parkin, Phys. Rev. B **52**,16041 (1995)

23. N. Ishimatsu, H. Hashizume, S. Hamada, N. Hosoito, C. S. Nelson, C. T. Venkataraman, G. Srajer, J. C. Lang, Phys. Rev. B **60**,9596 (1999)

24. S. Demirtas and A. R. Koymen, Journal of Applied Physics **95**, 4949 (2004)

25. R. M. White, Theodore H. Geballe, Long Range Order in Solids, Academic Pr, London (1979)

26. S. W. Biernacki ,Phys Rev B **68,**174417 (2003)

27. E. Warburg, Ann.Phys.**13,** 141(1881)

28. P. Langevin, Ann.Chem.Phys.**5**, 70 (1907)

29. P. Debye, Ann.Phys.**81**,1154(1926)

30. W. F. Giaque, J.Amer.Chem.Soc.49,1864,(1927)

31. V. K. Pecharsky, K. A. Gschneider Jr. Journal of Magnetism and Magn. Mat, **200**, 44(1999)

32. P. J. von Ranke, S. Gama, A. A. Coelho, A.de Campos, A. Magnus, G. Carvalho, F. C. G. Gandra, and N. A. de Oliveira, Phys. Rev. B 73,014415(2006)

33. J. Herrero-Albillos et al, Phys Rev B **73**,134410(2006)

34. C. Rong and J.P. Liu Applied Phys Letter **90**,222504(2007)

35. G. J. Liu, J. R. Sun, J. Shen et al Applied Phys Letter **90**, 032507(2007)

36. K. A. Gschneider, V. K. Pecharsky and A. O. Tsokol, Rep Prog. Phys **68**,1479(2005)

37. O. Tegusa, E. Bruck, L. Zhang, K. H. J. Buschow, F. R. de Boer, Physics B **319**, 174 (2002)

38. A.I. Akhiezet, V. G. Bar'yakhtar, and M.I.Kagano, Soviet Phys.-Uspekhi **3**, 567 (1961)

39. R. P. Joenk, Journal of Applied Phys, **34**, 1097 (1963)

40. T. Krenke, E. Duman, M. Acet ,E. F. Wassermann, X. Moya, L. Manosa, A. Planes, Nature Materials, **4**,450 (2005)

41. Y.Q. Zhang, Z.D. Zhang, J. Alloys Comp, **365**,35(2004)

42. Z. D. Han, D. H. Wang, C. L. Zhang, H. C. Xuan, B. X. Gu and Y. W. Du, Apply.Phys.Let.**90**,119902(2007)

43. X. Zhang, B. Zhang, S. Yu, Z. Liu, W. Xu, G. Liu, J. Chen, Z. Cao and G. Wu ,Phys Rev B **76**,132403(2007)

44. J. E. Mahan Physical Vapor Deposition of Thin Films(John Wiley & Sons, New York 2000)

45. B.D. Josephson, Phys. Letters **1**, 251, 1962

46. J.C. Gallop SQUIDs, The Josephson Effect and Superconducting Electronics (Adam Hilger, 1991)

47. S.S. Swithenbby SQUIDs and their applications in the measurement of weak magnetic fields. J Phys E: Sci. Instrum. 1980, 13:801-813.

48. J. Clarke, A. I. Braginski The SQUID Handbook,(Wiley-VCH Verlay, Weinheim,2004)

49. M. McElfresh Fundamentals of magnetism and magnetic measurements featuring Quantum Design's Magnetic Property Measurement System, Quantum Design, 1994

50. W. S. Kim, W. Kleeman, J. Tappert, W. Kenue, J. Appl. Phys **84**,4384 (1998)

51. G. A. Bertero, T.C. Hufnagel, B.M Clemens, R. Sinclair Journal of Materials Research **8**,771 (1993)

52. J. Colino, J. P. Andres ,and J .M. Riveiro, Phys. Rev. B **60**, 6678 (1999)

53. D. J. Webb , R. G. Walmsley, K. P Arvin, P. H. Dikinson, T. H. Geballe and R.M. White, Phys. Rev. B, **32**, 4667 (1985)

54. O. S. Anilturk, A.R. Koymen, Phys Rev. B **68**,0244309(2003)

55. B. Altuncevahir, A. R. Koymen, J. Appl. Phys **90**,2939,(2001)

56. B. Altuncevahir, A. R. Koymen, J. Appl. Phys **89**,6822 (2001)

57. B. Altuncevahir, A .R .Koymen, Journal of Magnetism and Magnetic Materials **261**, 424 (2003)

58. J. L. Prieto, M. G. Blamire, and J. E. Evetts Phys. Rev. Letter **90**,027201 (2003)

59. R. Ranchal, C. Aroca, M. Maicas, E. Lopez, J. Appl. Phys. **102**, 053904 (2007)

60. A. Pogorily, E. Shypil, and C. Alexander, Journal of Magnetism and Magn. Mat **286**,493 (2005)

61. R. Ranchal, C. Aroca, E. Lopez J.Appl.Phys **100**,103903 (2006)

62. R.E. Camley, W. Lohstroh, G.P. Felcher, N. Hosoito and H. Hashizume, Journal of Magnetism and Magn. Mat. **286**, 65 (2005)

63. S. Demirtas, M. R Hossu, R.E. Camley, H.C. Mireles, A.R. Koymen, Phys. Rev. B **72**, 184433 (2005)

64. S. Demirtas, R.E. Camley, A. R. Koymen, Appl. Phys. Lett. **87**, 202111 (2005)

65. Zhi-Pan Li, Casey W. Miller, Igor V. Roshchin, and Ivan K. Schuller, Phys. Rev. B **76**, 014423 (2007)

66. A. L. Dantas and R. E .Camley Phys. Rev. B **75**,094436 (2007)

67. A.L. Dantas, A.S.W.T. Silva, G.O.G Reboucas, A.S. Carrico, R.E. Camley, J. Appl. Phys. **102**, 123907(2007)

68. M. R. Hossu, A. R. Koymen , J. Appl. Phys. **99**, 08C704 (2006)

69. K. A. Jr. Gschneider, V. K. Pecharsky, D. Fort, Phys. Rev. Lett. **78** 4281(1997)

70. K. A .Jr. Gschneider, V. K. Pecharsky, Annu. Rev. Matter. Sci. **30** 387(2000)

71. X. Y. Liu, J.A. Barclay, R. B. Gopal, M. Foldeaki, R. Chahine, T. K. Bose, P.J. Schurer, J. L. LaCombe J. Appl. Phys. **79,** 163 (1996)

72. C. S. Arnold, D. P. Pappas, A. P. Popov, 1999 Phys. Rev. Lett. **83** 3305

73. M. Kuz'min, M. Richter, Appl. Phy. Lett. **90,** 32509 (2007)

74. S. Chaudhary, P. Garg, S. Rajput, Solid State Commun. **132** 293 (2004)

75. P. Poddar, J. Gass, D.J. Rebar,S. Srinath, H. Srikanth, S. A. Morrison, E. E. Carpenter, J. Magn. Magn. Mater.**307**, 227 (2006)

76. V. D. Mello, A. L. Dantas, A. S. Carrico, Solid State Communication, **140**,447 (2006)

77. R. Skomski, C. Binek, T. Mukherjee, S. Sahoo and D. J. Sellymyer, J .Appl.Phys,**103**,07B329 (2008)

78. M. R. Hossu, Y. Hao, A. R. Koymen, J. Phys.: Condens. Matter **20**, 215224 (2008)

.

BIOGRAPHICAL INFORMATION

Maria R. Hossu earned a Bachelor of Science in Physics at Bucharest University, Romania in 1991.

In 2003 she became graduate student at University of Texas at Arlington, where she received the Master of Science in Physics in May 2005.